

# **Seismic Behaviour of Reinforced Concrete Buildings with Moment Resisting Frames and Frames with Structural Walls Subjected to Near and Far-Fault Ground Motions**

*Thesis Submitted in partial fulfilment  
of the requirements for the degree  
of*

**Doctor of Philosophy in Civil Engineering**

By

**Patnala V S Neelima**

(Roll No. 201512644)



**INTERNATIONAL INSTITUTE OF  
INFORMATION TECHNOLOGY**

**HYDERABAD**

International Institute of Information Technology, Hyderabad  
(Deemed to be University)  
Hyderabad – 500032, India

January 2023



## Certificate

This is to certify that the work contained in this thesis, titled "*Seismic Behaviour of Reinforced Concrete Building with Moment Resisting Frames and Frames with Structural Walls Subjected to Near and Far-Fault Ground Motions*" by Patnala V S Neelima (Roll No. 201512644) has been carried out under my supervision and is not submitted elsewhere for a degree.

Ramancharla Pradeep Kumar

Professor (on Leave)

Earthquake Engineering Research Centre

International Institute of Information Technology Hyderabad

Director

CSIR-Central Building Research Institute

Roorkee, Uttarakhand

...



## Abstract

One of the significant causes of life loss during an earthquake is the collapse of structures in the near-fault regions. Broadly, two sets of parameters affect the structural response, namely: (i) characteristics of structures, like configuration, stiffness, strength, and ductility, and (ii) characteristics of ground motions. Usually, the former are dependent on the latter. But the latter is derived independently by geologists, seismo-tectonists, seismologists, geotechnical engineers and structural engineers. Often, the considered seismic hazard has uncertainties arising from the way strong ground motion is considered in the near-fault regions. To understand and quantify the hazard in the near-fault regions, the ground motions characteristics are examined of the strong motion records of 1999 Chi-Chi, Taiwan earthquake. It is observed that the ground motions in the near-fault region exhibit higher PGA values on the hanging wall side as compared to the footwall side.

Further, the behaviours of two reinforced concrete buildings with moment resisting frames of five and ten storeys are studied when subjected to two types of horizontal near-fault ground motions with and without velocity pulse. The responses observed and the damage caused in the moment frame buildings owing to these near-fault ground motions are identified. It is observed that the near-fault ground motions with pulse induce higher drift demands compared to those without pulse and far-fault ground motions. Also, the response of the structure subjected to near-fault ground motion with pulse indicate the impulsive action that requires a revised mitigation strategy other than the conventional earthquake resistant design procedures. Inclusion of a structural wall is identified as a simple solution to control the damage arising from near-fault ground motion effects. The maximum drift demand on the structures with structural walls with SPD of 2.75%, 3.75% and 9% are studied and improved performance is observed as the structural plan density of structural walls is increased.



## Acknowledgements

I express my deepest gratitude to my thesis supervisor and guide, **Prof. Ramancharla Pradeep Kumar** for extending his constant motivation and unwavering support on me. I derived an unshakable inspiration even just by his presence during my research journey.

I am grateful for my thesis reviewers **Prof. C V R Murty, Dr. B Radhika and Dr. Sunitha Palissery** for providing me the intense and thoughtful guidelines through their timely reviews. Their reviews have given a lot of insights in shaping the research carried out.

I feel happy to extend my regards to all my **colleagues at IIIT Hyderabad** for extending their emotional support throughout my journey at the college. Working in teams with them has helped me to learn many co-curriculum skills required in the real world. I truly cherish the moments spent together in this journey.

I owe my sincere gratitude and affectionate regards to my research colleague and husband **Mr. P R N Vyas**, for his constant faith on me in completing this journey. His constant motivation next to my supervisor has given me a lot of strength at low phases of research life. Also, I emotionally thank my **parents-in-law and the extended family** for respecting my educational goals and supporting me at all the times including the rough phases of life during the journey.

I deeply owe reverence to my **parents** who have taught me the fundamentals of education and trained me to take up many challenges of life that have helped me to dream big. They have given the required ambience in life to find out my interests and pursue my dreams.

Last but not the least, I am grateful to almighty not only for giving me many opportunities but also to give my daughter **Baby P Lalitha** without whose support, it would have been impossible to complete this task. Her learned adaptability has given me sufficient scope to focus on my career.



# Table of Contents

	<i>Page</i>
<b>Certificate</b>	<b>i</b>
<b>Abstract</b>	<b>iii</b>
<b>Acknowledgements</b>	<b>v</b>
<b>Table of Contents</b>	<b>vii</b>
<b>List of Figures</b>	<b>ix</b>
<b>List of Tables</b>	<b>xxv</b>
<b>List of Symbols</b>	<b>xxvii</b>
<b>1. Introduction</b>	<b>1</b>
1.1 Introduction	1
1.2 Literature Review	2
1.2.1 Structural Damages during Past Earthquakes	2
1.2.2 Characteristics of Near and Far-Fault Ground Motions	8
1.2.2.1 Hanging-Wall Effect	8
1.2.2.2 Directivity Effect	12
1.2.2.3 Fling Step Effect	19
1.2.3 Response of Structures to Near and Far-Fault Ground Motions	21
1.2.3.1 Near-Fault Ground Motions	21
1.2.3.2 Directionality Effects in Near-Fault Ground Motions	27
1.2.3.3 Design Improvements for Structures Subjected to Near-Fault Ground Motions	29
1.2.3.4 Far-Fault Ground Motions	32
1.3 Gap Areas	35
1.5 Objectives of Study	36
1.6 Scope of Study	36
1.7 Organisation of the Thesis	37
<b>2. Characteristics of Near and Far-Fault Ground Motions</b>	<b>39</b>
2.1 Background	39
2.2 Recorded Strong Ground Motions	40
2.3 Observations	44
2.4 Conclusions	45

<b>3. Effect of Near-Fault Ground Motions on Frame Buildings</b>	<b>47</b>
3.1 Background	47
3.2 Ground Motions Considered	47
3.2.1 Horizontal Ground Motions	48
3.2.2 Vertical Ground Motions	50
3.3 Analytical Model of Building	51
3.3.1 5-Storey	55
3.3.2 10-Storey	55
3.4 Nonlinear Time History Analysis	55
3.4.1 Horizontal Shaking	56
3.4.1.1 5-Storey	56
3.4.1.2 10-Storey	65
3.4.2 Vertical Shaking	70
3.5 Observations	74
3.6 Conclusions	76
<b>4. Effect of Near-Fault Ground Motions on Frame Buildings with Structural Walls</b>	<b>79</b>
4.1 Background	79
4.2 Ground Motions Considered	80
4.3 Analytical Model of Building	80
4.4 Nonlinear Time History Analysis	82
4.4.1 Horizontal Shaking	82
4.4.2 Vertical Shaking	90
4.5 Observations	91
4.6 Conclusions	93
<b>5. Summary and Conclusions</b>	<b>95</b>
5.1 Summary	95
5.2 Conclusions	96
5.3 Possible Future Work	97
<b>6. References</b>	<b>99</b>

## List of Figures

## List of Tables

<i>Table</i>	<i>Title</i>	<i>Page</i>
2.1	Number of recording stations in each soil type (Data Source: COSMOS)	36
3.1	Engineering characteristics of ground motions considered in the study in fault normal direction	44
4.1	Improvement in the Maximum Inter-Storey Drift (%) at each storey of 5-story structure subjected to near-fault ground motions with pulse in 4 earthquakes	81

*Blank Page*

## List of Symbols

$f_c$	Characteristic compressive cylinder strength of unconfined concrete
$f_{ck}$	Characteristics compressive cube strength of unconfined concrete
$f_{sc}$	Stress in reinforcement steel in compression
$f_u$	Ultimate strength of reinforcement steel
$f_y$	Yield strength of reinforcement steel
$g$	Acceleration due to gravity
$h_{eff}$	Effective height of SDOF system
$l_b$	Clear span of beams
$l_c$	Clear span of columns
$l_p$	Effective length of plastic hinge
$l_{pc}$	Length of plastic hinge
$A_c$	Gross area of concrete
$A_g$	Gross area of RC section
$A_h$	Seismic coefficient
$A_{sc}$	Area of reinforcement steel in compression
$A_{st}$	Area of reinforcement steel in tension
$D$	Overall depth of beam
$E_c$	Modulus of elasticity of concrete
$E_D$	Energy dissipated by hysteretic damping
$EI$	Flexural rigidity of RC section
$E_s$	Modulus of elasticity of reinforcement steel
$H$	Lateral force
$H_D$	Design lateral force
$H_e$	Elastic maximum lateral force
$H_{max}$	Maximum lateral force
$H_y$	Lateral force at yield
$I_b$	Second moment of area of RC beam section
$I_c$	Second moment of area of RC column section
$I_{eff}$	Effective second moment of area of RC section

$I_g$	Gross second moment of area of RC section
$K_{eff}$	Effective stiffness of SDOF system
$K_i$	Initial lateral stiffness of building
$L$	Span of beam
$M$	Flexural strength
$M_u$	Ultimate flexural strength
$M_y$	Flexural strength at yield
$N_D$	Design life of structure
$N_R$	Return period of earthquake
$P$	Axial force
$PF_1$	Mode participation factor
$P_u$	Axial load capacity of RC section
$R$	Response reduction factor
$R_\mu$	Ductility reduction factor
$s$	Scale factor
$S_a$	Spectral acceleration
$S_a/g$	Design acceleration spectrum value
$S_d$	Spectral displacement
$S_v$	Spectral velocity
$t$	Time instant
$T$	Fundamental natural period of a structure
$T_p$	Pulse period
$V_B$	Base shear
$W$	Seismic weight of building
$Z$	Zone factor
$\gamma_s$	Partial safety factor of reinforcement steel
$\gamma$	Unit weight of material
$\gamma_c$	Partial safety factor of concrete
$\delta_u$	Ultimate drift
$\delta_y$	Yield drift
$\varepsilon_c$	Strain in concrete
$\varepsilon_{c,max}$	Maximum compressive strain in extreme compression fibre of concrete

$\varepsilon_{csc}$	Strain in concrete in compressive at centre of reinforcement steel bars in compression
$\varepsilon_r$	Fracture strain of longitudinal reinforcement steel
$\varepsilon_{sc}$	Strain at centre of reinforcement steel bars in compression
$\varepsilon_{sh}$	Tensile strain at the commencement of strain hardening in reinforcement steel bars
$\varepsilon_{st}$	Strain at centre of extreme layer of reinforcement steel in tension
$\varepsilon_{su}$	Fracture strain of transverse reinforcement steel bars
$\varepsilon_u$	Ultimate strain in longitudinal reinforcement steel bar
$\varepsilon_0$	Strain in unconfined concrete at extreme compression fibre at peak stress level (from Mander Model)
$\varepsilon_{cc}$	Strain in extreme compression fibre of core concrete
$\varepsilon_{cu}$	Ultimate strain in extreme compression fibre of unconfined concrete
$\varepsilon_{co}$	Strain in extreme compression fibre of unconfined concrete at peak stress level
$\varepsilon_{sc}$	Strain in reinforcement steel in compression
$\varepsilon_s$	Strain in reinforcement steel
$\varepsilon_y$	Yield strain in reinforcement steel
$\varepsilon_{ccu}$	Ultimate strain in extreme compression fibre of confined concrete
$\eta$	Damping correction factor
$\varphi$	Curvature of a RC section
$\Phi$	Wavelet function
$\mu$	Ductility ratio
$\theta_p$	Plastic rotation of a frame member
$\theta_y$	Yield rotation of a frame member
$\theta_u$	Ultimate rotation of a frame member
$\xi$	Percentage of critical damping
$\xi_{eff}$	Effective damping
$\omega$	Fundamental natural frequency of the SDOF
$\Delta$	Lateral deformation
$\Delta_{roof}$	Lateral deformation at roof level of the building
$\Delta_u$	Ultimate lateral deformation of building
$\Delta_y$	Lateral deformation at yield of load-deformation curve of building

*Blank Page*

# 1 Introduction & Literature Review

## 1.1 INTRODUCTION

Earthquakes are sporadic but calamitous. There are two significant earthquake repercussions, namely life loss, and property loss. Although avoiding property loss is not possible, any small amount of life loss is a serious concern. Most of the first-world countries achieved zero life loss; however, they work to control the property loss. Since the practice of earthquake resistant design is relatively new in India, life loss is still alarming (Murty et al., 2012; Jain et al., 1993). From the experience of past earthquakes, the primary cause of life loss is the collapse of the buildings (Ramancharla and Murty, 2014).

Although the collapse of buildings is not acceptable, altogether avoiding the damage leads to an uneconomic and ill functional structure. Hence, the building must be engineered so that the secondary structural elements remain intact, and the critical elements undergo controlled damage. The building damage broadly depends on two kinds of parameters: structural parameters and ground motion characteristics. Therefore, the first step is to understand the building behavior when subjected to ground motion expected at a site during an earthquake event.

Three broad categories of parameters influence ground motion characteristics, namely source parameters, path parameters, and site parameters (Heaton and Hartzell, 1988; Oglesby et al., 2000; Udias et al., 2014). The parameters that are related to the rupture process of the earthquake are called source parameters. Some of the source parameters that influence the ground motion characteristics are directivity that is observed in the near-fault region (Archuleta, 1984; Hartzell and Heaton, 1983; Hartzell and Helmberger, 1982; Heaton and Helmberger, 1979; Olson and Apsel, 1982), the presence of asperities on the rupture plane that indicates considerably higher slip compared to the other parts of the rupture plane and causes high-frequency seismic waves, presence of barriers that do not rupture in an earthquake

and observe abrupt high-frequency stopping waves (Papageorgiou and Aki, 1983a, 1983b), radiation pattern that is pronounced at periods greater than 1 sec (Cormier and Spudich, 1984; Liu and Helmberger, 1985), presence of near-fault waves that decay rapidly with distance from the fault plane (Brune, 1970; Plafker, 1965; Thatcher, 1975). Path parameters are usually represented in the form of an attenuation law for a particular region. The usual form of the law involves distance from the source, magnitude, and focal depth (Boore and Atkinson, 1987; Joyner and Boore, 1982). Site parameters involve amplification of ground motion due to the presence of soft soils in the shallow depths of the site (Ishihara et al., 1981; Tsai, 1969), liquefaction in saturated cohesionless soils, that is indicated by an abrupt transition from a short period to long-period motion (Singh et al., 1988; Zeevaert, 1964), presence of basins that traps both the body and surface waves (Hanks, 1975; Liu and Heaton, 1984; Trifunac, 1976; Vidale, 1987), presence of waveguides with a low velocity that amplifies the ground motion.

But the basic understanding of the ground motions indicates that their characteristics are primarily different for recording stations located in the near-field and the far-Fault regions. As a result, the damage caused by these two types of ground motions on the structures is most likely to be different. Although the damage associated with different ground motions is not comparable due to many uncertainties, there is a considerable possibility of observing a damage pattern anticipated in the structures subjected to near-Fault and far-Fault ground motions.

## **1.2 LITERATURE REVIEW**

### ***1.2.1 Structural Damages During Past Earthquakes***

An earthquake ( $M_w$  7.3) that occurred on 28 June 1992 near Landers, California, observed many building failures. Although the earthquake revealed the lack of proper earthquake-resistant design principles in the existing building stock (Anderson and Bertero, 1997), it also helped to analyze the variation of ground motion characteristics for the fault plane. The ground motion recorded at Lucerne Valley station, which is at

2 km from the fault trace, shows directivity on the ground motions. Figure 1.1 shows the time history of the free-field ground motion recorded in East-West (EW) and North-South (NS) directions at Lucerne Valley station during the event. The maximum value of acceleration recorded in both directions is nearly equal to 0.8g with a significant vibration duration. Figure 1.2 shows the ground motion's elastic response spectra that reveal that the EW component is higher than NS for periods of approximately more than 1 sec (Anderson and Bertero, 1997).

In addition to the directivity, another critical issue in the near-fault ground motions is the large ground displacement that are imposed at base of the structure, usually known as static displacement. Lifeline structures that are installed in the ground are the most vulnerable to such ground motions. As a result, many hundreds of meters of pipelines present in the epicentral region are severely damaged; maximum horizontal displacement of 9.5 m is observed in and around Landers; 18<sup>0</sup> rotation of horizontal propane gas tanks at Landers Elementary School is observed during the 1992 Landers earthquake (Anderson and Bertero, 1997).

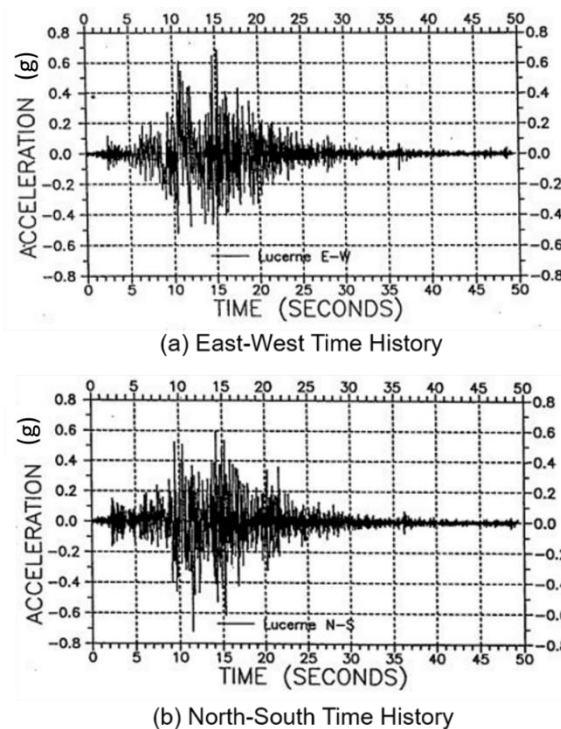


Figure 1.1 Ground motion time histories of recordings in East-West and North-South directions during 1992 Landers earthquake (Anderson and Bertero, 1997)

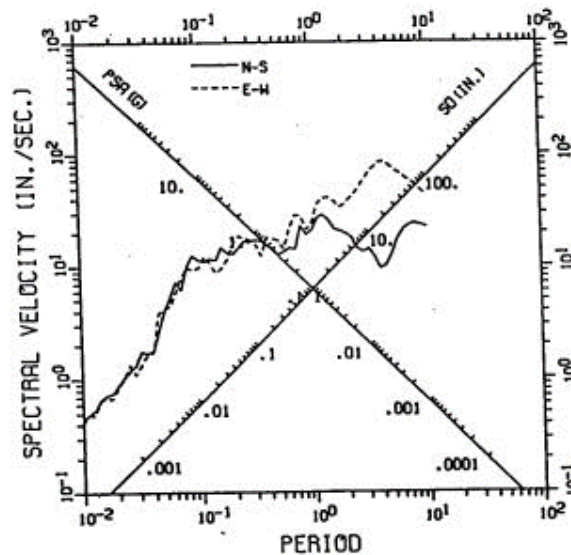


Figure 1.2 Elastic response spectra of velocity recorded at Lucerne Valley during 1992 Landers Earthquake (Anderson and Bertero, 1997)

Later in 1994, the Northridge earthquake that has occurred on 17 January in San Fernando Valley is one of the prominent events not because of the magnitude (Mw 6.8) but since it has tested the seismic performance of many modern buildings in the Los Angeles metropolitan area. On one hand, it revealed the structures that ignored earthquake-resistant features, and on the other, it highlighted the shortcomings of design principles. The structural damages occurred all around the epicenter at different distances (Todd et al., 1994). Figure 1.3 shows the structural damage during the earthquake.

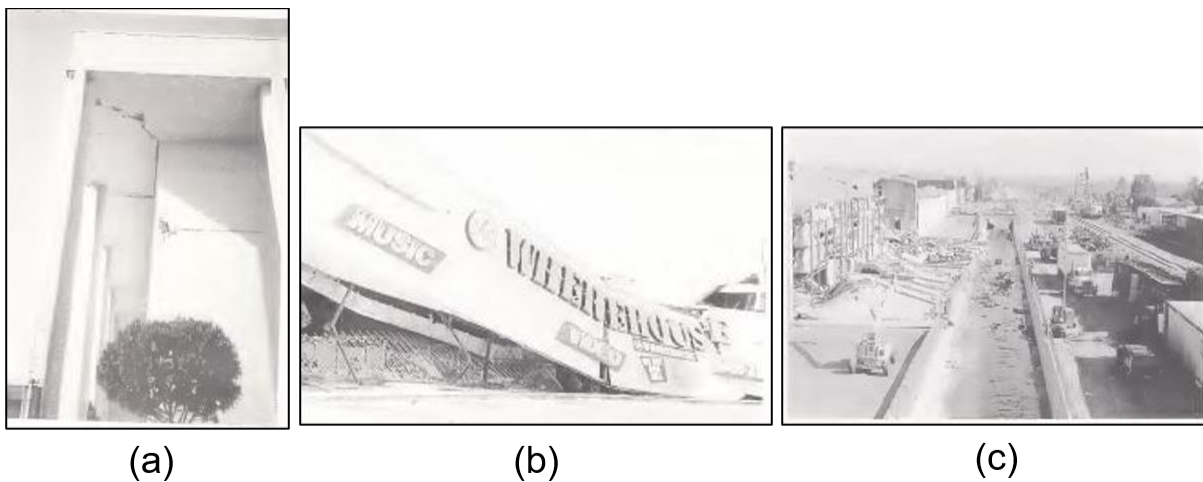
Since the damage is spread all around the area, there is a significant possibility of the varied intensity of ground shaking at different locations within few meters to few kilometres. A classic example of such a scenario is the damage that occurred at Northridge Fashion Mall. All the stores in the mall are moderately damaged with cracks in the façade, soffit, and cornice panels; however, severe damage occurred in the area south of the mall with concrete tilt-up of Levitz furniture store (Todd et al., 1994). Figure 1.4 shows the difference between damage of buildings at Northridge Fashion Centre and buildings around it.



(a) Locations of buildings severely damaged

(b) Severity of buildings damaged by assigned red (solid squares) and yellow (open squares) tags

Figure 1.3 Structural damages during 1994 Northridge earthquake (Todd et al., 1994)



(a)

(b)

(c)

Figure 1.4 (a) Horizontal cracks in the facade, soffit, and corners at Northridge Fashion Centre (b) Collapse of single-storey Warehouse south of Northridge Fashion Centre (c) Concrete tilt-up of a south wall of Levitz furniture store south of Northridge Fashion Centre (Todd et al., 1994)

A remarkable failure of a 5-storied structural system occurred at the Kaiser Permanente Office building on Balboa Avenue in Granada Hills. Figure 1.5 shows the failure pattern of the building. The second floor is crushed, and the non-structural end

walls completely collapse with other stories intact (Todd et al., 1994). Although the exposure of bare frame suggests that the structure has a strong beam - weak column system, the failure of joints at second storey requires further investigation in the direction of the type of ground motion applied on the structure. Similar damage was observed at the six-storey Barrington building on Olympic Boulevard (Todd et al., 1994).

Since the damages discussed are related to (RC) buildings, the lack of proper execution may be an apparent reason; however, this earthquake also witnessed moderate to severe failure of steel-framed buildings. Although the fundamental principles of design are confirmed (Tremblay et al., 1995), many structural damages need a detailed understanding of the causes for such failures.

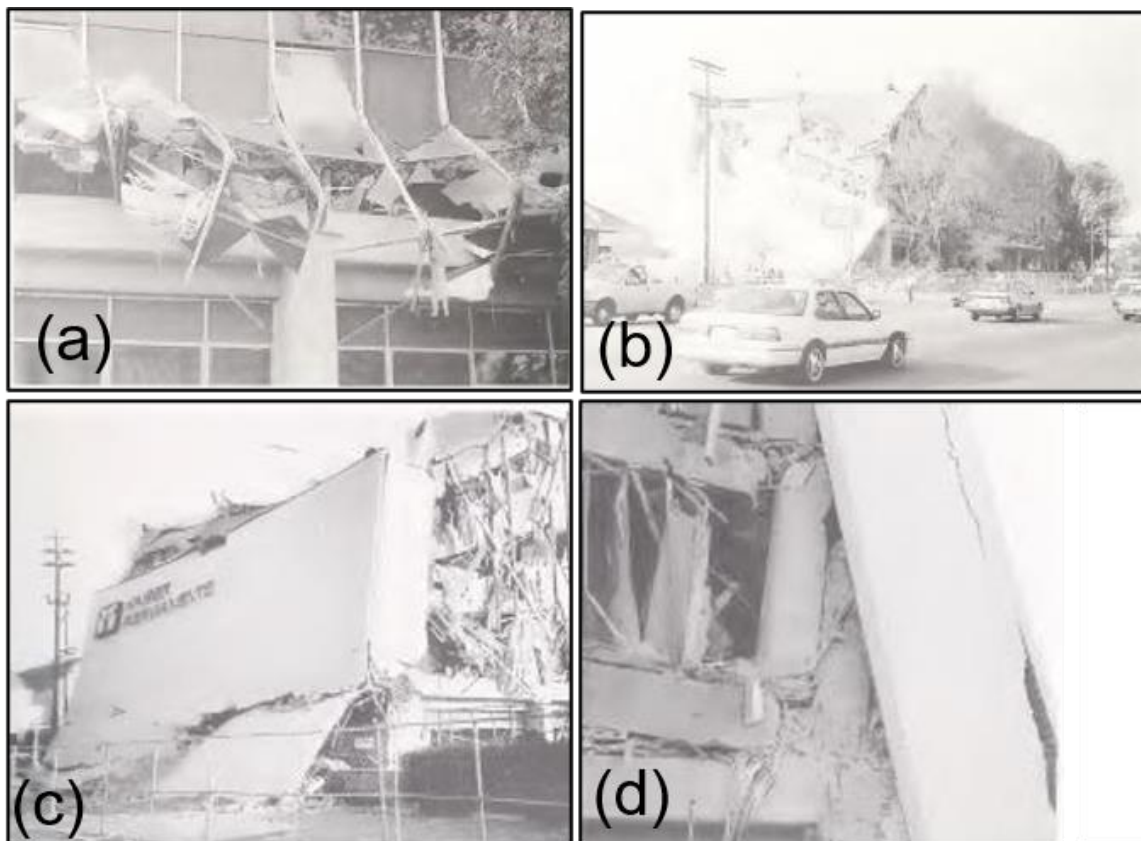


Figure 1.5 Damage to Kaiser Office Permanente building (a) Collapse of the second storey and fully intact first floor (b) Collapse of end wall on the south (c) Collapse of end wall on the north (d) Exposed concrete frame revealing deep beams suggests strong beam-weak column configuration (Todd et al., 1994)

One such anomaly surfaced in the damage state of two buildings, both located in the epicentral area. The First Interstate Bank building with a two-storey steel frame is located 2 km north of the epicenter. The building is built in 1970 and retrofitted in 1991 contains X-bracings using connecting plates on the façade wall. During the earthquake, moderate to severe uplift of the columns was observed at the base of the columns displacing the tiles and stucco covering the column. As a result, the connecting plates at the uplifted columns showed severe buckling and bending (Figure 1.6) (Tremblay et al., 1995).

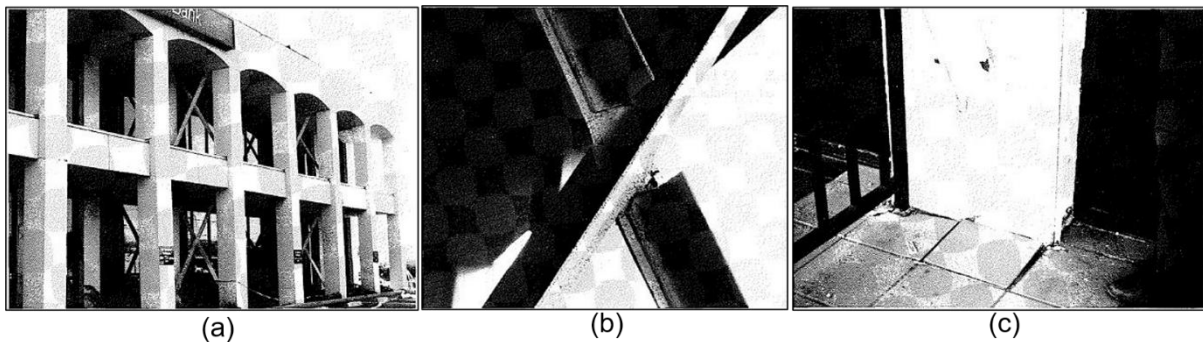


Figure 1.6 (a) View showing steel X-bracings in the facade of First Interstate Bank building (b) Buckling of connecting plate at brace intersection (c) Uplift of the column at the base of the X-bracing (Tremblay et al., 1995)

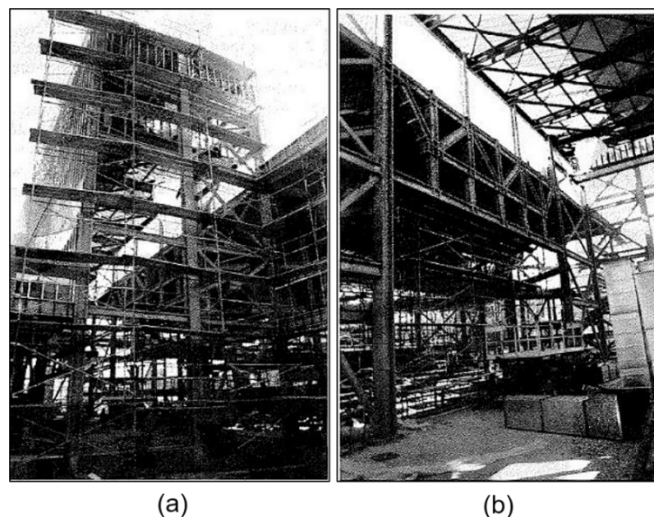


Figure 1.7 (a) Exterior view (b) Interior view of Student Union building with bracing system (Tremblay et al., 1995)

On the other hand, an under-construction 4-storey building (Student Union building) in California State University campus located 3 km from the epicenter has not shown any failure (Tremblay et al., 1995). Figure 1.7 shows the exterior and interior view of the Student Union building at California State University without any damage.

## ***1.2.2 Characteristics of Near and Far-Fault Ground Motions***

### **1.2.2.1 Hanging-Wall Effect**

The variations in the ground motion characteristics are fundamentally due to the variations in faulting mechanisms. The broad categories of faulting mechanisms are reverse fault, normal fault, and strike-slip faulting. Generally, reverse and normal faulting mechanisms are generated on inclined faults (non-vertical), and strike-slip mechanisms are generated on almost vertical faults. Hence, in the reverse and normal mechanisms, the earth's surface acts as a stress boundary for the seismic waves traveling from the inclined fault plane.

The reflections of the seismic waves at the earth's surface modify the normal stress on the fault plane that induces the coupling of shear stress and normal stress on the fault. As a result, the ground motion on the surface in the near-Fault region is significantly affected. Simulating the thrust and normal faulting mechanisms (with dip angles  $30^\circ$ ,  $45^\circ$ , and  $60^\circ$ ) reveals the particle velocity difference on the earth's surface (Oglesby et al., 2000). Figure 1.8 shows the simulation of stresses along the dip of the faults considered during initiated earthquake rupture.

Due to the initiated nucleation at  $t = 0$  sec, with the generated stress at  $t = 0.4$  sec, a typical shear crack stress pattern (Andrews, 1976a, 1976b; Ida, 1972) is formed at  $t = 2.5$  sec. As the crack propagates, the normal stress on the fault starts reducing ahead of the crack tip and increases behind the crack tip.

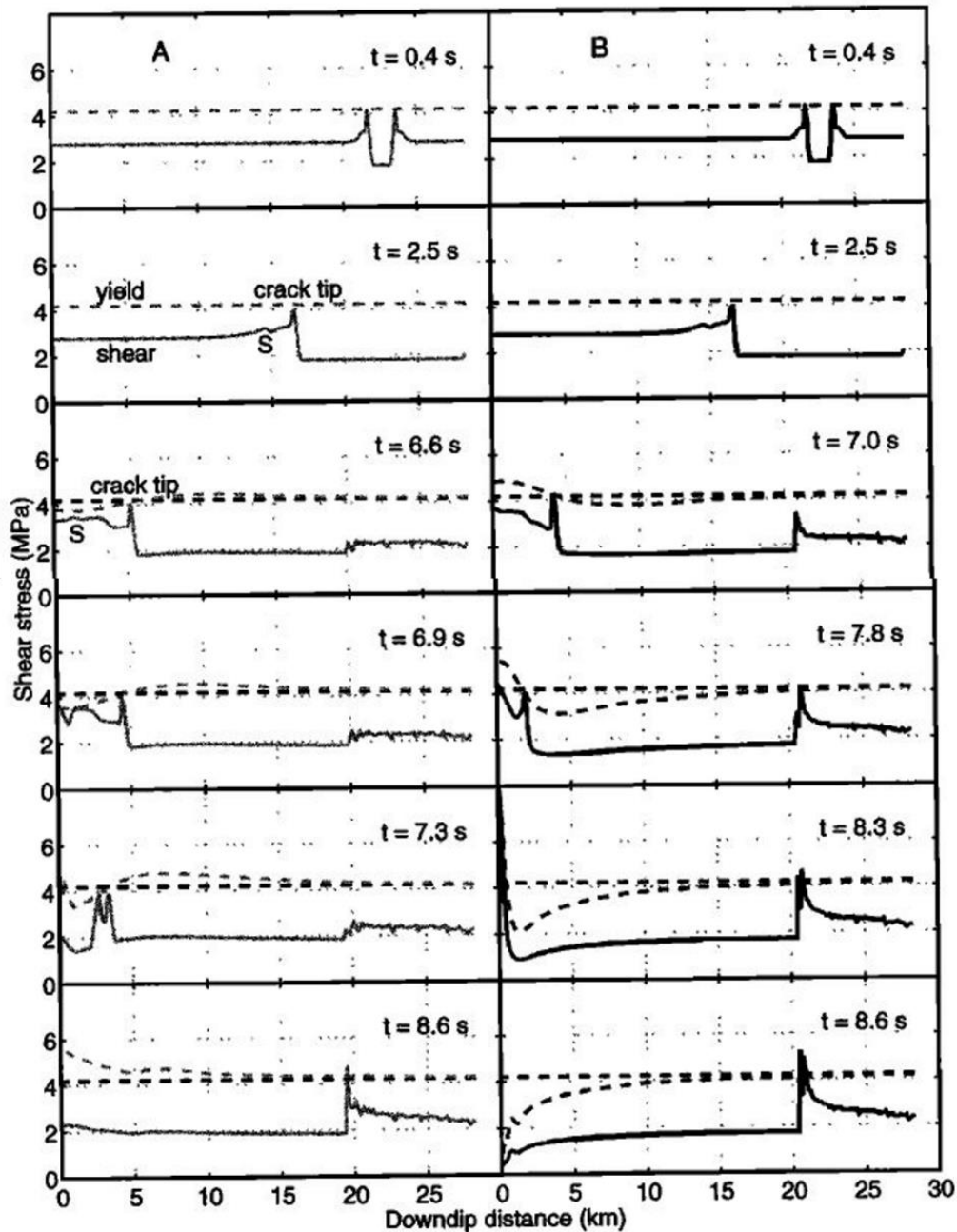


Figure 1.8 Snapshots of stresses along  $45^\circ$  dipping (a) normal and (b) thrust faults during earthquake rupture. The solid curves denote shear stress, and the dashed curves denotes yield stress. (Oglesby et al., 2000)

A normal fault achieves this phase at 6.6 sec and by thrust fault at 7.0 sec. Further decrease in normal stress resulted in the initiation of secondary crack on the fault plane at 6.9 sec for normal fault and 7.8 sec for thrust fault. The crack reaches the surface in a normal fault, and the fault plane is completely ruptured by  $t = 8.3$  sec. However, after the crack reaches the surface in thrust faults, the shear stress drops

from greatly increased yield stress to a greatly decreased sliding frictional level at time  $t = 8.6$  sec. This reduced stress amplifies the secondary slip, resulting in a strong breakout phase (Oglesby et al., 2000). This difference in normal and thrust faults increases with an increase in dip angle. Therefore, it is obvious to observe higher ground motion amplitudes in the near-field region when generated from a thrust fault than a normal fault or strike-slip fault.

Another way to evaluate the hanging wall effect is through an empirical approach which is possible if many recorded ground motions are available. Since 1999 Chi-Chi, Taiwan earthquake is one of those earthquakes that has been recorded at a maximum number of stations; the event-specific attenuation characteristics are used to estimate the empirical relationships for Peak Ground Acceleration (PGA), Peak Ground Velocity (PGV), and Spectral Intensity (SI) (Shabestari and Yamazaki, 2003). The empirical form of the equation includes the closest distance to the seismogenic part of the fault plane and a constant near-source saturation effect that is obtained from the nonlinear least square analysis (Shabestari and Yamazaki, 2003).

Figure 1.9 shows the predicted values of PGA, PGV, SI, and IJMA to the closest distance to the fault. The hanging wall stations show significantly large ground motion variations compared to the footwall stations at the same closest distance. Further, the residuals of the empirical equations are used to evaluate the hanging wall effect. A piecewise continuous functional form is introduced for PGA residuals' distance dependence on the hanging wall stations (1.1). The proposed empirical model for PGA on the hanging wall showed ~50% higher values than the mean attenuation for all the sites over the limited range of seismogenic distance from 5 to 25 km. But, on the footwall, it does not show a significant difference from the mean attenuation relation in the 1999 Chi-Chi, Taiwan, earthquake (Shabestari and Yamazaki, 2003) given by

$$HW_{effect} = \begin{cases} \frac{c_1}{2} \left[ \cos \left( \frac{\pi(r - x_1)}{x_2 - x_1} + \pi \right) + 1 \right] & x_1 < r < x_2 \\ Prd(r)_{Hangingwall} - Prd(r)_{All} & x_2 \leq r \leq x_3, \\ \frac{c_2}{2} \left[ \cos \left( \frac{\pi(r - x_3)}{x_4 - x_3} \right) + 1 \right] & x_3 < r < x_4 \end{cases} \quad (1.1)$$

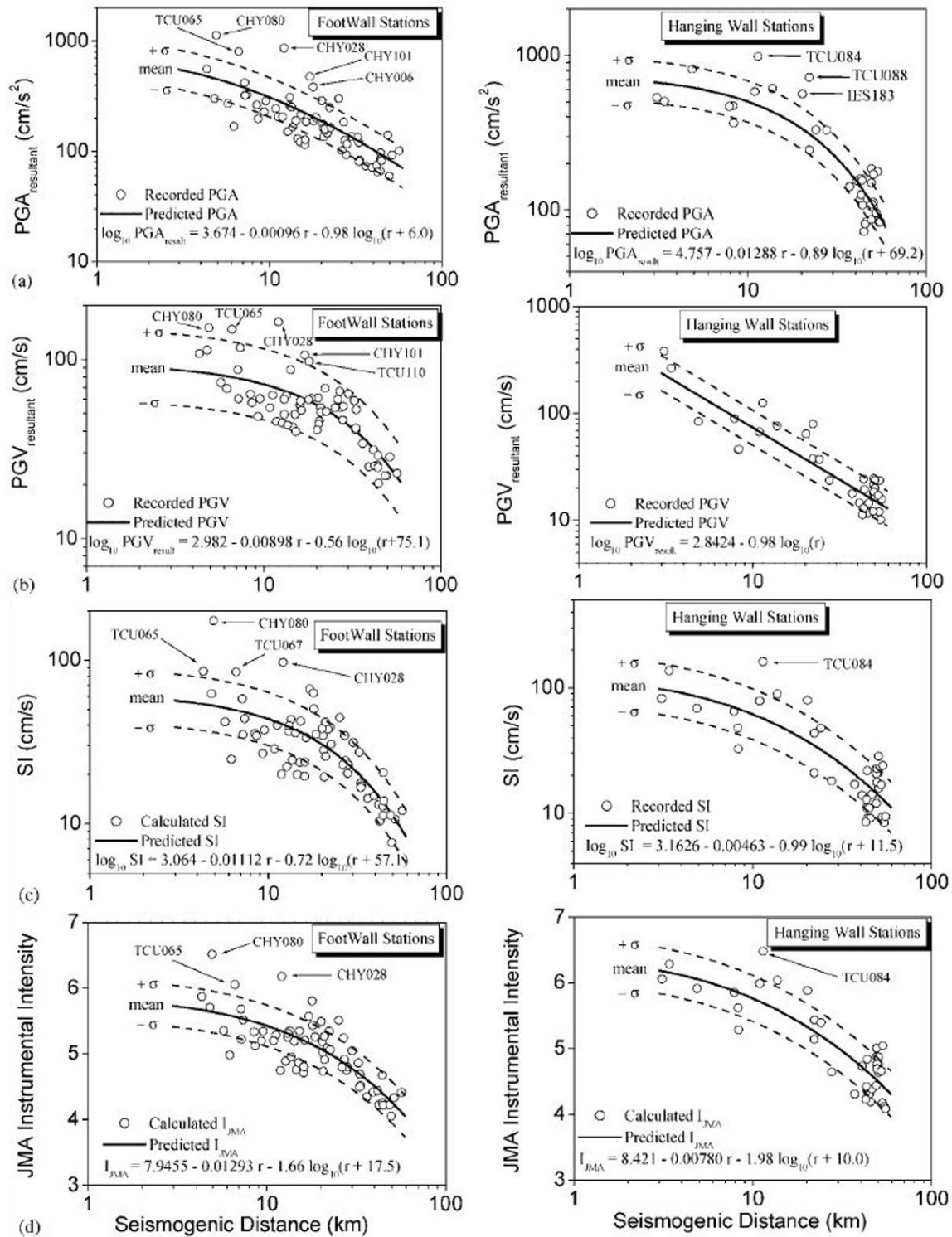


Figure 1.9 Predicted values of: (a) PGA, (b) PGV, (c) SI and (d)  $I_{JMA}$ , by the attenuation relationship for the footwall and hanging wall sites in 1999 Chi-Chi, Taiwan earthquake (Shabestari and Yamazaki, 2003)

### 1.2.2.2 Directivity Effect

Directivity is the phenomenon of time compression effect that is caused due to the coincidence of shear waves and the rupture propagation towards a particular location—the accumulation of seismic waves in one direction results in a sudden increase in the amplitude of ground motion. The seismic wave indicating large-amplitude resembles an impulse that occurs for a short time interval and is usually referred to as a pulse.

When the shear wave coincides with the rupture propagation, the pulse in the ground motion is generated in the fault normal component since the maximum value of the radiation pattern of the SH waves is orientated along the normal direction to the fault. Since, the rupture propagation and the SH wave radiation is aligned along the strike of the fault in a strike-slip earthquake, directivity effect can be readily observed in strike-slip faults than the dip-slip fault (Somerville and Graves, 1993). On the other hand, the radiation pattern of the SV waves observes minimum value in the direction of rupture. Figure 1.10 shows the radiation pattern of SH and SV waves that are emitted from a vertical strike-slip fault.

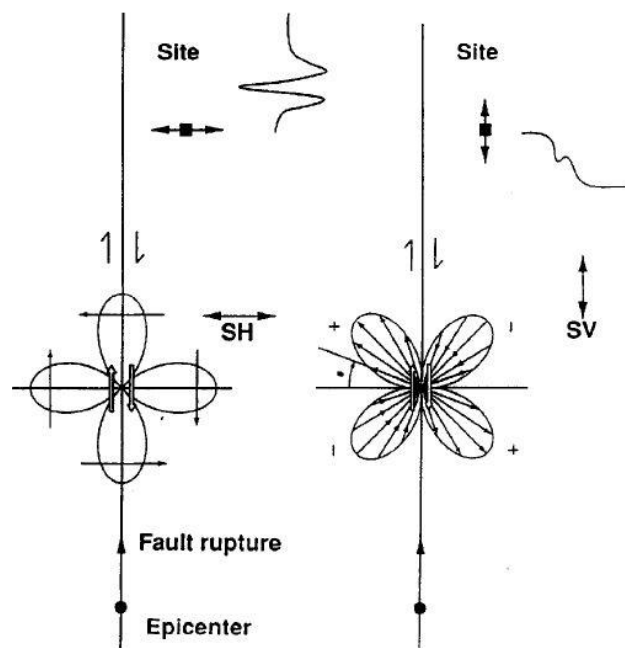


Figure 1.10 Pictorial representation of directivity effects for a vertical strike slip fault (Somerville and Graves, 1993)

This effect is more pronounced in strike-slip earthquakes than thrust earthquakes since the conditions are readily met in the former. For strike-slip earthquakes, the shear wave direction and rupture direction coincide and generate a directivity effect at locations parallel to the fault strike. Whereas for dip-slip earthquakes, the coincidence of directions of shear wave and rupture can generate directivity only at stations just about the hypocentre (Somerville and Graves, 1993). This ground motion is recorded at Pacoima Dam Station during the 1971 San Fernando Valley earthquake (Figure 1.11).

To carry out sufficient mitigation measures, it is required to know the extent of ground motions affected by directivity. A detailed study with varying fault dip and rake angles measures the ground velocities and displacements, thereby calculating the area subjected to large-amplitude long-period ground motions through finite element analysis (Aagaard et al., 2004). The simulations are performed for five pairs of fault dip and rake angles for each of the two hypocentres; one relatively shallower than the other.

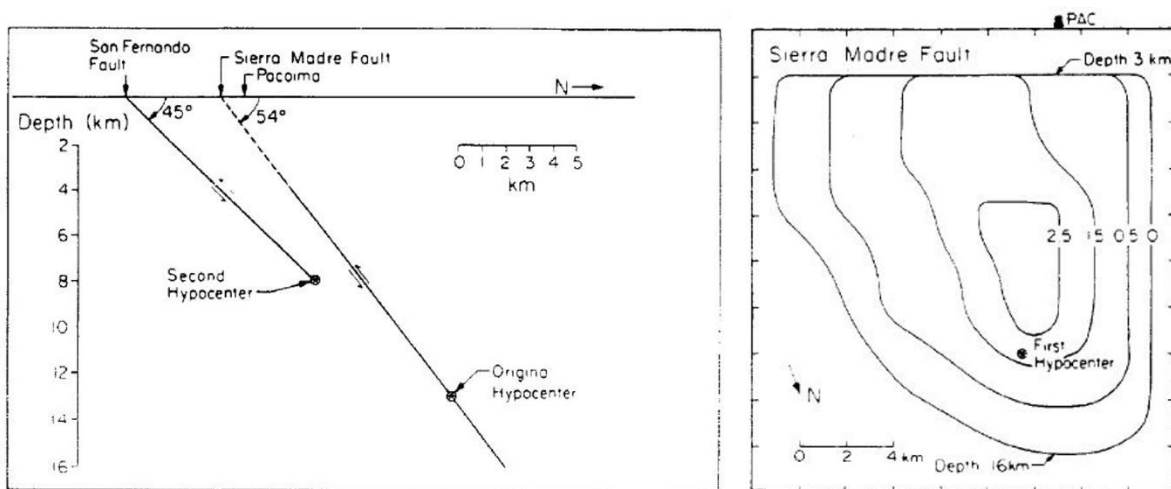


Figure 1.11 Relation of Pacoima Dam recording station to the rupture of the 1971 San Fernando Earthquake (a) Vertical section normal to the fault (b) Location of Pacoima Dam Station directly above the hypocentre and large inferred slip on the rupture surface between the hypocentre and Pacoima (Somerville and Graves, 1993)

The difference between maximum amplitude and maximum peak-to-peak amplitude of two consecutive peaks is studied and is found to be distinctly different for ground motions with a double-sided pulse that is usually observed in those that are affected by directivity. Therefore, maximum displacement and maximum peak-to-peak velocity are considered parameters to measure ground motion intensity. Figure 1.12 shows the distribution of maximum displacements and maximum peak-to-peak velocity on the ground surface around the fault trace for different scenarios considered. In the case of shallow hypocentre, as the dip increases from  $90^{\circ}$  to  $60^{\circ}$ , the maximum displacements on the hanging wall increase. The maximum peak-to-peak velocity is maximum towards the north, indicating directivity (Aagaard et al., 2004).

Further, when the dip angle reaches  $30^{\circ}$ , the relatively more minor amplitude of maximum displacement and peak-to-peak velocity indicates the presence of directivity on the ground motions since the rupture direction is nearly perpendicular to the slip direction. However, the maximum value of peak-to-peak velocity indicates the presence of static displacement at sites very near to the fault plane. In the case of deep hypocentre, the effect of directivity in pure strike-slip fault is decreased by one-third compared to shallow hypocentre. However, for the thrust fault, the amplitudes are almost double at the sites in the near-fault region (Aagaard et al., 2004).

Figure 1.13 shows the area on the ground surface where the maximum displacement and maximum peak-to-peak velocity exceed a given value for different locations of hypocentres. The pure thrust fault results in the smallest area subjected to a given level of peak-to-peak velocity for shallow hypocentre. However, there is a lack of consistent trend when the hypocentre is deep, especially in maximum peak-to-peak velocity, since the maximum displacement almost follows the slip distribution (Aagaard et al., 2004).

For strike-slip faulting, the shaking is most severe for unilateral rupture, while for thrust faulting, the shaking is most severe for up-dip rupture from a deep hypocentre. Also, the directivity is maximum in the regions where the rupture propagates parallel to the slip. Figure 1.14 shows the summary of the effect of fault geometry and slip rake angles on rupture directivity (Aagaard et al., 2004).

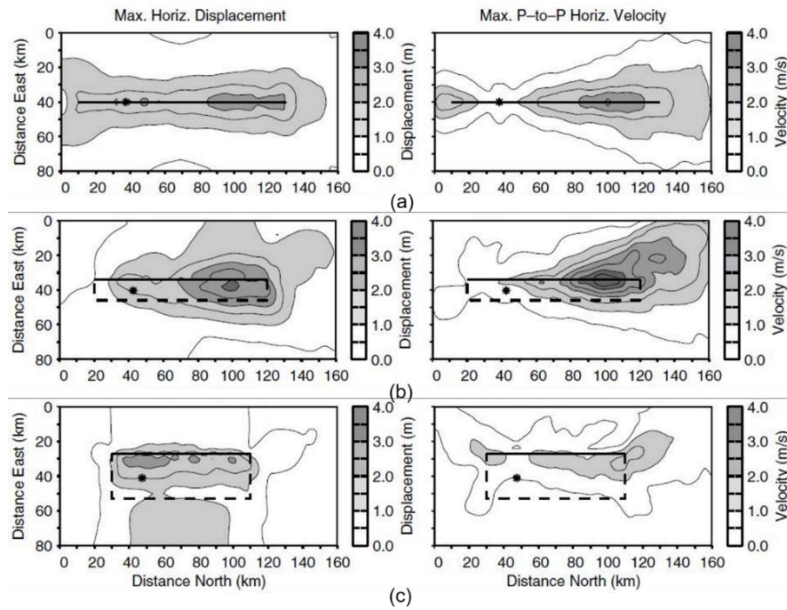


Figure 1.12 Maximum horizontal displacements and maximum peak-to-peak horizontal velocities on the ground surface for scenario (a) Dip90Rk0HySh (Pure Strike Slip fault with dip: 90°, Rake: 0°, Shallow Hypocentre) (b) Dip60Rk45HySh (dip: 60°, Rake: 45°, Shallow Hypocentre) (c) Dip30Rk90HySh (Pure Thrust fault with dip: 30°, Rake: 90°, Shallow Hypocentre) (Aagaard et al., 2004)

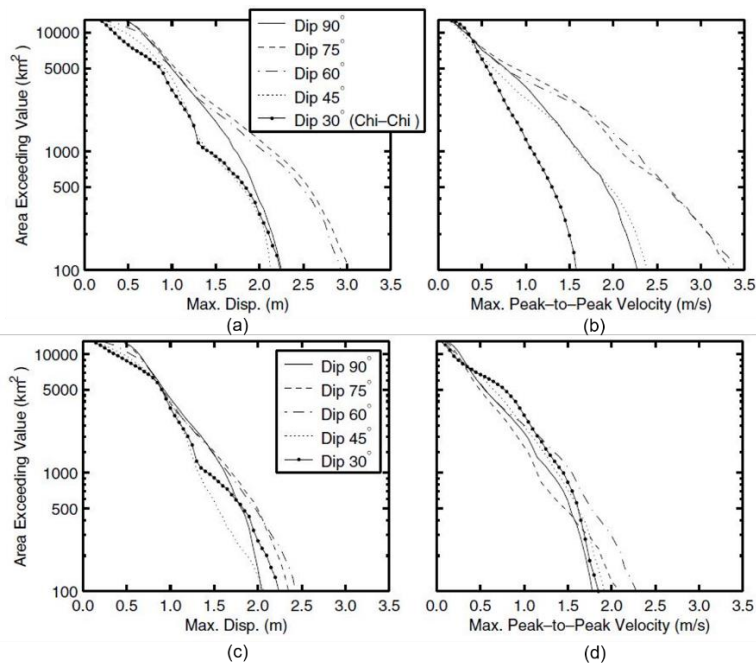


Figure 1.13 (a) Area on the ground surface where the (a) maximum horizontal displacements exceed a given value for shallow hypocentre (b) maximum peak-to-peak horizontal velocities exceed a given value for shallow hypocentre (c) maximum horizontal displacements exceed a given value for deep hypocentre (d) maximum peak-to-peak horizontal velocities exceed a given value for deep hypocentre (Aagaard et al., 2004)

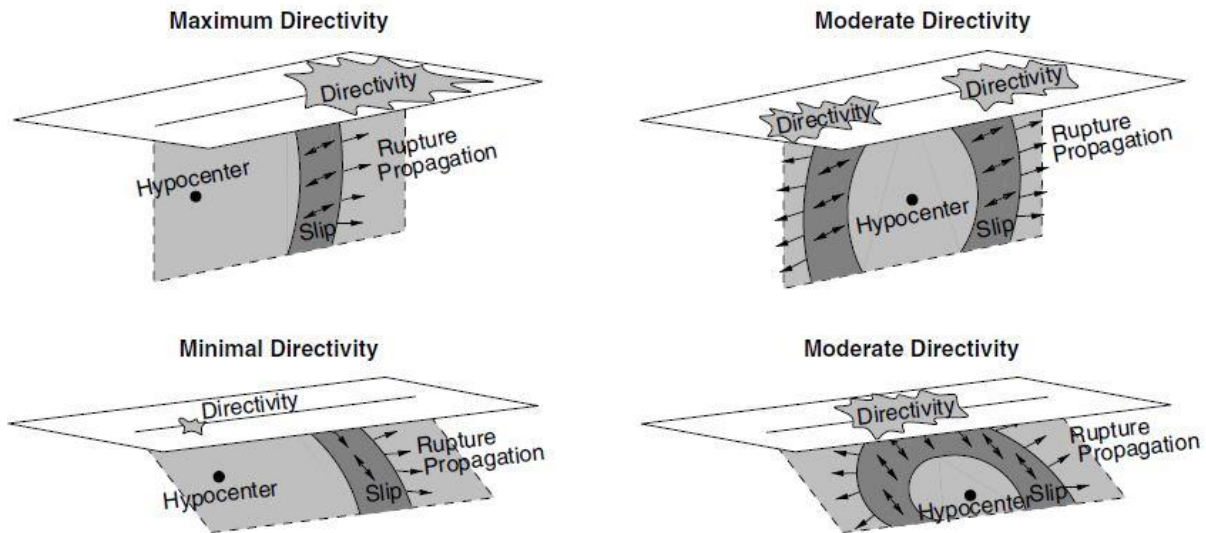


Figure 1.14 Effects of fault geometry and slip rake angle on amount and location of rupture directivity by the size and location of the splotch on the ground surface. The top row illustrates two cases for a vertical fault with oblique motion, and the bottom row illustrates two cases for a shallow-dipping fault with thrust motion. The left column corresponds to shallow hypocentre, and the right column corresponds to deep hypocentre (Aagaard et al., 2004)

Since the rupture directivity is the most predominant near-fault effect, it is essential to quantify the characteristics of the ground motion with such long-period velocity pulses. A wavelet-based processing technique identifies and characterizes the ground motions with such pulses (Baker, 2007). The algorithm identifies the pulse-like ground motion as a record with a short duration pulse that occurs early in the velocity time history and has the largest amplitude. Since for both the strike-slip and dip-slip faults, forward directivity typically occurs in the FN direction, the FN components are only assumed to have pulses. However, it is reasonable to identify the pulse characteristics and not the causal mechanism since the purpose of the study is to understand the damage that is likely to be caused to the building when it is subjected to such ground motions (Baker, 2007).

To identify the existence of the pulse in the ground motion, the algorithm has to distinguish between the pulse and non-pulse components of the ground motion. Since this distinction is not binary, the records are initially ranked depending on the pulse parameters. Then the existence of pulse is identified based on a threshold value of the considered parameters. To make such a ranking, wavelet analysis is used. In

this wavelet analysis, the prototype function is referred to as a mother wavelet, and this function is scaled and translated in time to form a set of “basis” functions (Baker, 2007). The wavelet basis function at time  $t$  is defined mathematically as:

$$\Phi_{s,t}(t) = \frac{1}{\sqrt{s}} \Phi\left(\frac{t-l}{s}\right), \quad (1.2)$$

where  $\Phi(\cdot)$  is the mother wavelet function,  $s$  is the scale parameter that dilates the wavelet, and  $l$  the location parameter that translates the wavelet in time. The Daubechies wavelet of order four is used as the mother wavelet.

To identify the existence of pulse, first, the coefficient of the considered mother wavelet is determined as the most significant value by convoluting the wavelet with the ground motion. The coefficient obtained indicates the strength of the signal resembling the wavelet. Therefore, it represents the energy of the wavelet present in the ground motion. This procedure results in obtaining the period and location of the wavelet in the ground motion (Baker, 2007). Any signal  $f(t)$  can be represented as a liner combination of “basis” functions, and the coefficients for that linear combination are determined by the following convolution integral (1.3):

$$C_{s,l} = \int_{-\infty}^{\infty} f(t)\Phi_{s,l}(t) = \int_{-\infty}^{\infty} f(t) \frac{1}{\sqrt{s}} \Phi\left(\frac{t-l}{s}\right) dt, \quad (1.3)$$

Then, the wavelet is subtracted from the original ground motion, and the residual ground motion is used to obtain the next coefficient. To obtain the next coefficient, the wavelet located a plus or minus one half of the width of the original wavelet is considered. To obtain detailed characteristics of the pulse, ten coefficients are calculated in a similar procedure. Finally, the largest of these coefficients is the velocity pulse that is specific for the near-fault ground motions. This procedure calculates the coefficient for the wavelet irrespective of the type of ground motion. Hence, for non-pulse-like ground motions, the extracted pulse is typically a minor feature resulting in the same residual ground motion as the original ground motion (Baker, 2007).

To establish a threshold value of the pulse, a parameter defined as “pulse indicator” is developed using linear discriminant analysis on a large dataset of ground

motions. The distinction between the pulse-like and non-pulse-like ground motion is defined in terms of two parameters, namely “PGV ratio” and “energy ratio.” The ratio of PGV of residual record to that of the original record is referred to as PGV ratio. The ratio of the energy of the residual record to that of the original record is referred to as the energy ratio. Regression analysis is used to establish the following predictive equation (1.4). The pulse indicator has values between 0 to 1, with higher values indicting the pulse and lower values indicating the non-pulse-like ground motions. To qualify a ground motion to be pulse like, a threshold value of 0.85 is used as the pulse indicator (Baker, 2007) given by:

$$PulseIndicator = \frac{1}{1 + e^{-23.3+14.6(PGVratio)+20.5(energyratio)}} \quad (1.4)$$

In general, the near-fault effects are represented by velocity pulse that is observed early in the ground motion. Therefore, to ensure the pulses are extracted from the ground motion, the late-arriving pulse is identified by computing the original record's cumulative square velocity (CSV) and the extracted pulse. To ensure the pulse extracted is due to near-fault effects, the time at which the CSV reaches 20% of the maximum value in the original ground motion is more significant than when the CSV reaches 10% of the maximum value in the extracted pulse. In other words, the arrival of the extracted pulse is ensured to be before most of the ground motion (Baker, 2007).

Another aspect of identifying the velocity pulses due to near-fault effects is that these pulses are observable also in low-intensity ground motions since the velocity time history is very simple. In low-intensity ground motions, a sudden peak value of velocity is also visualized as impulsive relative to the other parts of the ground motion. However, such ground motions cannot be categorized as affected by near-fault effects. Therefore, a threshold value of 30 cm/sec is used to qualify a ground motion to be pulse-like affected by the near-fault effects (Baker, 2007).

### 1.2.2.3 Fling-Step Effect

Another most important phenomenon observed in the ground motions recorded in the near-fault region is the effect of fling-step, also called static displacement. The ground motions with fling-step indicate static, permanent

displacement at the end of the ground displacement time history, which is visible as a single-sided pulse in the velocity time history of the ground. This is observed in the direction parallel to the strike for strike-slip earthquakes and parallel to the dip for the dip-slip earthquakes. Hence, for dip-slip earthquakes, both fling-step and forward directivity motions occur in the fault normal direction. The ground motion can be assumed to be two parts; pulse component and non-pulse component. The velocity waveform of these pulses is modeled by a mathematical function characterized by three parameters related to amplitude, duration, and location of pulse and are validated through a numerical study (Yadav and Gupta, 2017).

A ground motion data set of 20 ground motions are considered, and the fling pulses are extracted using the five-point moving average method. It is observed that the shape of the velocity pulse closely resembles the normal distribution function for the velocity of pulse (Yadav and Gupta, 2017) that can be defined as:

$$v_p(t) = \frac{a}{\sigma} e^{-\frac{(t-t_{loc})^2}{2\sigma^2}}, \quad (1.5)$$

where  $t_{loc}$  represents the location of the velocity pulse,  $\sigma$  the duration  $T_p$ , and  $a$  represents the amplitude of velocity pulse. Figure 1.15 shows the time histories of acceleration, velocity, and displacement due to the proposed form of fling-step pulse (Yadav and Gupta, 2017).

But observing the fling step in processed ground motion is seldom possible since processing involves baseline correction and filtering of specific frequencies to correct the error caused due to noise and baseline offsets from tilting and transducer response. Filtering consists of applying a low and high-pass filter in the frequency domain and typically removes the static offset from records (Boore and Bommer, 2005).

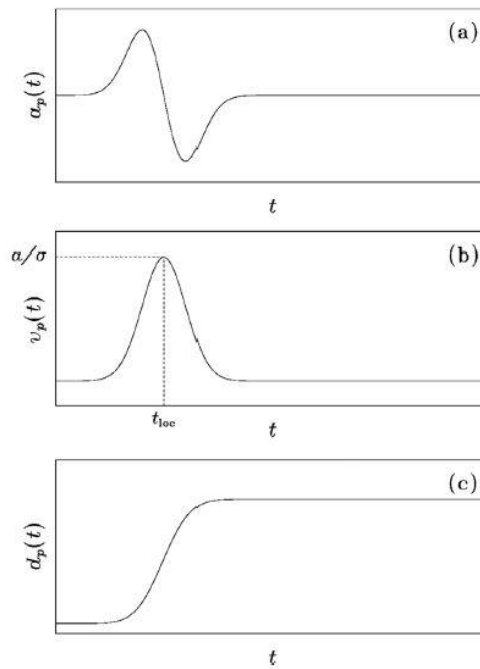


Figure 1.15 Time-histories of (a) acceleration (b) velocity and (c) displacement for proposed fling step pulse (Yadav and Gupta, 2017)

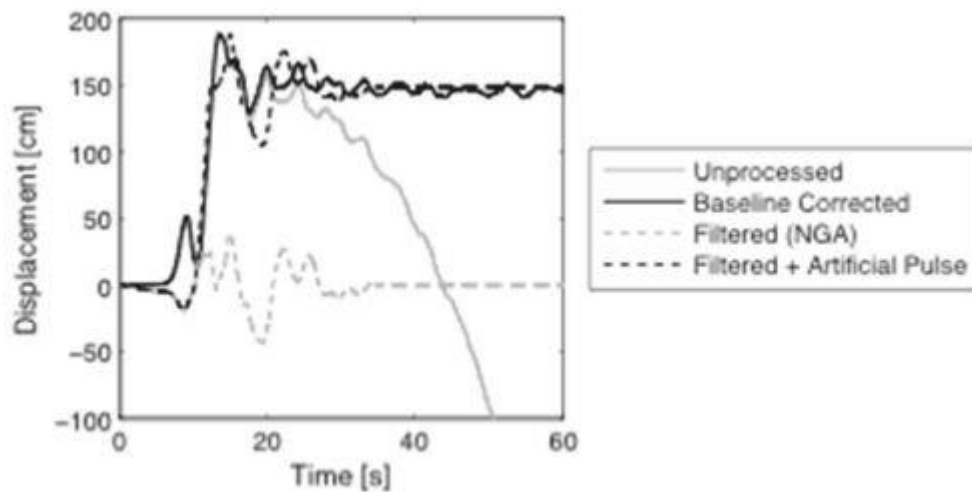


Figure 1.16 Comparison of different corrections for displacement time history from the YPT station in the 1999 Kocaeli, Turkey earthquake (Burks and Baker, 2014)

Baseline correction removes baseline offsets by fitting and subtracting a linear trend from the velocity time history and preserving static offset (Boore, 2001). Figure 1.16 shows the displacement time history from the YPT station in the 1999 Kocaeli, Turkey earthquake (Burks and Baker, 2014).

## 1.2.3 Response of Structures to Near and Far-Fault Ground Motions

### 1.2.3.1 Near-Fault Ground Motions

The severity of the ground motion is precisely understood through the building response that is subjected to it. It is easy to analyze and understand the behavior of simple building models than the original structure itself. Observing and analysing the behavior of uniform shear beams subjected to idealized pulses representing the velocity pulses in near-fault ground motions gives a deep insight into the building behavior as a whole (Hall et al., 1995). Figure 1.17 shows the uniform shear beam subjected to two kinds of idealized ground motions with pulses. Ground motion A has forward only with a duration of pulse  $T_p/2$  representing fling effect and ground motion B has forward and backward pulse with a duration  $T_p$  representing directivity effect in near-fault ground motions, where  $T_p$  is the duration of pulse in the ground motions considered (Hall et al., 1995).

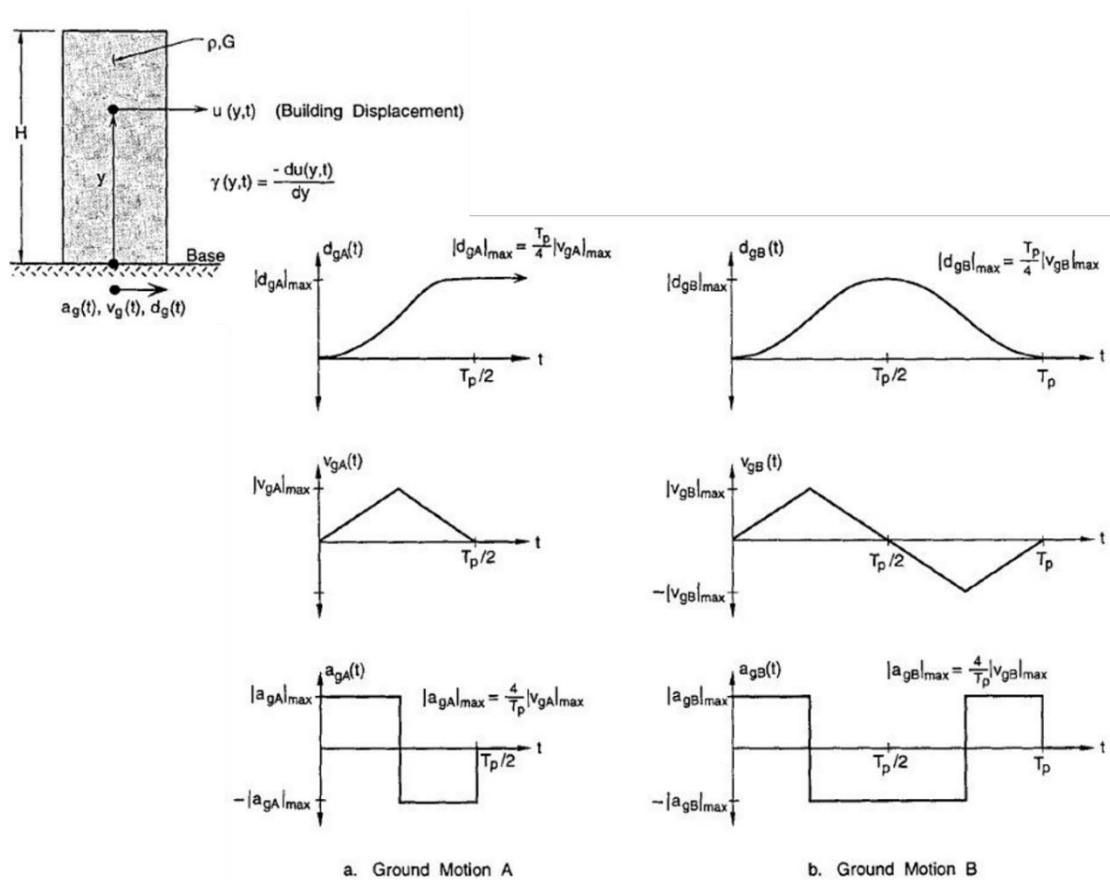


Figure 1.17 Idealised multi-storey building modelled as an elastic shear beam subjected to simple pulse-type ground displacement motions A (forward motion only) and B (forward and backward motion) (Hall et al., 1995)

An analytical study of the behavior of the shear beam in a linear state reveals that the amplification of ground motion at the top of the beam depends on the ratio  $T_p/T$ , where  $T$  is the fundamental period of the building. Also, the amplification of ground motion B is almost double that of ground motion A. In the inelastic range, the lateral force coefficient that is the shear strength at the building base is critical for the ground motion B with a forward and backward pulse. To relate the behavior of the shear beam to the wave propagation in the building, the back phase of the ground displacement pulse, which creates a negative shear strain, occurs as the negative reflection of the shear wave off the top of the building arrives doubles at the base. Because the building responds more slowly when it yields, a ground motion having a pulse period exceeding the building's elastic period may be the most severe (Hall et al., 1995).

Similarly, a study to identify the salient response characteristics to describe the near-fault ground motions by simple equivalent pulses and use them to represent behavior attributes of structures (Alavi and Krawinkler, 2004). Elastic and inelastic demands are evaluated on SDOF and MDOF systems with two base shear strength coefficients by applying a set of 15 near-fault ground motion records with forward directivity. Storey ductility ratio, defined as the ratio of maximum storey drift normalized by the storey yield drift, is used to quantify the response of the MDOF system. Figure 1.18 shows the storey ductility demands for the ground motions considered for both the MDOF systems. It is evident that the maximum storey ductility demand occurs in the upper portion for strong structure, and it occurs in the lower portion for the weak structure. Also, the near-fault ground motion exhibit non-uniform ductility demands unlike the ordinary ground motion represented by mean curve with uniform ductility demands (Alavi and Krawinkler, 2004).

Figure 1.19 shows the strength and period dependence of storey ductility distributions for NR94rrs (1994 Northridge (NR) earthquake recorded at Rinaldi Receiving Station(rrs)) ground motion. With a reduction in the base shear strength, the ductility demands in the upper portion stabilize and grow no more. Further strength reduction results in a migration of the maximum demand towards the base.

This phenomenon is not observed for structure with a period  $T=0.5$  sec, which is shorter than the effective pulse period (Alavi and Krawinkler, 2004).

The maximum ductility demands occur close to the base for these structures regardless of the base shear strength. This is justified by the large elastic storey shear demands in the upper portion of the long period structures ( $T > 1.0$ ), where they reach the storey shear capacity first, resulting in early yielding in the upper stories (Alavi and Krawinkler, 2004).

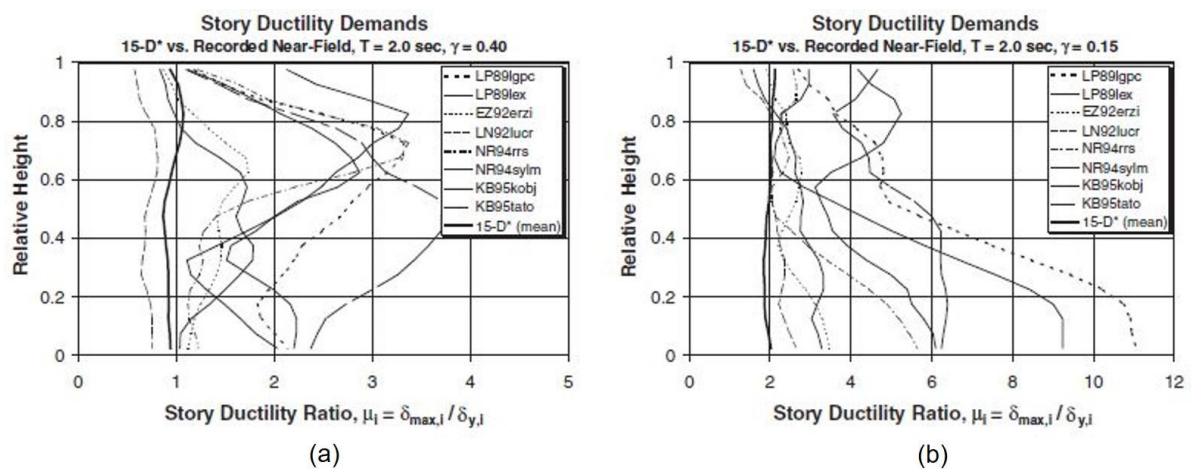


Figure 1.18 Storey ductility demands for MDOF system with (a) base shear coefficient = 0.40 and (b) base shear coefficient = 0.15 when subjected to near-fault and ordinary ground motions (Alavi and Krawinkler, 2004)

Although ductility demand gives a brief idea of the structural response to ground motion, evaluation of damage is required to formulate proper mitigation measures. The seismic response of steel moment frames is evaluated using the equivalent pulses representing fling step effect and directivity effects in near-fault ground motions (Kalkan and Kunnath, 2006). Three existing steel special moment-resisting frame buildings (4-storey, 6-storey, and 13-storey) were selected to evaluate the seismic demands. 21 records categorized into three sets of ground motions (far-fault, near-fault with directivity, and near-fault with fling) are considered for nonlinear time history analysis on two-dimensional frames from each building (Kalkan and Kunnath, 2006).

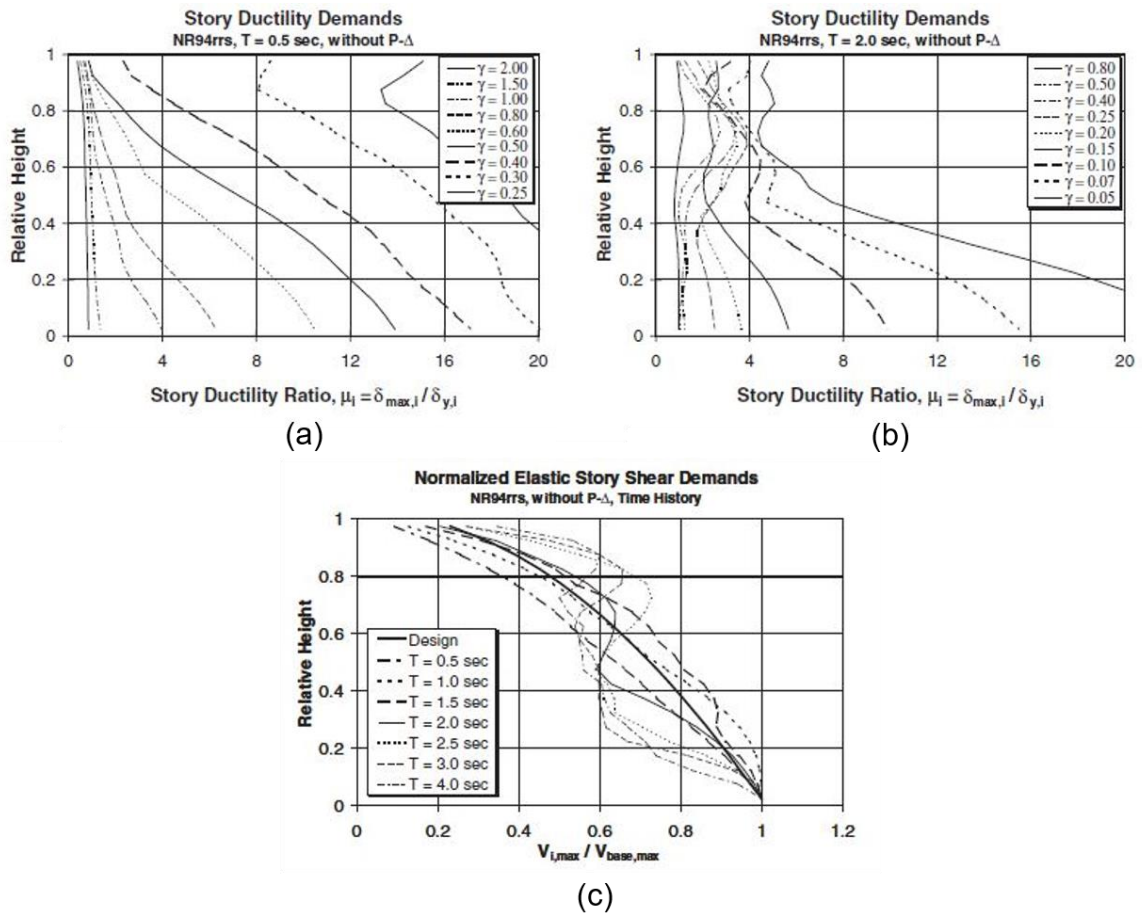


Figure 1.19 Dependence of storey ductility demands on base shear strength for NR94rrs record for natural period (a)  $T = 0.5$  sec and (b)  $T = 2.0$  sec; (c) Normalised elastic storey shear demands for NR94rrs record (Alavi and Krawinkler, 2004)

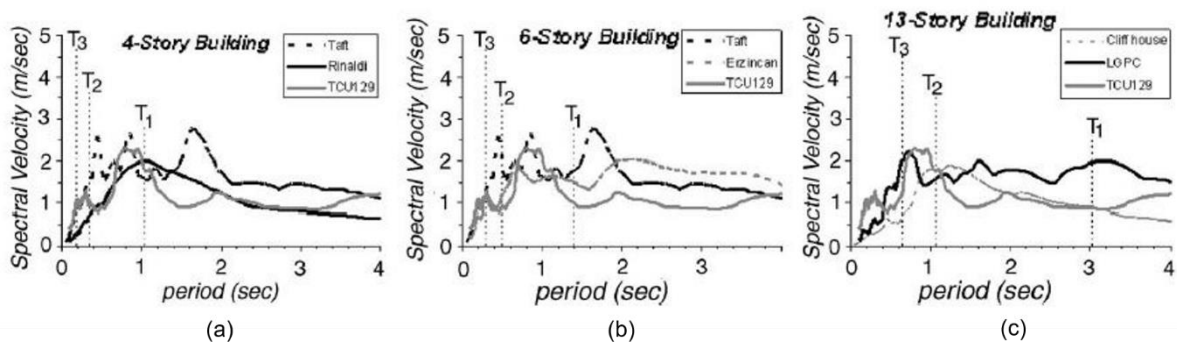


Figure 1.20 Velocity spectra of selected ground motions (Kalkan and Kunnath, 2006)

The results of the nonlinear time history revealed that the higher mode effects of the three buildings are triggered for critical records in all three sets that lead to the shift in demands from the lower to the upper stories. To ascertain the contribution of the higher modes, the acceleration and velocity spectra of the ground motions are inspected collectively.

Figure 1.20 shows the velocity spectra of the selected ground motion with highlighted first three modal periods for the three buildings. For a 4-storey building, two records activated the higher mode effects resulting in increased demands in upper and intermediate stories. Similarly, three records for 6-storey and another three records for 13-storey structures activate the higher mode effects and hence higher demands in upper and intermediate stories. The spectral velocities for the records at higher mode periods are much larger than that for the fundamental period, keeping in mind that a shift to the right of the spectra is to be expected as the yielding of components occur. It is observed that the demands in lower levels for records with fling step were significantly higher than the records with forward directivity that have predominant higher mode effects (Kalkan and Kunnath, 2006).

**Error! Reference source not found.** shows the severity of near-fault ground motions having forward directivity and fling step compared to the far-fault motions at the component level. The demands on the interior column on the first storey level of a 6-storey building experiencing the greatest demand among each ground motion category are presented (Kalkan and Kunnath, 2006).

The greatest deformation demands in near-fault shaking are associated with fewer reversed cycles of loading. This effect is due to the presence of long-duration high-amplitude pulses in near-fault records, causing dissipation of sudden energy in a short period in a single or few excursions. On the other hand, the energy demand for the far-fault motion tends to gradually increase over a longer duration causing an incremental build-up of input energy. It can be concluded that ground motions with smaller input energies can cause peak demands. Also, the gradual build-up of input energy for far-fault records results in increased reversed inelastic cyclic action and low-cycle fatigue damage. At the same time, near-fault motions are characterized by

fewer inelastic displacement cycles followed by several cycles of elastic action. This effect is described by the term “plastic cycle,” which is defined as the cycle in which peak-to-peak amplitude exceeds twice the yield rotation. For the critical column in Figure 1.21, there are 20 half plastic cycles during the response of far-fault records, while there are only six half plastic cycles each for the near-fault motion with forward directivity and fling step effects. Therefore, it is understood that the cumulative damage resulting from plastic cycles is much more significant than implied by the peak ductility demand and should not be ignored when assessing the component's performance (Kalkan and Kunnath, 2006).

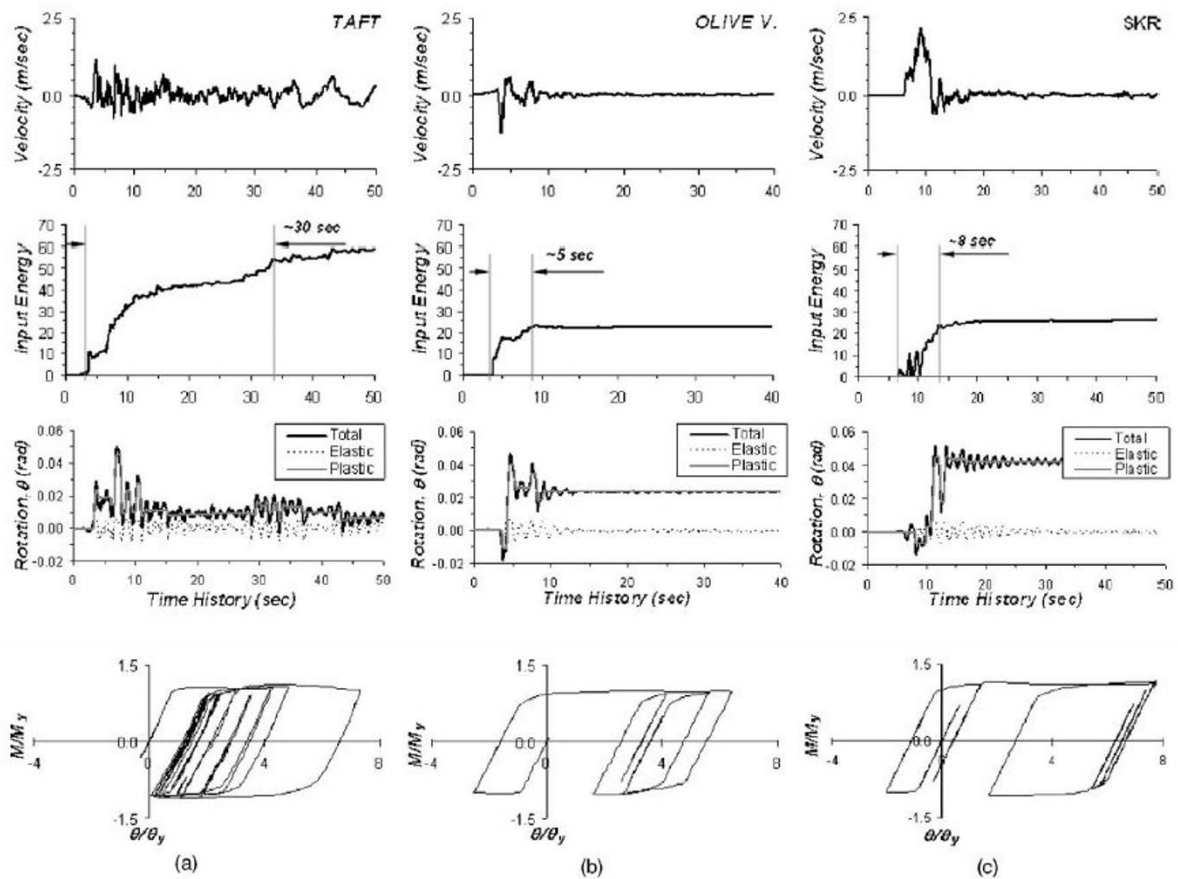


Figure 1.21 Cyclic demand for a typical column subjected to (a) far-fault motion (Taft), (b) near-fault motion with forward directivity (Olive V.) and (c) near-fault ground motion with fling step (SKR) (Kalkan and Kunnath, 2006)

### 1.2.3.2 Directionality Effects in Near-Fault Ground Motions

It is understood that near-fault ground motions exhibit unique characteristics due to various phenomena that are specific to the region. Each of these phenomena (directivity or fling) dominates ground motion characteristics in a specific direction of measurement. However, the direction in which the ground motion characteristics are critical need not be the critical direction for the structural response. A study to find out the most harmful component of ground motion for the nonlinear response along the structural axis of a tall building is performed (Archila, 2014). To understand the problem, a case study on 44 stories reinforced concrete building is performed through nonlinear time history analysis when subjected to near-fault ground motion recorded at Hotville Post office station, located at 7.7 km from the fault plane, during the 1979 Imperial Valley earthquake. Figure 1.22 shows the analysis cases and the resultant displacement response at each floor (Archila, 2014).

Figure 1.22 indicates that the displacement response is maximum when FN is applied along the structural axis, which is reasonably agreeable since the directivity effect is usually predominant in the FN direction of ground motion. However, the FN component is indicated to be one of the responses among various values that are generated at different orientations of the ground motion. Figure 1.23 shows the displacement response of the structure along the structural axis for other orientations of the ground motion. Neither FP nor FN generates the critical response in the structure (Archila, 2014).

A parametric study using synthetic pulses with varying velocity pulse amplitude and duration revealed that elastic and inelastic maximum peak displacement responses occur when  $T_p/T$  lies between 1 and 3, where  $T_p$  is the duration of the pulse, and  $T$  is the fundamental period of the structure. Further, the study defines a new parameter, “Conditioned Maximum Velocity (CMV)” that satisfies the amplitude and duration criterion. The amplitude criterion indicates that “the amplitude of velocity pulse should be maximum among all the orientations of ground motion to produce the critical response. The duration criterion describes that “since the duration of velocity pulse that produces the largest displacement response

on SDOF is longer than fundamental period, the critical response can be expected along an orientation of the ground motion where the strong velocity pulse has duration longer than the translational first mode period of building” (Archila, 2014).

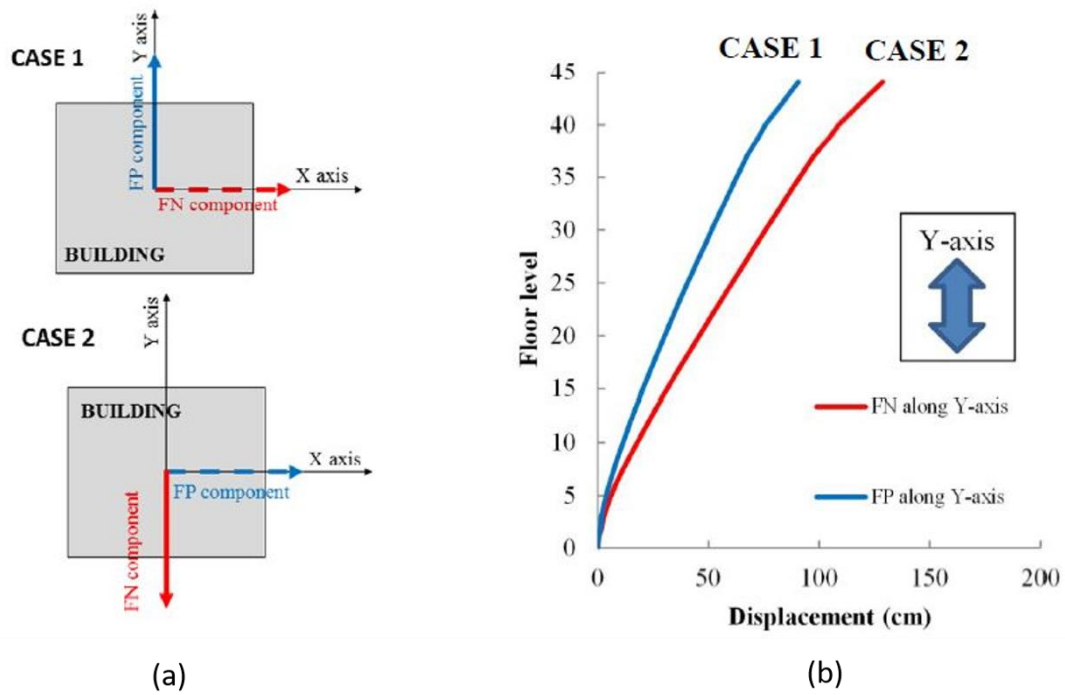


Figure 1.22 Envelopes of nonlinear displacement responses along Y axis for cases 1 and 2 (a) Orientated ground motion cases 1 and 2 (b) Responses along Y axis (Archila, 2014)

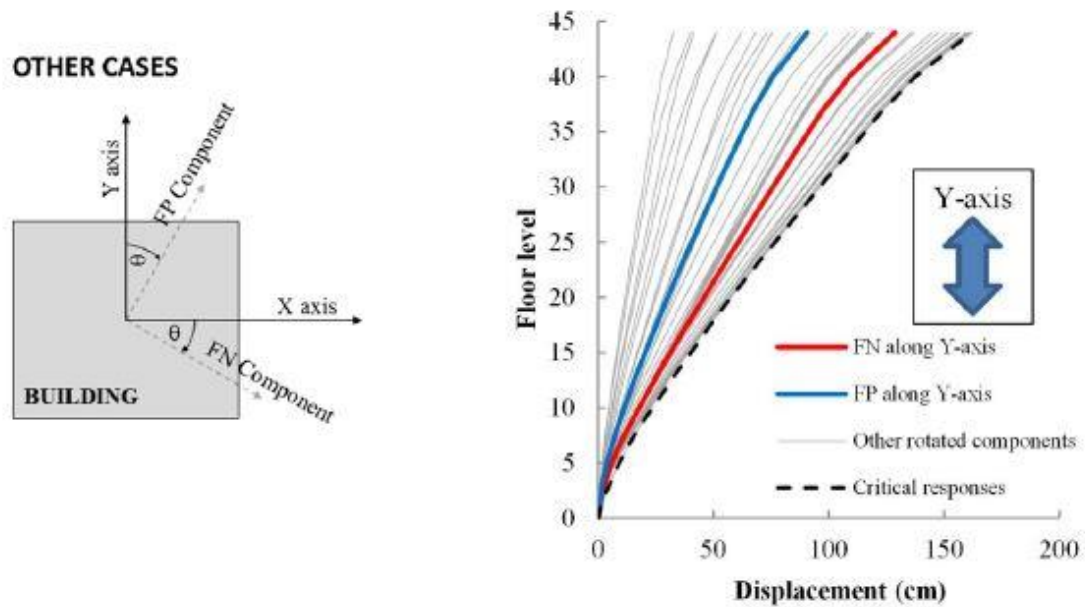


Figure 1.23 Sensitivity of displacement response to ground motion characteristics (Archila, 2014)

Figure 1.24 shows the comparison between the critical displacement calculated from all the rotated components and the CMV ground motion proposed for a period of 1 sec, 2 sec, and 3 sec for an idealized SDOF system subjected to NGA 181 ground motion. This comparison suggests that the CMV could provide reasonable estimates of the critical displacement for the structure (Archila, 2014).

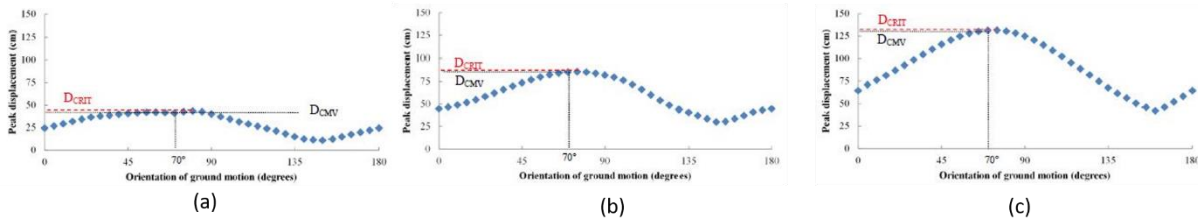


Figure 1.24 Orientation dependence of peak displacement for NGA181 ground motion of SDOF system with base shear coefficient 0.2 and period (a)  $T = 1$  sec, (b)  $T = 2$  sec and (c)  $T = 3$  sec (Archila, 2014)

### 1.2.3.3 Design Improvements for Structure Subjected to Near-Fault Ground Motions

Although the structural damages occurred in the past earthquakes can mostly be attributed to improper construction practices, the question that is still prevalent is the reason for the failure of code-compliant buildings. This suggests a requirement for the improvement of the current design procedures adopted in the standard codes.

The important issue of structures subjected to near-fault ground motions is the non-uniform distribution of story ductility demands. Strengthening techniques for multi-story frame structures are explored with the objective of reducing maximum drift demands (Alavi and Krawinkler, 2004). Two possible solutions are explored. In general, an ideal story shear strength distribution would result in a uniform distribution of story ductility over the height, to efficiently use the energy dissipation capacity available in all elements. But for those structures subjected to near-fault pulse-like ground motions, similar strength distribution leads to large variations of ductility demands over the height.

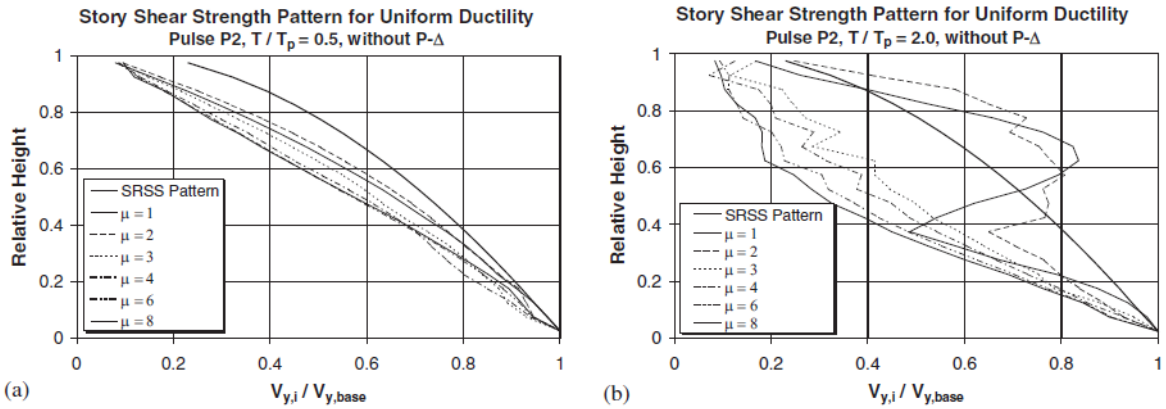


Figure 1.25 Storey shear strength distributions normalised by base shear strength for uniform ductility over height: (a)  $T/T_p = 0.5$ ; and (b)  $T/T_p = 2.0$

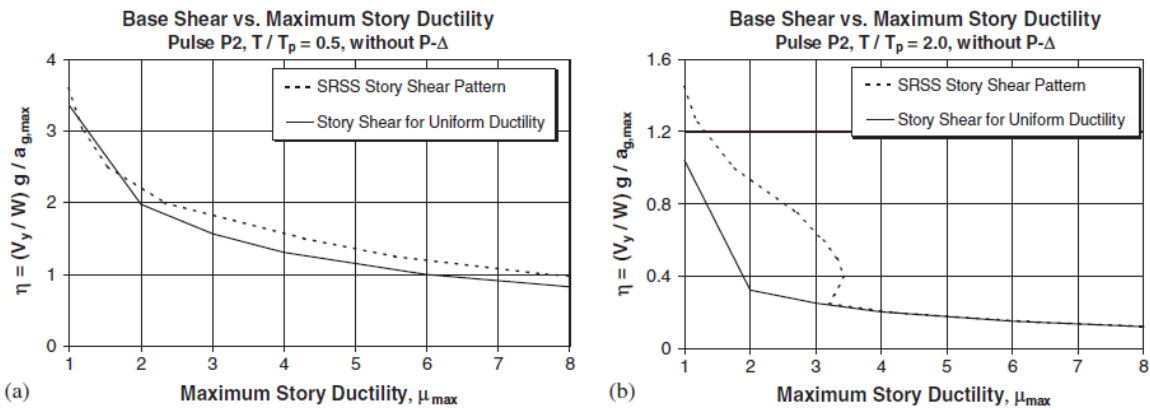


Figure 1.26 Base shear strength demands for specific target ductilities, SRSS and uniform ductility story shear strength distributions, pulse P2: (a)  $T/T_p = 0.5$ ; and (b)  $T/T_p = 2.0$

Storey shear strength distributions that induce uniform ductility over the height of frame structures can be found through an iterative process in which story shear strengths are varied until a targeted uniform story ductility is achieved. Figure 1.25 shows the storey shear strength distribution for two structures with  $T/T_p = 0.5$  and 2.0, respectively. The shear strength distribution is estimated for different target ductilities ranging from 1 (elastic behaviour) and 8 (highly inelastic).

For the structure with  $T/T_p = 0.5$ , the shear strength pattern is almost similar for all values of target ductility ratio. But for the structure with  $T/T_p = 2.0$ , the shear strength distribution randomly varies between target ductility ratio of 2 and 3. Relatively, high strength is required around 2/3<sup>rd</sup> up the structure for close to elastic

behaviour ( $\mu=1$  and  $2$ ), whereas for a uniform ductility of  $3$  or larger the required strength is high at the base and decreases rapidly with height.

Figure 1.26 illustrates the relation between base shear strength demands and maximum story ductility. For structure with  $T/T_p = 0.5$ , the SRSS distribution pattern and required distribution to achieve uniform ductility does not vary distinctly. On the other hand, for structure with  $T/T_p = 2.0$ , the base shear strength required for a specific  $\mu_{max}$  strongly depends on the story shear strength distribution in the ductility range of  $\mu_{max} \leq 3.2$ , whereas for larger ductilities the required base shear strength is insensitive to the distribution of strength over the height. This study concludes that no single-story strength distribution will provide consistent protection at all performance levels and full range of structure periods (Alavi and Krawinkler, 2004).

The study further evaluates the improvement in the structure performance of the 20-story generic frame building by strengthening appropriately with structural walls. To investigate the effects of relative wall stiffness on seismic demands, the wall-to-frame stiffness ratio,  $k_w/k_f$ , is varied in the response evaluations. The frame stiffness  $k_f$ , is defined as the point load at the roof level that corresponds to a unit roof displacement. The wall stiffness  $k_w$ , is defined in a similar manner, assuming a fixed base and neglecting shear deformations. Two kinds of structural walls are considered with fixed base and hinged base to study the effect of change in fundamental period of the building which becomes rigid with fixed base and does not change with hinged base. Three types of strengthening with walls are evaluated that include dual systems with elastic walls, dual systems with inelastic walls. In all the cases, storey drift and force (shear and moment) demands are evaluated.

In the case of dual systems with elastic walls, the fixed walls are very effective in reducing the drift demands for the relatively stiff frame ( $T/T_p = 0.5$ ) but become much less effective in reducing the demands for the relatively flexible frame ( $T/T_p = 2.0$ ), in which case the addition of the fixed wall may even lead to an increase in the maximum drift demand (Alavi and Krawinkler, 2004). It is also observed that the hinged walls significantly reduce the large drifts in the upper portion of the strong structure and bottom portion of the weak structure. Also, with the consideration of p-

delta effects, a higher protection is observed since walls consistently reduce story drift demands of frame structures, especially excessive demands in the bottom stories.

When the structure is strengthened as a dual system with inelastic hinged walls, a pilot study is conducted to evaluate the effect of wall shear yielding on story drift demands for dual systems with hinged walls. It is observed that wall shear yielding only slightly reduces the effectiveness of the hinged wall in reducing the maximum story drift demand. Adding a hinged wall with limited shear strength can still effectively reduce the drift demands. Also, for elastic walls the shear drift demands are negligible compared to the total drifts, but the demands increase rapidly in the bottom portion of the wall once shear yielding occurs.

Similar pilot study is conducted to evaluate the effect of wall flexural yielding on story drift demands for dual systems with fixed walls. It is observed that for systems with relatively stiff frames the elastic wall reduces the drifts very effectively (better than a hinged wall). This effectiveness slightly declines if frames are strengthened with very weak walls, but the benefits are still considerable. However, for systems with relatively flexible frames, the effectiveness of strengthening increases when the fixed wall yields in flexure. The reason is that when the fixed wall plastifies at the bottom, its behaviour approaches that of a hinged wall. The study concludes that the frame strengthened by fixed walls yielding in bending will lead to concentration of large plastic rotations in the bottom story.

#### **1.2.3.4 Far-Fault Ground Motions**

The existing 49 storey steel structure response when subjected to low amplitude, long period far-fault ground motion, and high amplitude relatively short duration period of near-fault ground motion is studied (Muin et al., 2020). The building is made up of steel moment-resisting frames with few braced frames in one direction. The fundamental period of the building is around 5.2 sec. The record represents the far-fault ground motion observed at ChiChi-002 station during the 1992 Chi-Chi earthquake in Taiwan. The near-fault is represented by the record observed

at Newhall station during the 1994 Northridge earthquake. The far-fault ground motion has a predominant period of 4 sec to 6 sec. Figure 1.25 shows the horizontal acceleration time history of far-fault and near-fault ground motions along with the comparison of pseudo displacement spectra of the two (Muin et al., 2020).

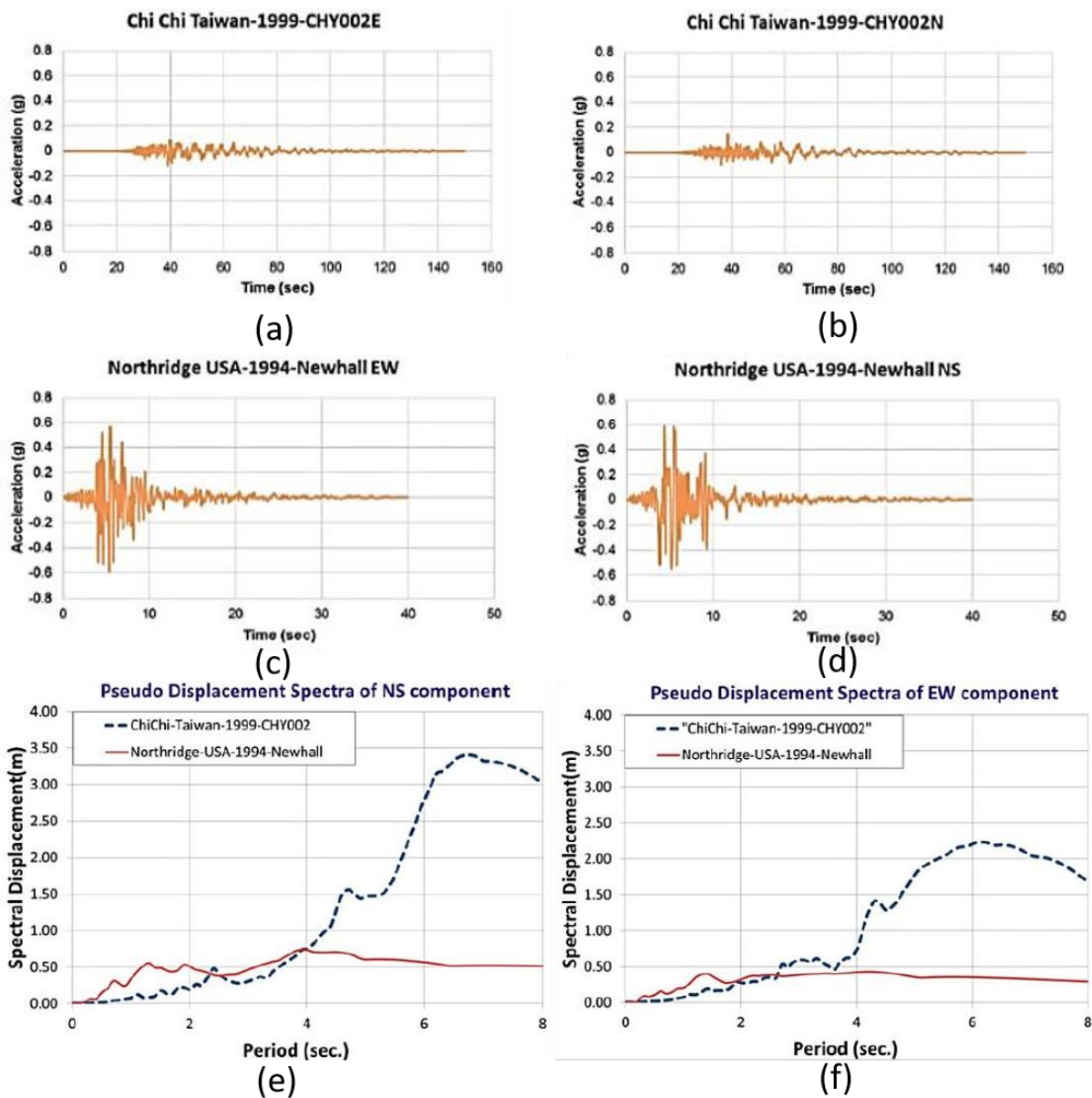


Figure 1.27 Pseudo acceleration spectra for the (a) far-fault in EW direction (b) Far-fault in NS direction (c) Near-fault in EW direction (d) Near-fault in NS direction; Comparison of pseudo displacement spectra for far-fault and near-fault ground motions in (e) NS direction (f) EW direction (Muin et al., 2020)

Figure 1.26 shows the roof drift response of the structure when subjected to near and far-fault ground motions. The near-fault ground motion with a PGA of 0.6g generates a maximum roof drift of only 0.7% for the braced frame, whereas the far-fault ground motion generates a maximum roof drift of 1.5% for the braced frame. The roof orbit plot shown in Figure 1.27 shows the structure vibrating predominantly in NS braced frame direction in response to the near-fault ground motion. For the far-fault ground motion, the EW shaking dominates initially. Later, EW and NS motions become couples and create a rotational twisting motion considerably larger than the motion due to the near-fault motion (Muin et al., 2020).

Also, it is observed that the response attenuation is considerably low for the far-fault ground motion compared to the near-fault ground motion. The drift response in the braced frame direction decreased 60% in five cycles (25.1 sec) for the near-fault ground motion, while it decreased 46.2% in five cycles (24.8 sec) for the far-fault ground motion (Muin et al., 2020).

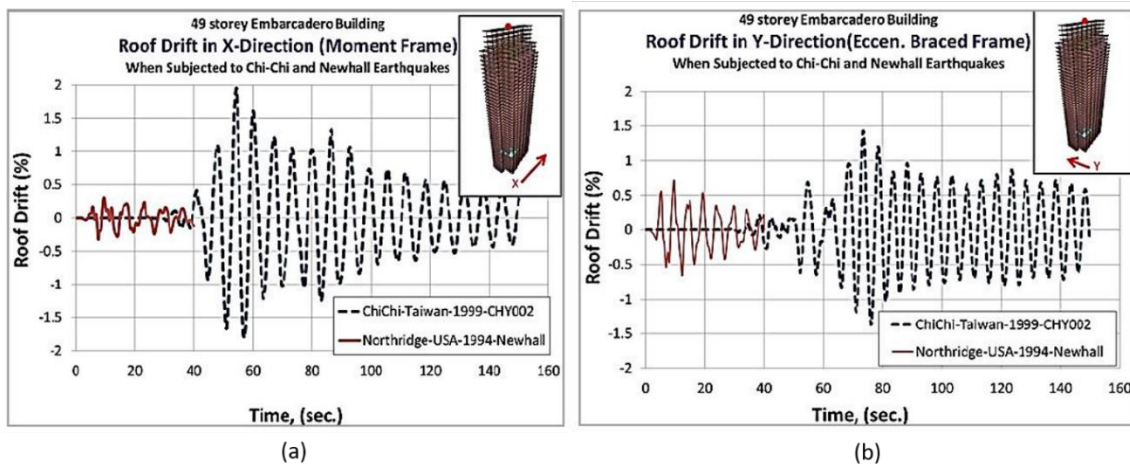


Figure 1.28 Displacement time history of the roof of the structure subjected to near and far-fault ground motions in (a) Moment frame along X direction (b) Braced frame along Y direction (Muin et al., 2020)

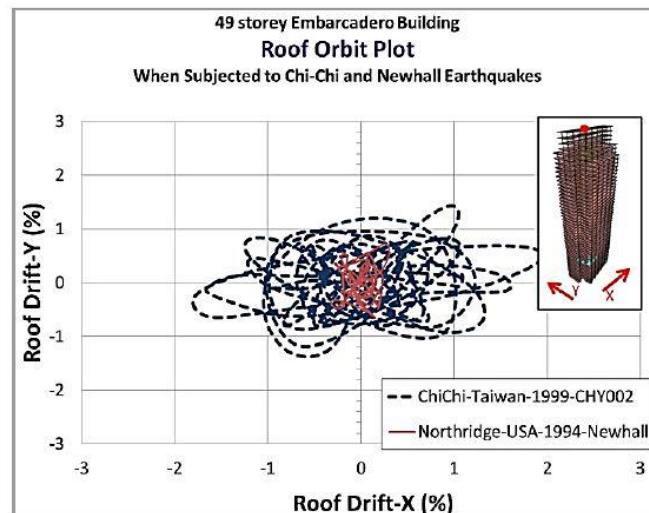


Figure 1.29 Roof orbit response of the structure to near-fault, strong and far-fault, weak earthquakes (Muin et al., 2020)

Similar attenuation is observed when the base shear response is considered. For the near-fault ground motion, the response decreases to 70% in five cycles, and for the far-fault ground motion, the response decreases to 43% in five cycles. This slow attenuation for the far-fault ground motion indicates that the structure is exposed to prolonged large cyclic forces that may result in buckling and low-cycle fatigue fractures (Muin et al., 2020).

### 1.3 GAP AREAS

The strong ground motions recorded close to the fault exhibit distinct characteristics than those recorded far away from the fault. Ground motions recorded close to the fault exhibit large velocity pulses ( $> 0.5$  m/s), owing to hanging wall, directivity, and fling step effects. A hanging wall increases the amplitude of ground motion due to multiple reflections at the earth's surface. Directivity induces a large amplitude velocity pulse with long periods. Fling step is the presence of residual displacement at the end of the ground motion. Although extensive research was undertaken to understand these effects through analytical studies, a clear direction is not available on how to incorporate near-fault and far-fault effects in structural design.

Literature suggests that the effects of these near-fault strong ground motions were studied extensively. But the following issues are yet to be discussed in detail:

1. The effects of near-fault ground motions on the structural behaviour are not derived using robust analytical 3D models of buildings.
2. The quantification of near-fault strong ground motion and its incorporation in structural design procedure, especially in the long period range.

## **1.4 OBJECTIVES OF THE STUDY**

To mitigate the structural damage in moment frame building, arising from near-fault strong ground motions with large amplitude short duration pulses, the sufficiency of current structural design procedures needs to be examined. Therefore, the objectives of the study are:

- A. To identify the differences in seismic responses of reinforced concrete moment frame buildings subjected to near-fault (with large velocity pulses) and far-field strong ground motions.
- B. To suggest a possible retrofit solution to mitigate the damage in moment resisting frame buildings.

## **1.5 SCOPE OF STUDY**

The thesis focusses on understanding the earthquake behaviour of RC buildings subjected to near-fault ground motions using 3D analytical model of the buildings. To address the mentioned gap areas in the section 1.3, the recorded strong ground motions are considered for carrying out the study rather than the idealised pulses. The ground motions considered are categorized into four sets; near-fault with pulse whose pulse period greater than fundamental period of building, near-fault with pulse whose pulse period less than fundamental period of building, near-fault without pulse and far-fault ground motions. Since due to directivity effect in the near-fault ground motions, the fault normal is usually critical than the fault parallel, the

study considered only the fault normal component with no residual slip for all the four categories of ground motions. In addition, to capture the correlation between damage and fundamental period of the building, typical 5- and 10-storey building are considered. In all cases, the buildings are considered to have moment frame as the basic structural system. Also, building with moment frame structural walls of different configurations are considered.

## **1.6 ORGANISATION OF THESIS**

Chapter 1 discusses the literature on the subject, and identifies the gap areas, write problem statement and state the objectives of the study. Also, the scope of work is stated, along with the methodology employed to carry out the study.

Chapter 2 discusses the strong ground motion accelerograms recorded during 1999 Chi-Chi earthquake to understand the characteristics of near- and far-fault ground motions.

Chapter 3 discusses the behaviour of moment frame buildings subjected to near and far-fault ground motions. The differences are established in the earthquake damage sustained under near-fault ground motions with and without velocity pulse.

Chapter 4 focusses on reducing the earthquake damage in moment frame buildings by the provision of structural walls in them. The improvements in the earthquake behaviours are discussed.

Chapter 5 presents the summary of work done, and states the conclusions drawn from the study. Suggestions are made for the design philosophy of the buildings when subjected to near- and far-fault ground motions.

...



## 2 Characteristics of Near and Far-Fault Ground Motions

### 2.1 BACKGROUND

To understand the seismic behaviour of buildings subjected to near-fault strong ground motions, it is essential to identify their predominant characteristics. A statistical study is carried out on the strong ground motions recorded during 1999 Chi-Chi earthquake. The earthquake occurred on 20 September 1999 near Chi-Chi town in Taiwan that recorded a magnitude of 7.6 $M_w$ . It is one of the largest earthquakes in Taiwan that occurred on land in the past hundred years with 2,470 fatalities, 11,305 injured and 1,00,000 structural damages. The earthquake resulted from the complex subduction phenomena (visible like a pretzel) between the Philippines and the Eurasian plates that lead to subduction of Philippines plate on the north-eastern coast and subduction of Eurasian plate on the southwestern coast. The earthquake had energetic aftershock sequence that occurred for 1 year and include 87 greater than magnitude 5, 13 greater than magnitude 6 and 7 greater than magnitude 6.5 earthquakes (Shin and Teng, 2001). Figure 2.1 shows the map of the aftershock sequence from 20 September 1999 to 19 October 2000.

This earthquake is one of those that are recorded extensively such that the total global holding of significant strong motion data increased five times after the event. More than 650 modern digital free-fault strong motion stations are installed within four years under the program called Taiwan Strong Motion Instrumentation Program (TSMIP). The rupture process and the seismic wave propagation are reconstructed using the recorded waveforms which revealed that the earthquake occurred on North-South trending East dipping (dip = 30<sup>0</sup>) surface fault called Chelungpu at a focal depth of 8 km (Shin and Teng, 2001). This causative fault is the boundary between western foothills and western plains starting from Shih-Kang in the north and terminating at Tungtou in the south with an azimuth of 5<sup>0</sup>. The faulting is mainly thrust action with a minor left lateral component in the South-East end. The total energy release of 2.1 x 10<sup>17</sup> Joules occurred in discontinuous jumping dislocations (Shin and Teng, 2001).

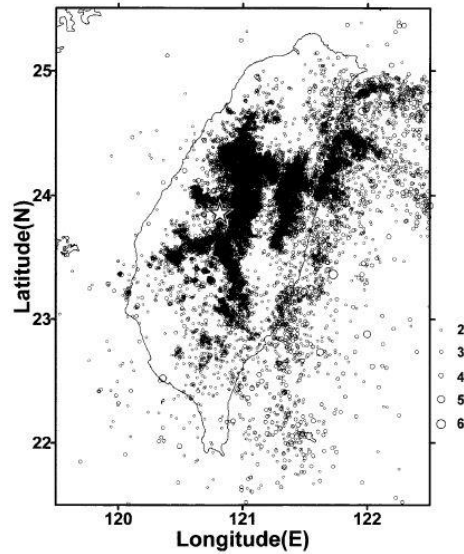


Figure 2.1 Map showing the Chi-Chi mainshock and aftershock sequence from 20 September 1999 to 19 October 2000 (Shin and Teng, 2001)

The extensive recording of the ground motions allows to observe and analyse the characteristics of near and far-fault ground motions generated from the same source in different set of propagation paths and site characteristics. Therefore, the recorded strong motion database is considered for the case study. The available ground motions at the recording stations in the horizontal directions are used to study the characteristics of ground motions.

## 2.2 RECORDED STRONG GROUND MOTIONS

The earthquake was recorded at 376 free-field stations located on different soil types. Based on the type of soil present at the recording station, stations are categorized into 5 types with varying shear wave velocity (Table 2.1). Because the earthquake occurred on a right lateral strike-slip fault, all those stations located on the right of the fault line are identified as hanging wall stations and those that are on left of the fault line are identified as footwall stations (Figure 2.2). The map shows that the recording stations are densely located on the footwall side and are sparse on the hanging wall side. As a result, very few recording stations are available on the near-fault region towards the hanging wall side.

Table 2.1 Number of recording stations in each soil type (Data Source: COSMOS)

Soil Type	Shear Wave Velocity (m/sec)	No. of Stations
Sb	760-1500	48
Sc	360-760	53
Sd	180-360	180
Se	<180	81
Unknown	-	14

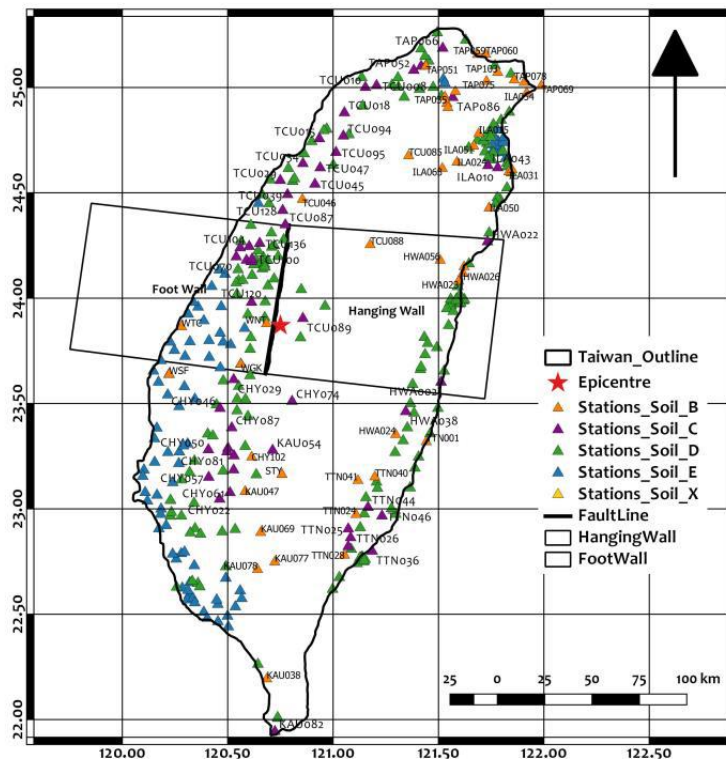


Figure 2.2 Map showing areas representing hanging wall and footwall (Data Source: COSMOS)

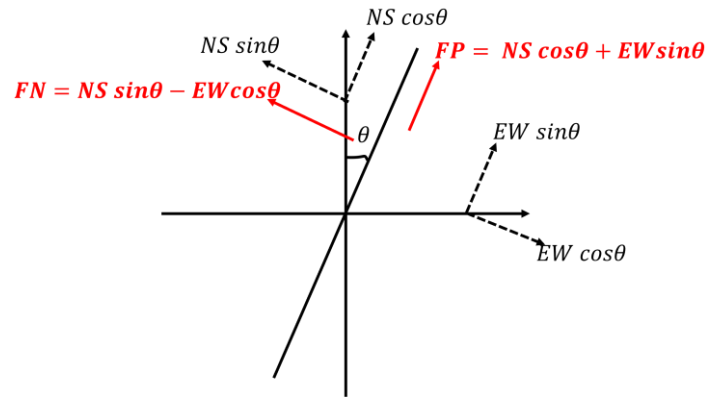


Figure 2.3 Method to transform horizontal ground motion recorded with respect to North into Fault Normal and Fault Parallel directions

The corrected accelerograms at the recording stations are obtained for the study (COSMOS). At each station, two horizontal components along NS and EW are utilized. Literature suggests that the ground motion characteristics are critical in the directions along the fault plane and across the fault plane. Hence, the direction cosines of the acquired horizontal components along the fault line (Fault Normal) and across the fault line (Fault Parallel) are estimated using the azimuth of the fault (Figure 2.4).

The peak ground acceleration (PGA) is extracted from the accelerograms obtained at all stations. A plot of epicentral distance and PGA for footwall stations and hanging wall stations are separately shown in figure 2.5 and 2.6, respectively. A statistical trendline is fit for the distance and PGA relationship. On the hanging wall, the stations are located till 100km from the fault plane, however on the footwall, the stations are located within 50km from the fault plane. In the near-fault region, the ground motion amplitude on the hanging wall stations is nearly twice that of footwall stations. This observation reinforces that the ground motions recorded during this earthquake undergo the phenomena of hanging wall effect.

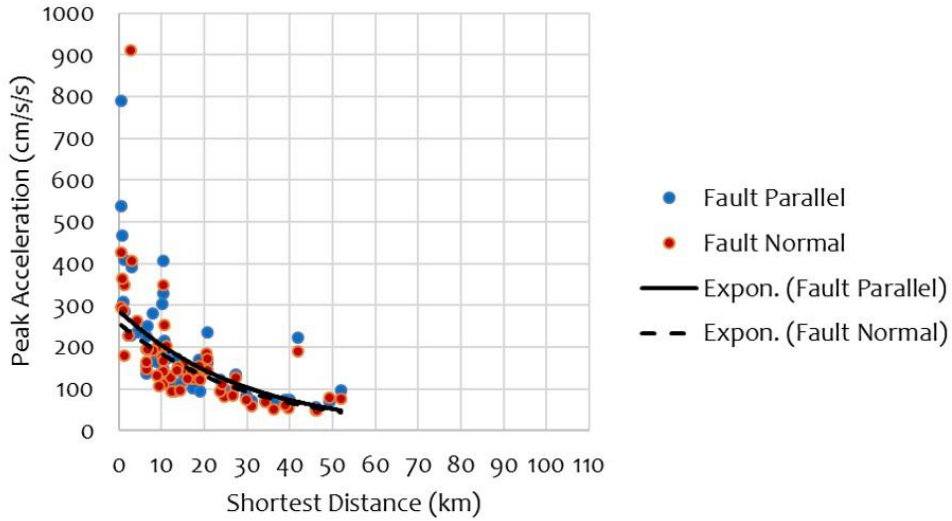


Figure 2.4 Peak Ground Acceleration (PGA) recorded in Fault Normal and Fault Parallel directions with respect to the shortest distance of station from fault plane on the footwall (Data Source: COSMOS)

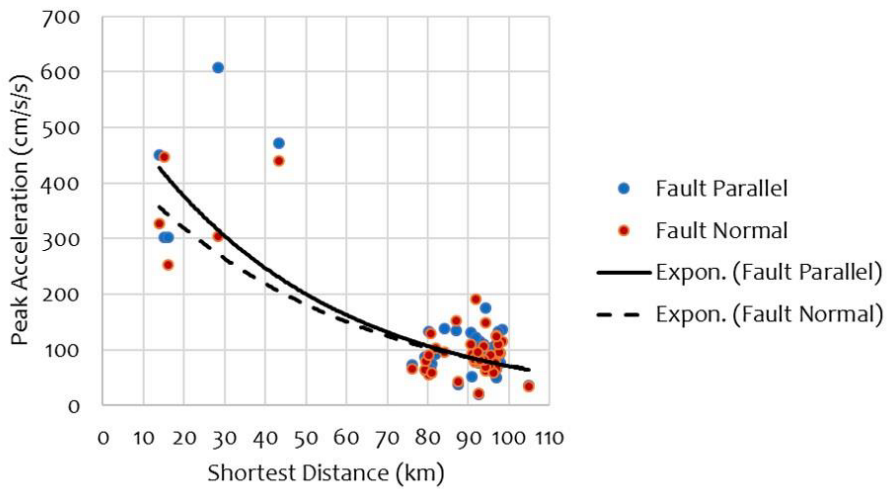


Figure 2.5 Peak Ground Acceleration (PGA) recorded in Fault Normal and Fault Parallel directions with respect to the shortest distance of station from fault plane on the hanging wall (Data Source: COSMOS)

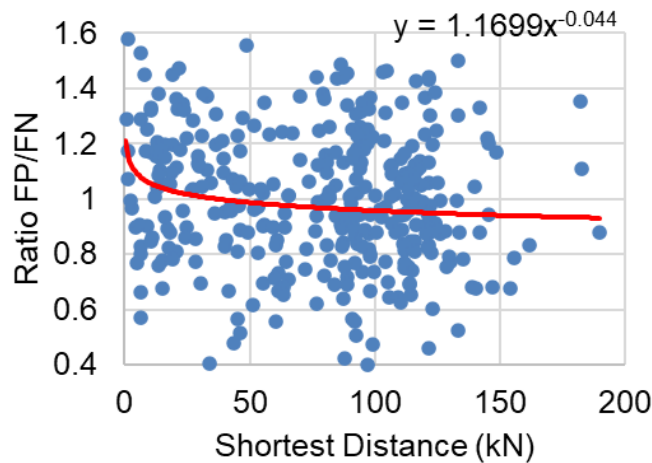


Figure 2.6 Ratio of Peak Ground Acceleration (PGA) between Fault Normal and Fault Parallel directions with respect to the shortest distance from the fault plane

The relationship between shortest distance and the recorded PGA values also indicate that the amplitude of fault parallel component is higher than the fault normal in the near-fault region at both the hanging wall and footwall stations (Figure 2.6). With increase in the distance away from the fault plane, the difference in amplitudes of fault parallel and normal decreases and is almost negligible. Also, the difference in both the components is high for stations on the hanging wall side than the footwall side. Therefore, these difference in characteristics of the ground motions are required to be summarised in the preceding sections.

### 2.3 OBSERVATIONS

The study revealed the predominant characteristics of strong ground motion influenced by hanging wall effect. The observations are as follows:

1. The maximum PGA on the hanging wall is nearly two times higher than the maximum PGA on the footwall. Also, the maximum value on both the sides of the fault line occurs in the near the fault. This is due to the hanging wall effect present in the near-fault strong ground motions.
2. Although the hanging wall effect requires all the stations on the hanging wall side to have higher PGA values. But the studies indicate some exceptions at certain locations with higher values at footwall stations. This uncertainty can be attributed to the fault mechanism of the earthquake which is predominantly

thrust with considerable amount of strike-slip action at the north of the fault plane and sometimes also to the local site conditions at recorded stations.

3. Another characteristic of hanging wall effect that is noticed from this study is the difference in PGA values of FP and FN in the near-fault region. It is observed that the PGA values in the FP are higher than those in the FN. This behaviour may be largely attributed to the faulting mechanism of the earthquake. In a pure thrust faulting mechanism, it is intuitive to observe higher PGA values in the FN direction at a near-fault station since the resultant direction of slip is upwards and in the direction of FN. But since this earthquake is caused due to mixed faulting mechanism with considerable strike-slip component, majority of the stations near the end of the fault plane indicate higher FP components. Therefore, although the faulting mechanism consists of thrusting action, the higher average PGA on FP indicate predominant strike slip faulting mechanism.

## 2.4 CONCLUSIONS

Apart from these observations, in general, the near-fault region of any earthquake is considered to be less than 20 km – 30 km as prescribed by different agencies. But the present study indicates a highly sensitive characteristics of ground motion with hanging wall effect in the near-fault region that requires a particular definition of near-fault region apart from the distance parameter. Combining all the observations and interpretations of the characteristics of near-fault ground motions that exhibit hanging wall effect, the procedure to identify the near-fault region of the earthquake can be established. It is understood that the hanging wall effect is highly sensitive to the faulting mechanism of the earthquake. For a pure thrust faulting mechanism, it may be derived that the PGA ratio of FN and FP component is greater than one can be termed as a condition to define the near-fault region. On the other hand, if a complex faulting mechanism exists, the PGA ratio should be dependent on

the predominant slip direction. For the present case study, the PGA ratio of FP to FN is observed to be greater than one in the near-fault region. Therefore, it can be said that the PGA ratio of FP and FN can be reliably utilized in defining the near-fault region in addition to the distance of the station from the fault plane.

The case study highlights the prominence of ground motion characteristics that vary with the near and far-fault regions. Since the near-fault ground motion observe peculiar phenomena like directivity, hanging wall etc, the ground motions exhibit specific characteristics. Hence, the conventional methods to design the structures present in the near-fault region may not be sufficient to ensure the safety of such structures.

...

*Blank Page*

## **3 Effect of Near-Fault Ground Motions on Frame Buildings**

### **3.1 BACKGROUND**

In an earthquake, safety of buildings is of utmost importance to limit life loss. The prominent building typology in most of the cities in India is the reinforced concrete moment resisting framed buildings. Knowledge of their behaviour when subjected to near and far fault ground motions helps in adopting sufficient mitigation measures.

In the near fault region, the ground motion characteristics are highly influenced by source mechanism. However, in the far fault region, they are influenced predominantly by path followed by the seismic waves. Therefore, it is proposed to carry out the study when ground motions are recorded during two source mechanisms, i.e., i) reverse faulting, and ii) strike slip faulting. The predominant difference in both the source mechanisms is the directivity present in the ground motions. Due to directivity effect present in the ground motions, a short duration impulse appears in the record in the initial time instants. The behaviour of the structure is highly influenced by the period of the pulse present in the ground motion. The ratio of pulse period to the structure's natural period defines the maximum response and the damage that is likely to occur. Therefore, the study also includes the ground motions with pulse periods higher and lower than building's natural period.

### **3.2 GROUND MOTIONS CONSIDERED**

To understand the effect of fault mechanisms on the behaviour of buildings, two earthquakes in each of the source mechanisms are considered. 1995 Northridge earthquake and 2004 Japan earthquake are predominantly reverse/thrust faulting mechanism; 1999 Turkey earthquake and 2004 Parkfield earthquake are predominantly strike slip earthquakes.

### 3.2.1 Horizontal Ground Motions

Four ground motions recorded in each earthquake namely near-fault with pulse whose pulse period is less than building's natural period, near-fault ground motion with pulse whose pulse period is greater than building's natural period, near-fault ground motion without pulse and far-fault ground motion are considered for the study. The ground motion data files are obtained from PEER NGA West 2 database and COSMOS virtual data centre after applying the baseline correction and filtering. The ground motions are selected based on a significant magnitude than  $M_w$  6. All the near-fault ground motions with a velocity pulse are from earthquakes of magnitude  $M_w$  between 6.5 and 7. Further, the recorded ground motions are converted to the normal and parallel components from each earthquake's fault motion characteristics, as shown in Figure 3.2. Table 3.1 shows the engineering characteristics of ground motions considered in each category. Further, the location of the pulse is identified using moving windows method using the Fourier transform. The Fourier transform of the moving window with a time duration equal to the pulse period is adopted to identify the maximum value of velocity. This maximum value indicates the pulse associated with the documented pulse period (Figure 3.1). Therefore, the start and end time of the pulse in the original ground motion is observed.

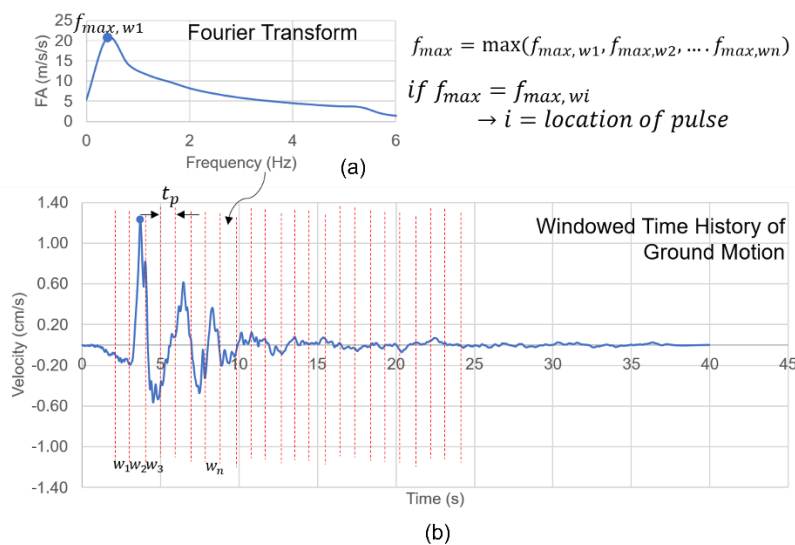


Figure 3.1 Procedure to identify the location of pulse using moving window method (a) Fourier Transform of a window (b) Time history of ground motion

Figures 3.3 and 3.4 show the acceleration and velocity response spectra of the ground motions considered, respectively. The plots of acceleration spectra also indicate the design spectrum as suggested by the Indian Standard Code of Practice for Earthquake Resistant Design of Buildings [IS 1893 (Part 1): 2016]. It is observed that almost all the ground motions considered are following the design spectrum without any differences between types of ground motions (namely near-fault with and without pulse and far-fault). But the plot of velocity response spectra of same ground motions indicates entirely different features as compared to the acceleration spectra. In the Northridge earthquake, it is clearly observed that the response of near-fault ground motion with pulse is predominant for structures with period greater than 1 sec. In both Japan and Turkey earthquakes, the structures with period greater than 0.5 sec observe higher response due to the far-fault ground motions. This amplification in the response may be due to the presence of long period waves that are usually predominant at distances far away from the fault. Lastly, in the Parkfield earthquake, the response of the structures with period greater than 0.5 sec are governed by the near-fault ground motions with pulse.

Therefore, it may be inferred that the conventional design procedures suggested by the structural code of practice that are based only on the acceleration response spectra are insufficient to incorporate the effects of near-fault ground motions in the design of earthquake resistant design of buildings.

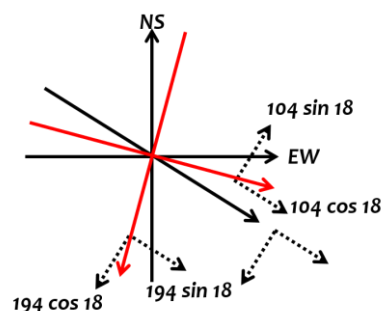


Figure 3.2 Directions of recorded (red) ground motions to North (NS), the azimuth of the fault plane (black-solid), and the normal and parallel (black-dotted) components of the recorded ground motions during the Northridge earthquake, 1995

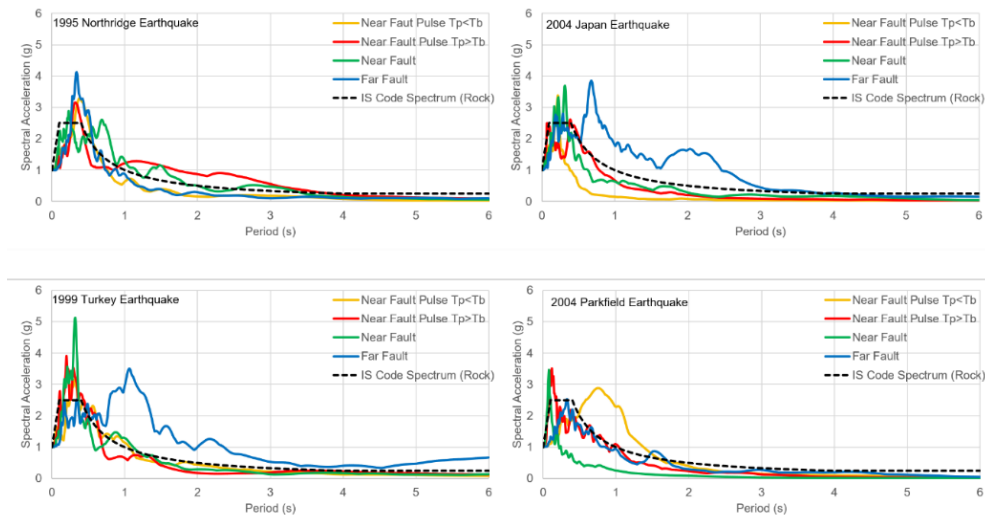


Figure 3.3 Acceleration response spectra of horizontal ground motions considered

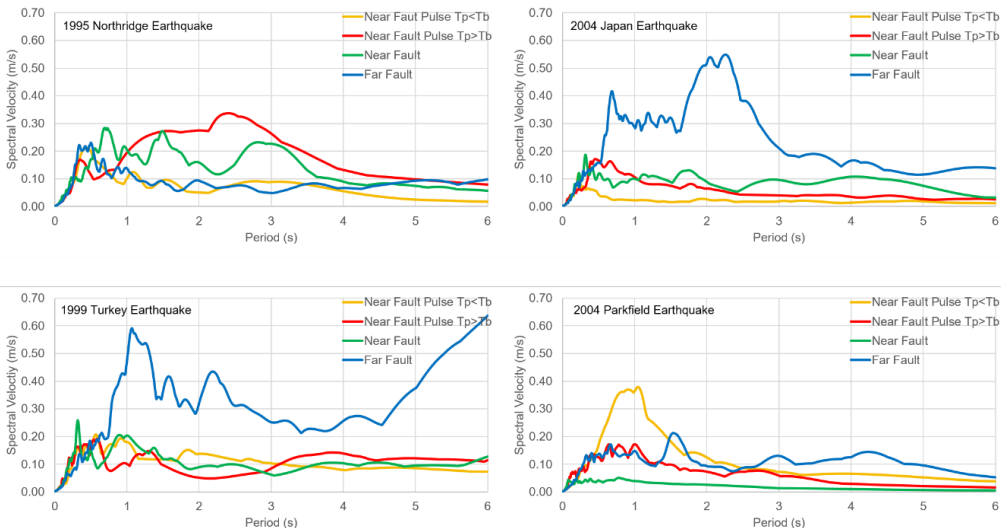


Figure 3.4 Velocity response spectra of horizontal ground motions considered

### 3.2.2 Vertical Ground Motions

Generally, structures experience a constant gravity of acceleration ( $g$ ) in the vertical direction all the time. If an earthquake of say,  $0.15g$  vertical acceleration shakes the building vertically then the net effect shall be added and subtracted in both the vertical positive and negative directions, respectively. It means the structure is experiencing an acceleration in the range of  $0.85g - 1.15g$ . But the structures are designed for a  $1.5$  load factor for dead and live loads that is much higher than the observed peak acceleration. Although, vertical accelerations do not have predominant

effects on normal buildings, they may become important in cases of structures present in the near-fault regions.

To observe the effect of vertical ground motions on 5 story structure. Four analysis cases, following the 30% rule suggested by IS 1893-2016 are considered i.e., (a) 100% Vertical ground motion, (b) 100% Vertical and 30% fault normal ground motion in longitudinal direction, (c) 100% Vertical and 30% fault parallel ground motion in transverse directions, and (d) Vertical, 30% fault normal in longitudinal direction and 30% fault parallel in transverse direction. The same cases are considered in the transverse direction also.

### **3.3 ANALYTICAL MODEL OF BUILDING**

Two buildings with 5-storey and 10-storey moment resisting frames with floor-to-floor height of 4.5 m and with bay width of 4 m in 6 x 4 no. of bays in x and y directions, respectively are considered for the study. The buildings are assumed to be ordinary residential and the gravity loads (i.e., dead and live loads) are applied accordingly. Lateral loads corresponding to seismic zone V are applied on the building according to IS 1893 (Part 1): 2016. Earthquake resistant design along with ductile detailing is performed considering the code prescribed 73 load combinations. The final cross-section details of the beams and columns are obtained with the required reinforcement. Since the designed buildings are regular, the first three predominant modes are translational.

The numerical model of bare frame is developed in SAP2000 v23 for performing nonlinear analysis. To obtain a considerable robustness in the model, the slabs (that are modelled as shells for performing the design) are applied as uniformly distributed load on beams in addition to URM infill wall load. For evaluating the structure's performance, the expected strength without partial safety factors is required to be evaluated. The expected mean strength of concrete suggested by IS 456: 2000 is calculated as

Table 3.1 Engineering characteristics of ground motions considered for the study in fault normal direction

<i>S.No.</i>	<i>Type of ground motion</i>	<i>Station Name</i>	<i>Closest Distance to Fault (km)</i>	<i>PGA (g)</i>	<i>Predominant period (s)</i>	<i>Effective Duration (s)</i>	<i>Pulse Period (s)</i>
1995 Northridge Eq.							
1	Near Fault with pulse $T_p < T_b$	Pacoima Dam	7.01	0.51	0.51	3.79	0.59
2	Near Fault with pulse $T_p > T_b$	Sylmar Olive View Med	5.30	0.73	2.41	5.76	2.44
3	Near Fault without pulse	Arleta Fire Station	9.50	0.24	0.78	13.88	-
4	Far Fault	Lake Hughes	40.00	0.27	0.51	17.74	-
2004 Japan Earthquake							
1	Near Fault with pulse $T_p < T_b$	NIG021	11.26	1.18	0.23	5.97	0.32
2	Near Fault with pulse $T_p > T_b$	NIGH11	8.93	0.53	0.41	9.37	1.79
3	Near Fault without pulse	NIG017	12.81	0.49	0.32	46.06	-
4	Far Fault	FKS020	101.86	0.036	2.46	50.09	-
1999 Turkey Earthquake							
1	Near Fault with pulse $T_p < T_b$	Bolu	12.04	0.68	0.54	8.90	0.88
2	Near Fault with pulse $T_p > T_b$	IGIRM	2.65	0.31	0.42	17.49	10.05
3	Near Fault without pulse	Lamont	11.46	0.11	0.33	15.31	-
4	Far Fault	Armont	131.45	0.006	9.10	32.23	-
2004 Parkfield Earthquake							
1	Near Fault with pulse $T_p < T_b$	Slack Canyon	2.99	0.29	1.02	5.17	0.85
2	Near Fault with pulse $T_p > T_b$	Parkfield: Eades	2.85	0.21	0.74	0.51	1.22
3	Near Fault without pulse	Parkfield Work Ranch	10.76	0.25	0.084	3.01	-
4	Far Fault	Fresno-VA Medical Centre	109.51	0.007	0.67	20.67	-

---

---

(3.1)

Since the relationship between expected strength and yield strength is not available in IS 456, it is considered from ASCE 41 – 17 as follows:

$$f_e = 1.25f_y \quad (3.2)$$

The nonlinear material strength of concrete is defined using Mander material model for both unconfined (i.e., cover concrete) and confined (i.e., core concrete) properties. Similarly, the nonlinear material strength of steel bars is defined using Park material model. The full moment of inertia ( $I_g$ ) of the cross sections is used for nonlinear analysis unlike the reduced  $I_{cr}$  used for design of building adopted based on the suggestion of practice code. The required reinforcement obtained from design is assigned to the beams and columns using *Section Designer* (i.e., detailing toolbox inbuilt in software). The moment curvature capacity of the section and the axial load and moment interaction (P-M) are automatically calculated from the defined section details.

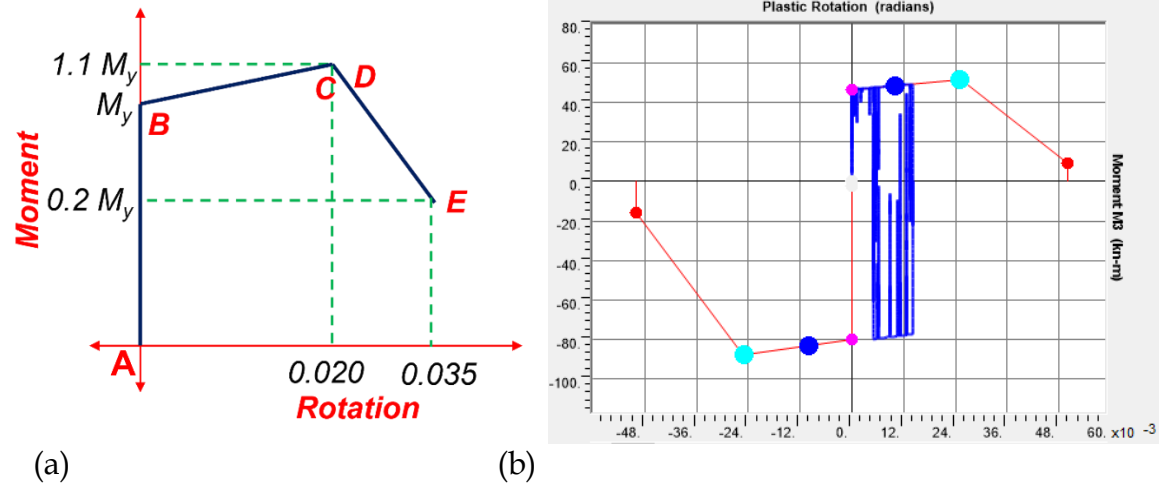


Figure 3.5 Moment-Rotation ( $M-\theta$ ) relationship (a) defined at the nonlinear plastic hinge, and (b) actual curve at a typical hinge location.

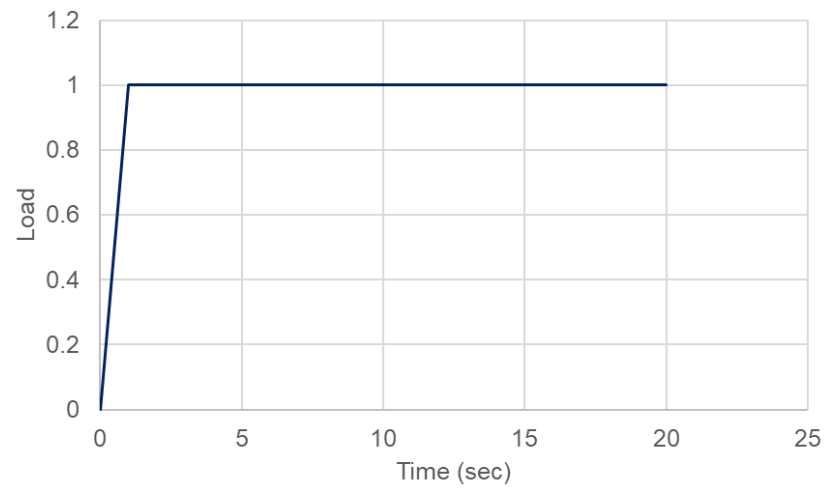


Figure 3.6 Ramp function to apply the dead load on the structure

Nonlinearity in beams is modelled using lumped plasticity approach defined at  $1/4^{\text{th}}$  of the depth of the member [ASCE 41 - 17]. However, in columns fibre lumped plasticity hinges are adopted. Fibre hinges are a hybrid method to incorporated fibre modelling that is highly precise with sufficient robustness with general lumped hinges. The length of the plastic hinge for both moment hinge and fibre hinge are taken as half of the depth of the member [ASCE 41 - 17].

In beams, the hinge behaviour is defined using a moment-rotation ( $M-\theta$ ) relationship for flexural hinges. It is defined using a scale factor equal to the yield moment ultimate rotation that is multiplied with the  $M-\theta$  curve. Figure 3.5 (a) shows the  $M-\theta$  defined for each nonlinear plastic hinge. The nonlinear hinge is active only when the member yields; till the yield the initial stiffness of the member determines the load carrying capacity. Five critical stages of hinge propagation are defined; point A where loading starts, point B where the member yields, (rotation is zero and moment corresponds to yield moment), point C where the moment in member reaches to 10% more than the yield, point D where the moment capacity decreases to 20% of yield moment, point E where the complete collapse of the member is observed. Beyond this the hinge will drop down to zero moment capacity.

The actual curve at a typical hinge location at a beam is shown in figure 3.5 (b). The hinge is observed to be following the defined  $M-\theta$  relationship.

In columns, the fibre hinges are defined at the material level defining the limit states for stresses and strains in the cross section. Therefore, each cross section provided is defined with fibre layout in the section designer. Each fibre is assigned with the material (confined, unconfined or reinforcement) based on its location in the section. Acceptance criteria for member level failure are defined

in three damage states: Immediate Occupancy (i.e., member observe spalling of concrete), Life Safety (i.e., yielding of steel bars) and Collapse (i.e., crushing of concrete).

### **3.3.1 5-Storey**

The natural period of the building with expected strength is obtained as 0.96 s and 1.03 s in longitudinal and transverse directions, respectively with a mass participation of 83% in first mode. The seismic weight of the structure is obtained as 35,720 kN. Beams in the first and second storey are of size 400 x 550 mm, third and fourth stories are of size 350 x 450 mm, fifth storey are of size 300 x 300 mm. The cross-section sizes of columns are maintained same throughout the height of the building with cross section 400 x 400 mm, for the corners, 450 x 450 mm and 450 x 500 mm for the edges, and 500 x 550 mm for the core columns.

### **3.3.2 10-Storey**

The natural period of the building with expected strength is obtained as 1.77 s and 1.85 s in longitudinal and transverse directions, respectively with a mass participation of 80% in first mode. The seismic weight of the structure is obtained as 82210 kN. Beams in the first six stories are of size 450 x 600 mm and top 4 stories are of size 400 x 500 mm. The cross-section sizes of columns are maintained through the height of the building with cross section 500 x 650 mm and 600 x 600 mm.

### 3.4 NONLINEAR TIME HISTORY ANALYSIS

The total dead load of the structure is applied in the form of a ramp function as shown in Figure 3.6 to avoid transient vibrations caused due to sudden application to total load. The ground motion is applied in continuation to the dead load after 20 sec. The acceleration time history is applied in the required direction with output time step equal to the recorded time step for a particular ground motion. Damping is specified based on the model time period and is equal to 5%. Modified Newton-Raphson method is used to derive the solution of the nonlinear problem.

The analysis is performed for the time equal to the total record time of the ground motion with the same time increment as the record. However, during the analysis if the structure develops the state of mechanism (i.e., if simultaneous collapse hinges are formed at the same level), the analysis is terminated. Therefore, the end of response is marked as the end of the ground motion or formation of collapse mechanism, whichever is observed first.

#### 3.4.1 *Horizontal Shaking*

The primary focus of the study is to observe the earthquake response of the moment resisting frame building that is designed by conventional earthquake resistant design principles, drift gives a simple representation of the earthquake resistance. Hence, Inter-storey Drift Ratio (IDR) calculated as the relative displacement between two consecutive stories is the primary comparison parameter. As an example, the IDR for the 5-storey structure subjected to near-fault ground motion with pulse recorded during 1995 Northridge earthquake.

Similarly, the damage observed is indicated by calculating the dissipated hysteretic energy from the hysteretic moment rotation relationship obtained from the analysis. The hysteretic energy is calculated as the sum of area under the hysteresis. The sum

of hysteresis energy thus calculated at each nonlinear hinge at a storey gives the energy dissipated at that storey. Similarly, the sum of all the nonlinear hinges in a structure yields the total hysteretic energy dissipated.

#### **3.4.1.1 5 Storey**

Figure 3.7 shows the ground motion time history and the IDR of 5-storey building with moment resisting frame in longitudinal directions when subjected to near-fault ground motion with pulse. It is observed that the structure attained inelastic drifts at the initial time instant after the start of the near fault double sided pulse. Another important aspect to observe is that the response after the pulse is mostly elastic which indicates that the ground motion might not contain high amplitude pulse. This observation shows that the structure can withstand the near fault ground motions if it can retain the high amplitude in short duration.

Figure 3.8 shows the force-deformation curve obtained for a building subjected to near-fault ground motion recorded during Northridge earthquake. It is observed that the building undergoes large inelastic drift in a single cycle.

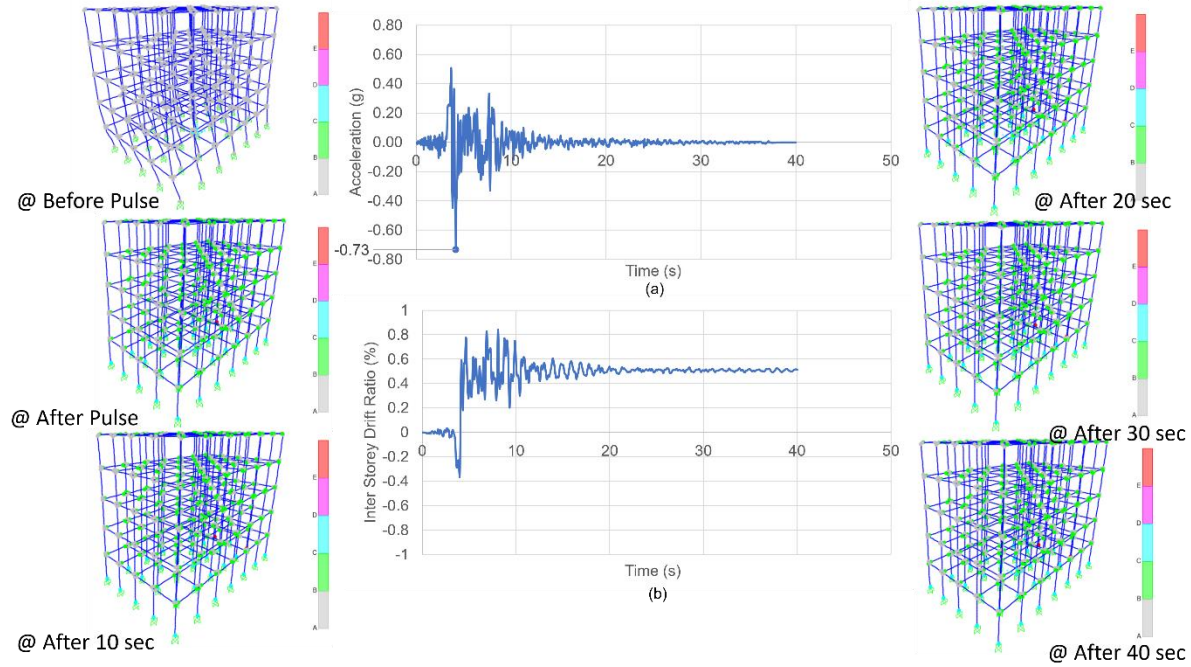


Figure 3.7 Plot of (a) Earthquake ground motion and (b) Inter Storey Drift Ratio (%) throughout the time history of 5-storey moment resisting frame building subjected to near-fault ground motion recorded during 1995 Northridge earthquake.

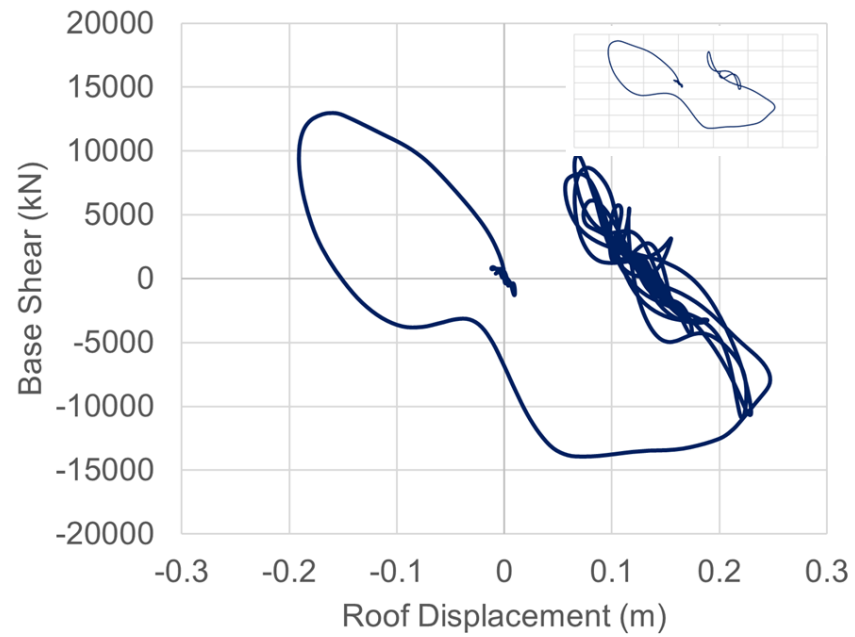


Figure 3.8 Force vs. deformation curve of the 5-storey building subjected to near-fault ground motion recorded during Northridge earthquake in the longitudinal direction.

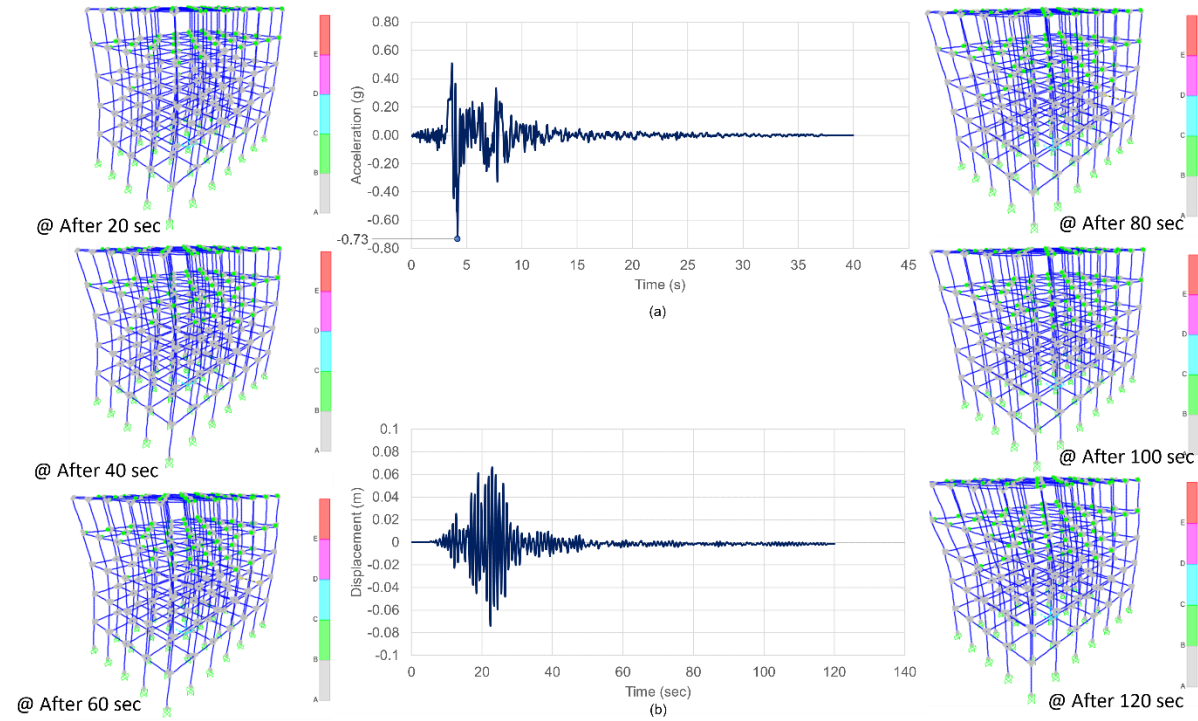


Figure 3.9 Plot of (a) Earthquake ground motion and (b) Inter Storey Drift Ratio (%) throughout the time history of 5-storey moment resisting frame building subjected to far-fault ground motion recorded during 1995 Northridge earthquake.

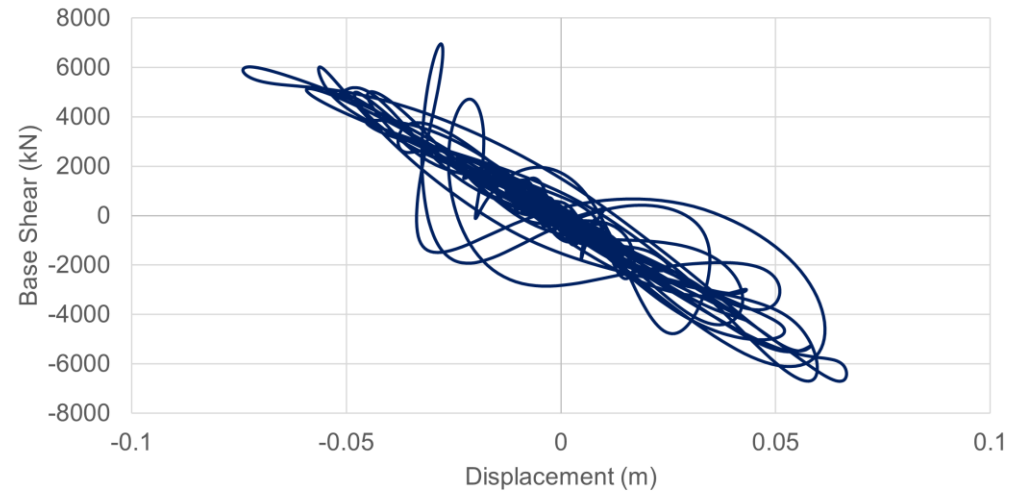


Figure 3.10 Force vs. deformation curve of the 5-storey building subjected to far-fault ground motion recorded during Northridge earthquake in the longitudinal direction

#### 3.4.1.1.1 Validation of Numerical Models

To validate the numerical models used, nonlinear static pushover analysis is performed on the typical 5-storey structure and compared with the nonlinear time history analysis. For performing the nonlinear static pushover analysis, the target displacement is applied as 4% of the height of the building (figure 3.11). The structure achieved 85% strength reduction by this drift. When subjected to far-fault ground motion recorded during 1995 Northridge Eq., the structure the structure obtained 0.3% drift from nonlinear time history analysis. This value is much less than the maximum drift obtained from nonlinear static pushover analysis. Hence, it can be concluded that the numerical model developed for the study is pertaining to the requirements.

#### 3.4.1.1.2 *Inter Storey Drift (%)*

The inter storey drift when subjected to the four ground motions recorded in the four earthquakes that are obtained at each floor is shown in the figure 3.12. It is observed that the maximum inter storey drift of the structure is 2% for the ground motion from Northridge earthquake. Also, the drift demand is observed to be high in the intermediate storeys (i.e., 2<sup>nd</sup> and 3<sup>rd</sup> storeys). Figure 3.13 shows the inter storey drift obtained at each floor when subjected to near-fault ground motions without pulse. It is observed that the maximum inter-storey drift is obtained when subjected to Japan earthquake. But unlike the near-fault ground motion with pulse, the maximum drift across the floors is less than 1% as compared to 2% in the former case. Also, the location of maximum drift is shifted to 3<sup>rd</sup> and 4<sup>th</sup> floors.

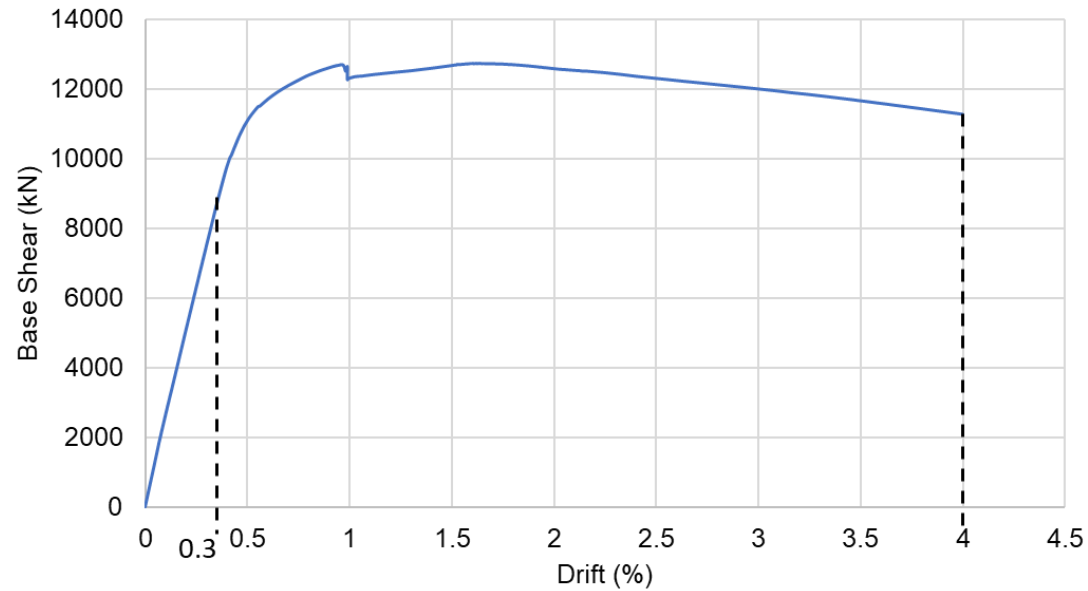
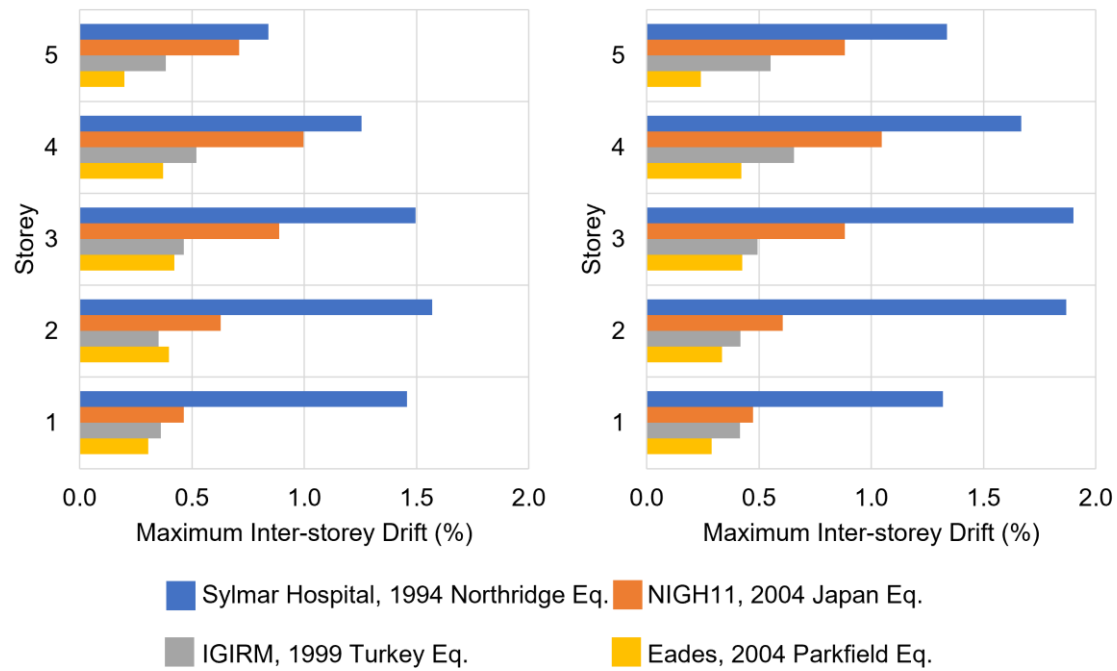


*Figure 3.11 Validation of numerical model by comparing displacement achieved through nonlinear static analysis and nonlinear time history analysis*

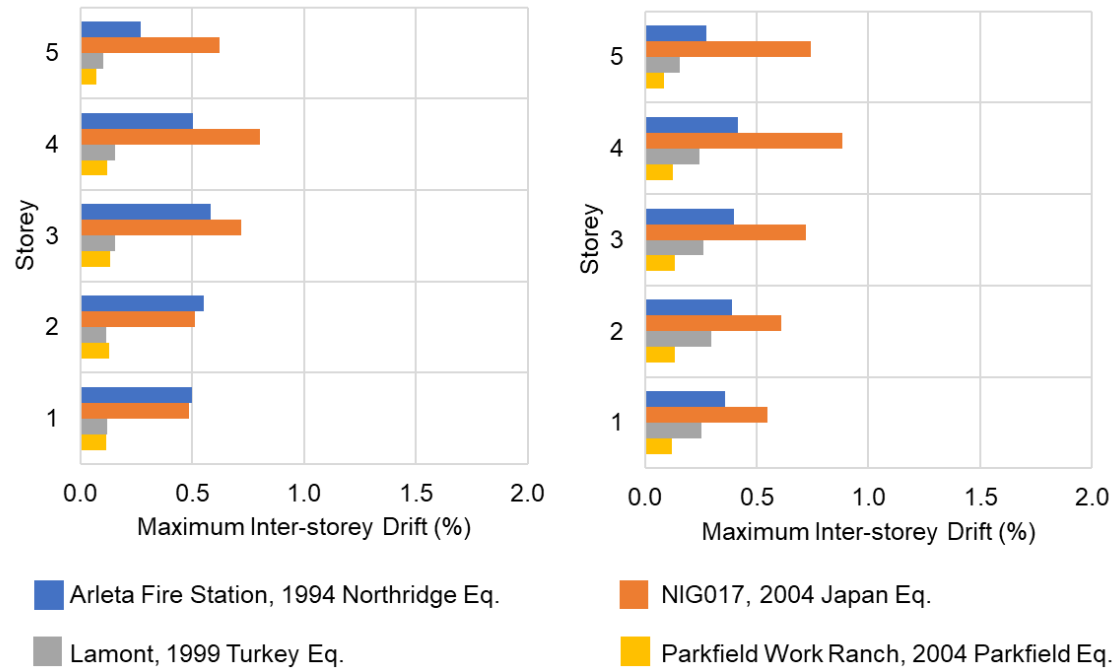
For the 5-storey building subjected to far-fault ground motions, the maximum inter storey drift at each floor is shown in figure 3.14. The drift demand is comparatively high for the Northridge earthquake with higher values in the intermediate storeys. But the value of maximum drift is less than 0.5% much less than those obtained for near-fault ground motions with pulse and near-fault ground motions without pulse.



(a)

(b)

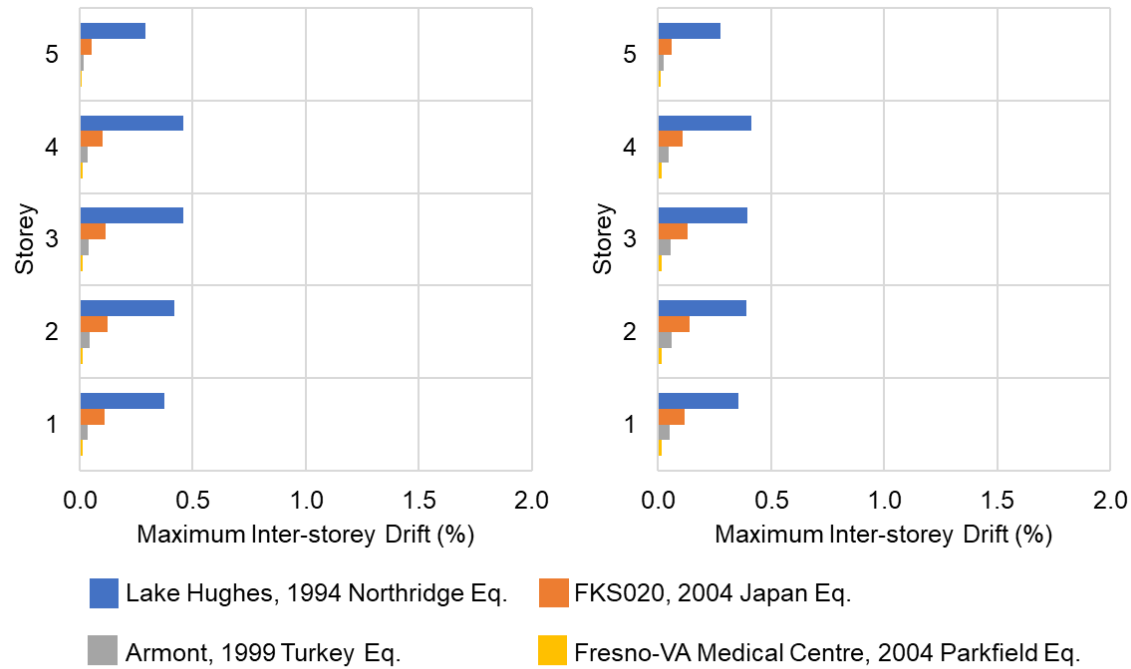
Figure 3.12 Maximum inter storey drift (%) of 5-storey building at each floor subjected to near-fault ground motions with pulse in (a) longitudinal, and (b) transverse direction



(a)

(b)

Figure 3.13 Maximum inter storey drift (%) of 5-storey building at each floor subjected to near-fault ground motions without pulse in (a) longitudinal, and (b) transverse directions



(a)

(b)

Figure 3.14 Maximum inter storey drift (%) of 5-storey building at each floor subjected to far-fault ground motions in (a) longitudinal, and (b) transverse directions

### 3.4.1.1.3 Energy

In addition to the drift demand, the comparison of input energy and the dissipated energy reveals the damage that would occur due to ground motion. Figure 3.15 shows the comparison of absorbed and dissipated energy of 5-storey structure when subjected to near-fault ground motions with and without pulse and far-fault ground motions in both the orthogonal directions of the

structure. It is observed that the Northridge earthquake imparted comparatively higher absorbed energy and hence higher dissipated energy. Also, the structure has not dissipated energy when subjected to far-fault ground motion which remained in elastic state.

Hysteretic energy dissipated by 5-storey structure at each floor when subjected to near-fault ground motions with pulse is shown in figure 3.16. It is observed that the dissipation of energy is higher in the 1<sup>st</sup> storey for the Northridge and Japan earthquake and higher in the intermediate storeys for the Turkey and Parkfield earthquakes. But it can be concluded that the near-fault ground motions observe higher dissipated energy in the lower storeys since the input energy imparted by the Northridge earthquake is considerably higher than the other ground motions.

Figure 3.17 shows the hysteretic energy dissipation by 5-story structure when subjected to near-fault ground motions without pulse in both the orthogonal directions. It is observed that the dissipation of energy shifted to the intermediate storeys (i.e., 3<sup>rd</sup> and 4<sup>th</sup> storey). Also, the value of maximum energy dissipation is nearly 40% of the input energy imparted.

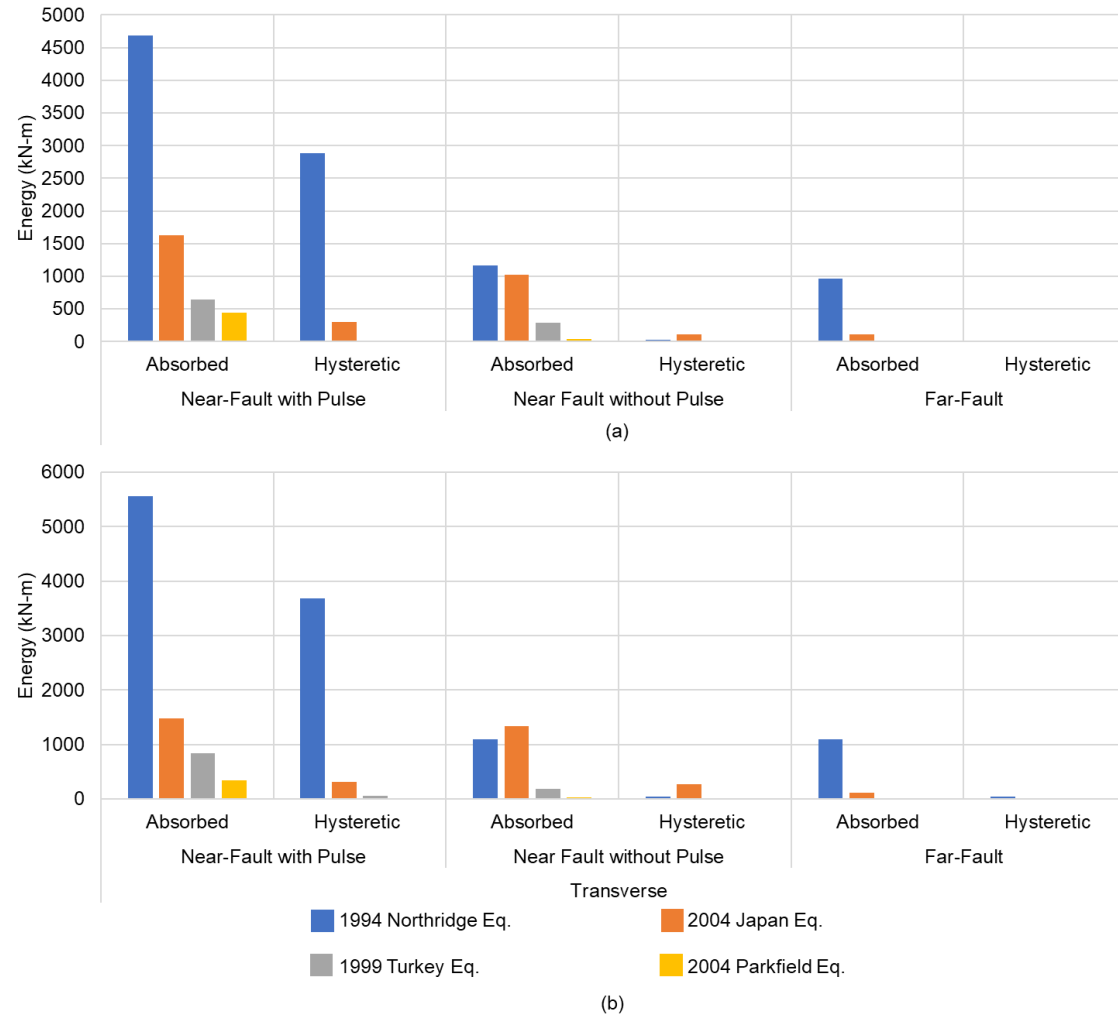


Figure 3.15 Comparison of absorbed energy and dissipated energy of 5-storey structure subjected to different ground motions in (a) longitudinal, (b) transverse direction

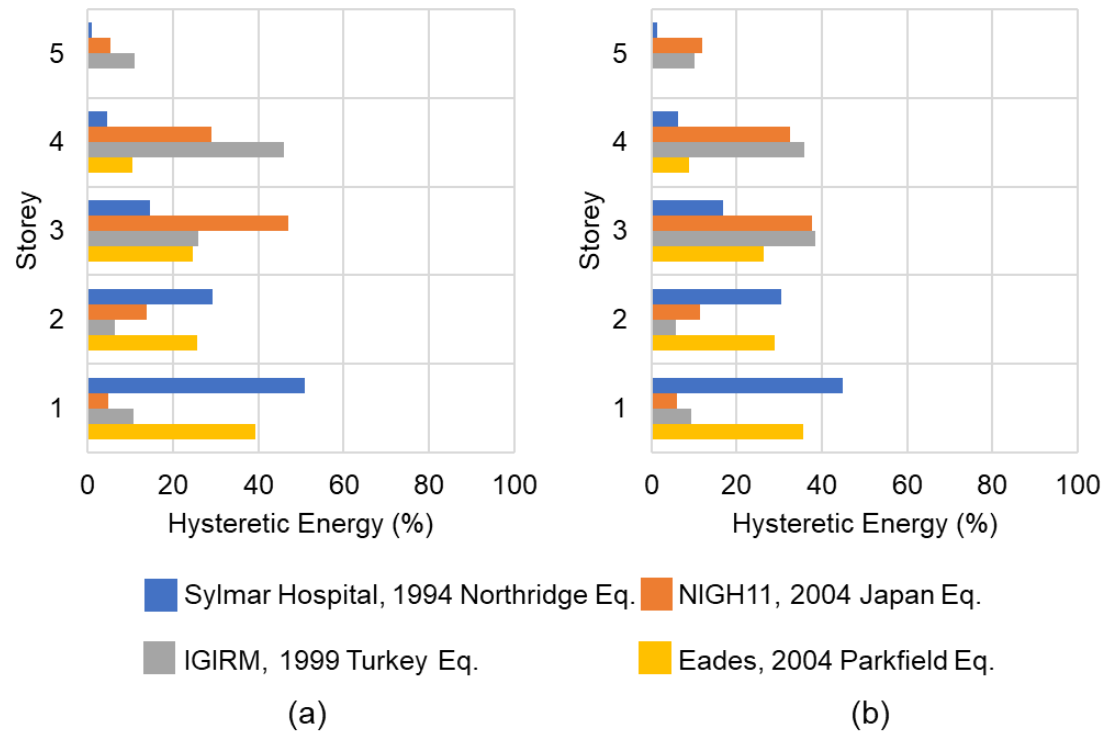


Figure 3.16 Hysteretic energy dissipated by 5-story structure subjected to near-fault ground motions with pulse in (a) longitudinal, and (b) transverse directions

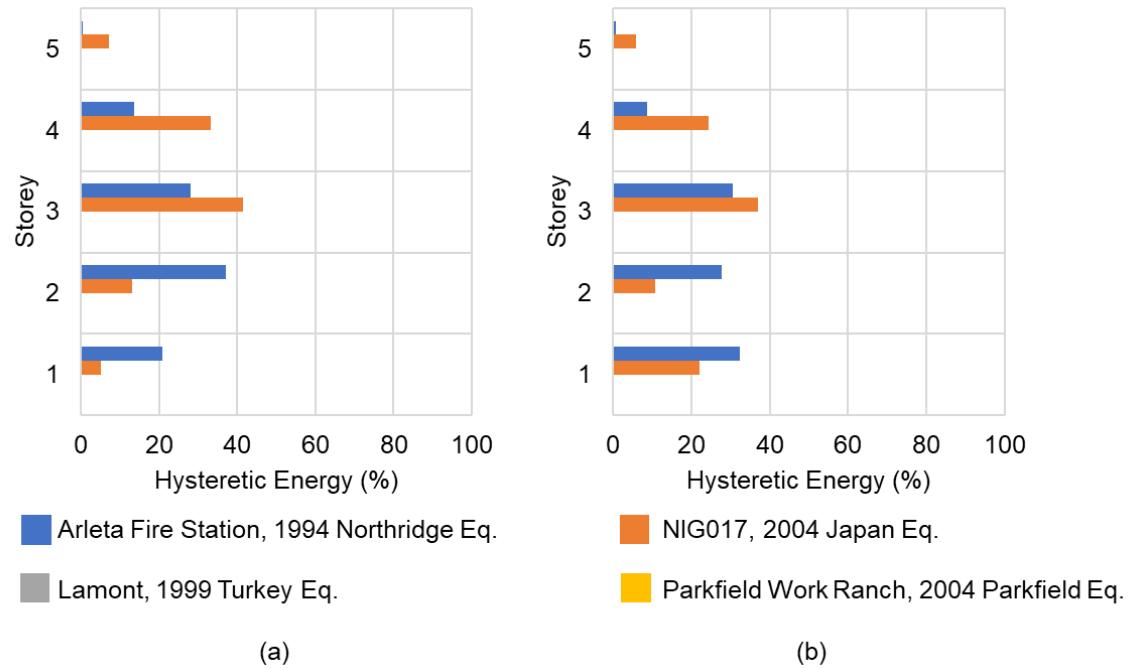


Figure 3.17 Hysteretic energy dissipated by 5-storey structure subjected to near-fault ground motions without pulse in (a) longitudinal, and (b) transverse directions

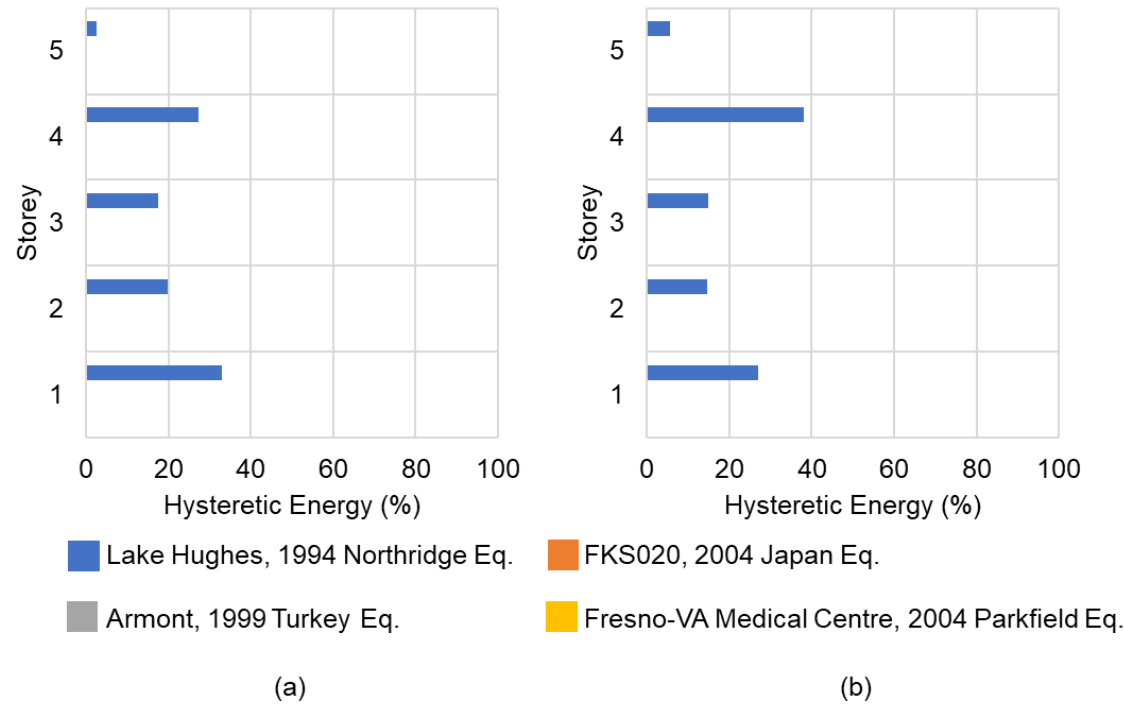


Figure 3.18 Hysteretic energy dissipated by 5-storey structure subjected to far-fault ground motions in (a) longitudinal, and (b) transverse direction

Similarly, figure 3.18 shows the hysteretic energy dissipated by 5-story structure when subjected to far-fault ground motions in both the orthogonal directions. It is observed that the structure remained in elastic state in all the cases except when it is subjected to Northridge ground motions. In this case also, the energy dissipation is higher in the 4<sup>th</sup> storey.

### 3.4.1.2 10 Storey

The response of the 10-Storey structure subjected to the same set of ground motions discussed in the previous section is also represented using maximum inter storey drift (%) and maximum input and dissipated energy which also indicates the expected damage that occurs.

#### 3.4.1.2.1 *Inter Storey Drift (%)*

The maximum inter storey drift at each floor obtained from nonlinear time history analysis of 10-Storey building subjected to near-fault ground motion with pulse is shown in figure 3.19. It is observed that the maximum drift is obtained in the lower floors (i.e., 2<sup>nd</sup> and 4<sup>rd</sup> floors). Also, the maximum drift across the floors is obtained for the Northridge earthquake. Similarly, the maximum inter storey drift when subjected to near-fault ground motions without pulse is shown in the figure 3.20. It is observed that higher drifts are obtained for both Northridge and Japan earthquakes. Also, the maximum drift is observed in the higher floors (i.e., 8<sup>th</sup> floor) of the structure. The value of the maximum drift is obtained less than 0.6%. This value of maximum drift further reduces to less than 0.4% when the structure is subjected to far-fault ground motions. This is shown in the figure 3.21 in which maximum inter-storey drift is indicated at each storey of the 10-storey structure.

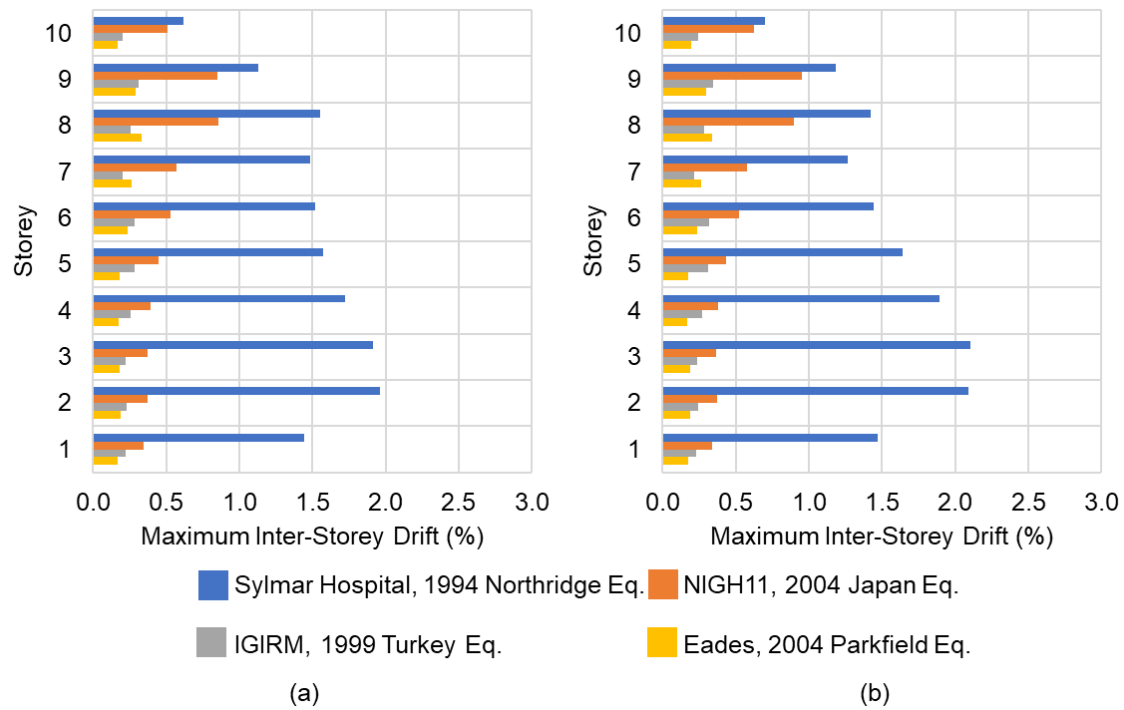


Figure 3.19 Maximum inter storey drift (%) of 10-storey building at each floor subjected to near-fault ground motions with pulse in (a) longitudinal, and (b) transverse direction

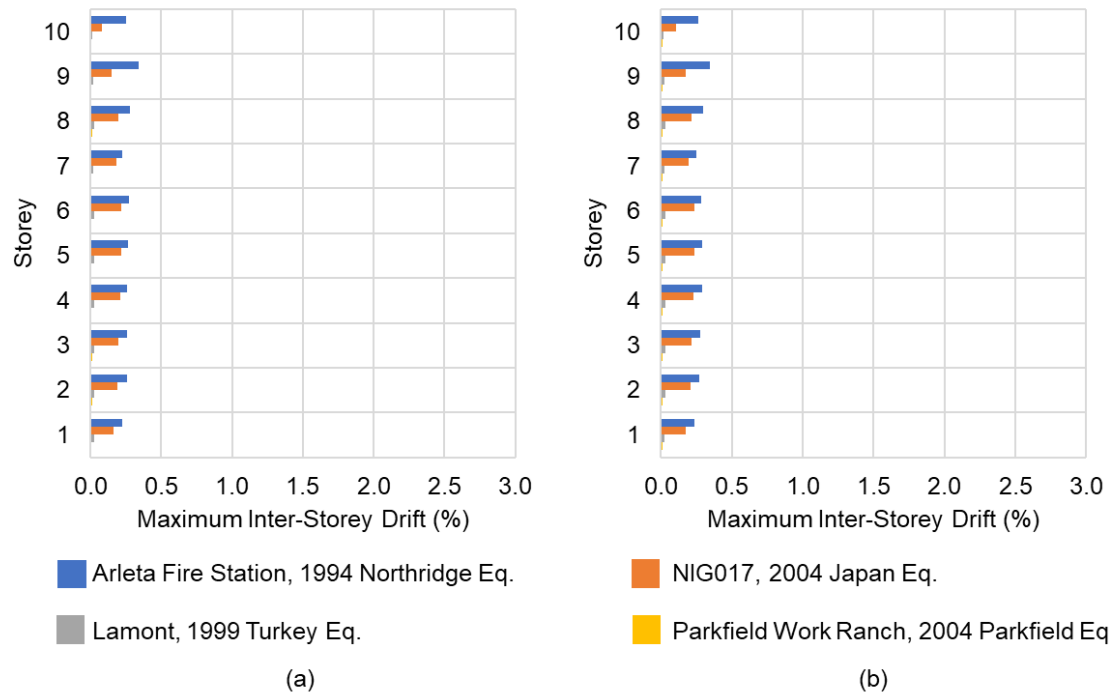


Figure 3.20 Maximum inter storey drift (%) of 10-storey building at each floor subjected to near-fault ground motions without pulse in (a) longitudinal, and (b) transverse direction

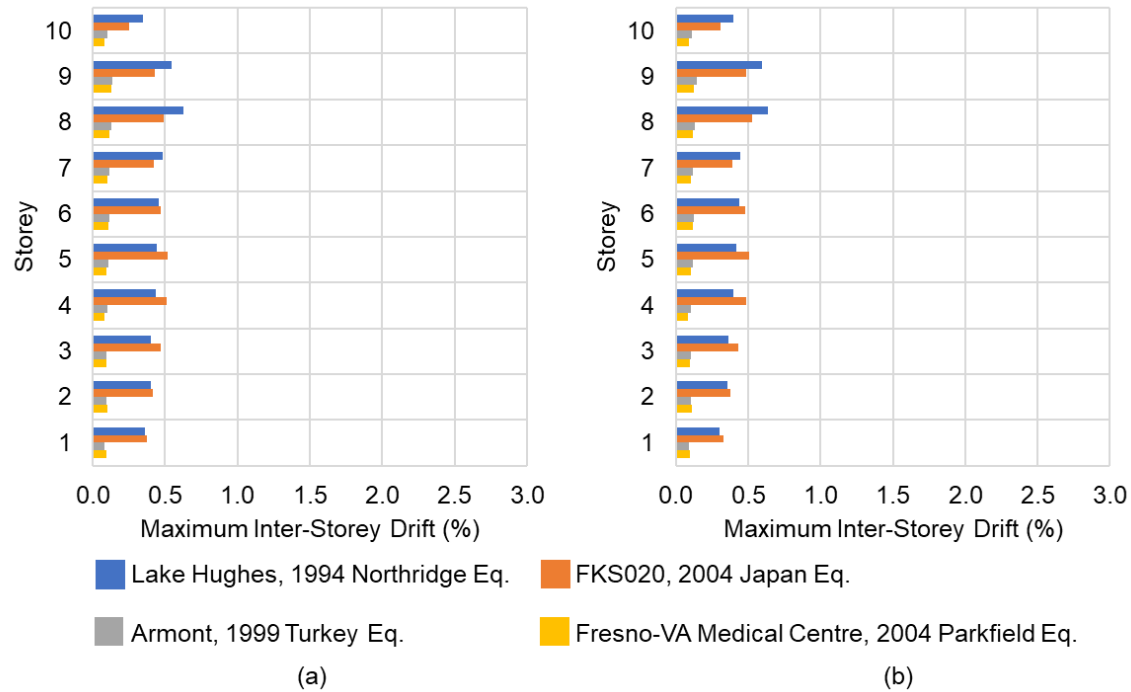


Figure 3.21 Maximum inter storey drift (%) of 10-storey building at each floor subjected to far-fault ground motions in (a) longitudinal, and (b) transverse direction

### 3.4.1.2.2 Energy

The figure showing the dissipated hysteretic energy in relation with the input energy when 10-storey structure is subjected to near-fault ground motions with pulse is shown in figure 3.22. It is observed that the Northridge earthquake results in higher input and hysteretic energy when subjected to near-fault ground motions with pulse. On the other hand, for both the near-fault ground

motion without pulse and far-fault ground motions, the structure remains in elastic state throughout the analysis. This behaviour can be justified by the small amount of input energy that is imparted to the structure.

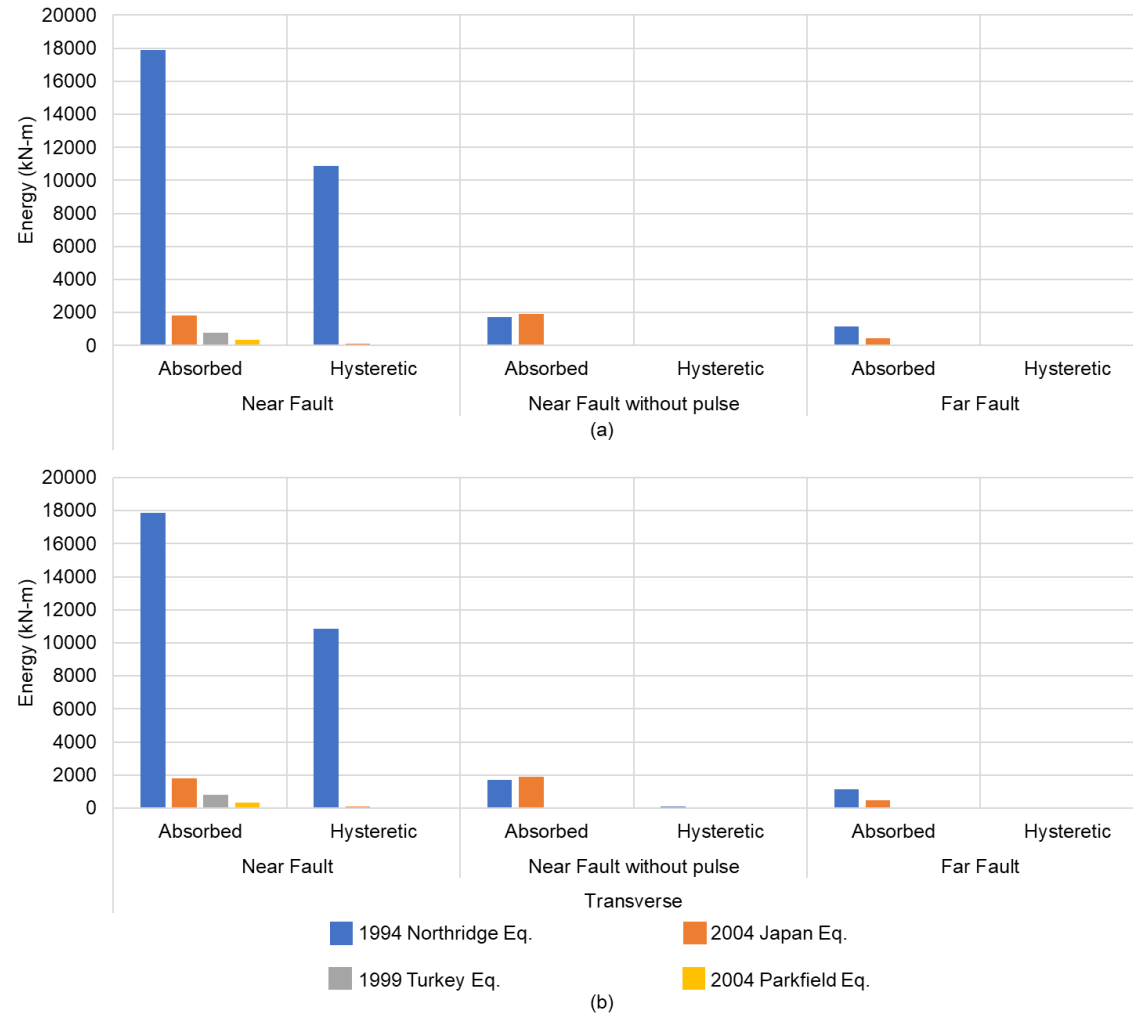


Figure 3.22 Comparison of input energy and dissipated energy of 10-storey structure subjected to different ground motions in (a) longitudinal, and (b) transverse direction

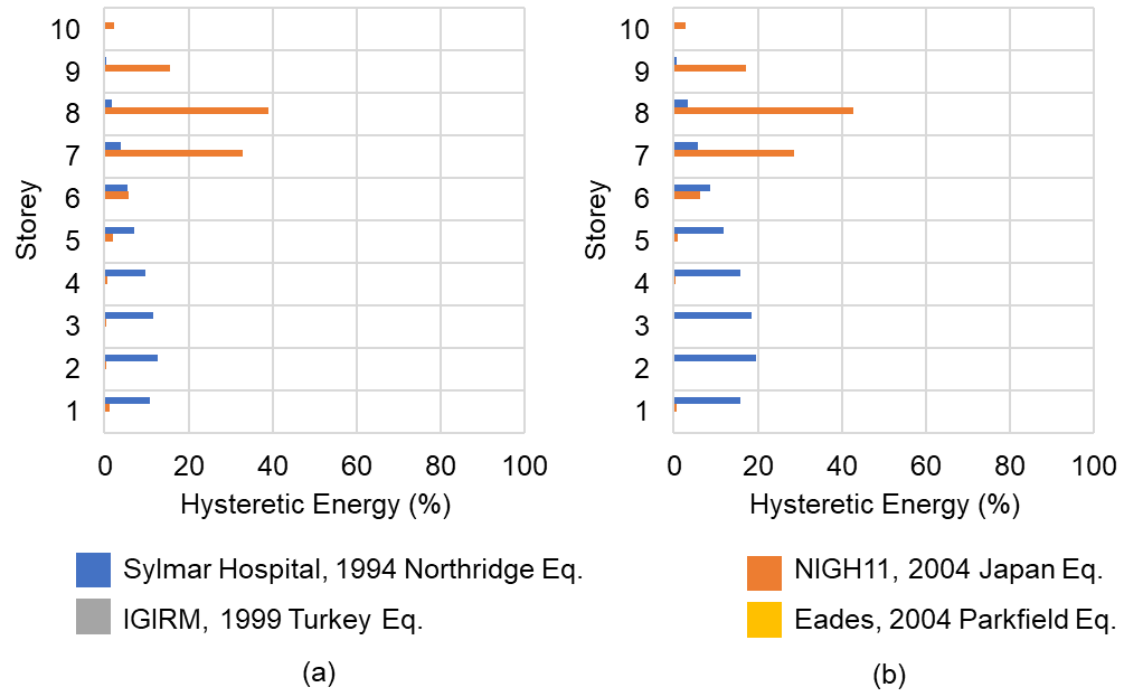


Figure 3.23 Hysteretic energy dissipated by 10-story structure subjected to near-fault ground motions with pulse in (a) longitudinal, and (b) transverse directions

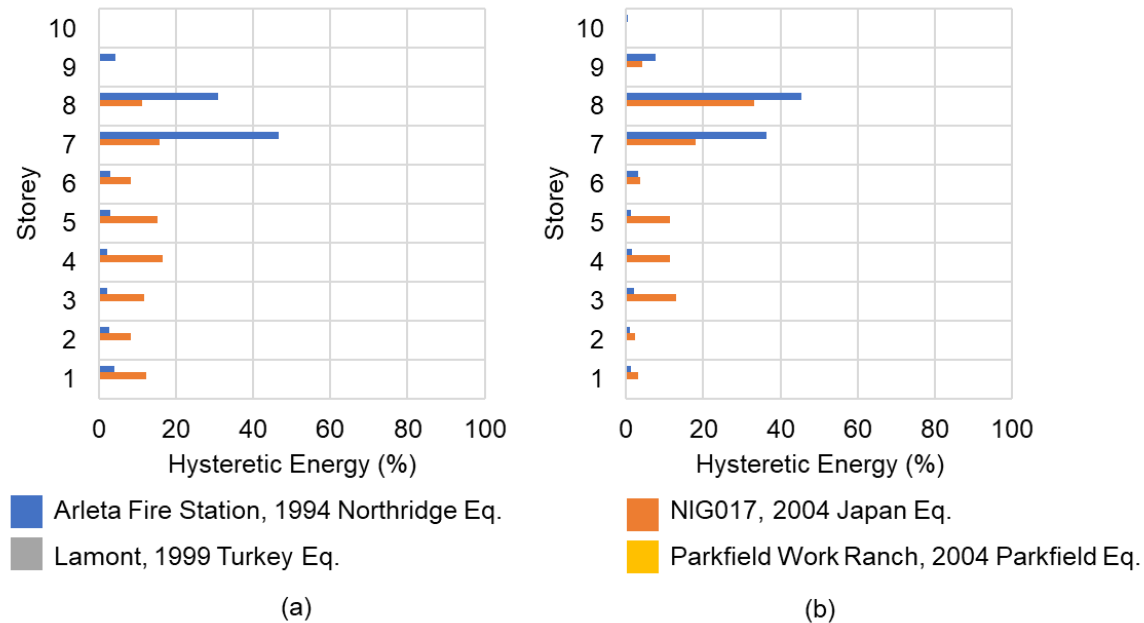
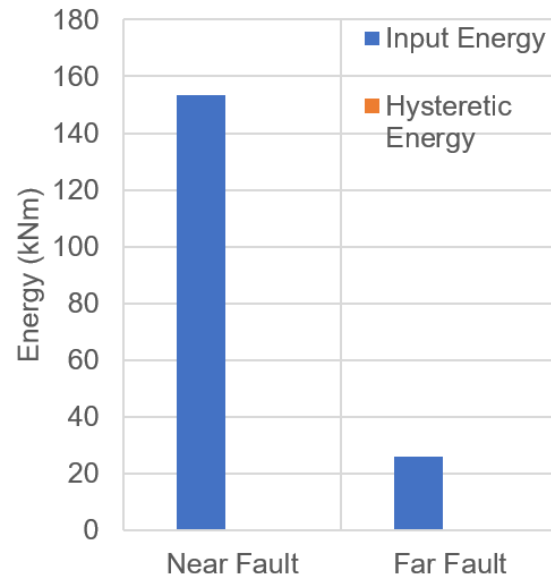


Figure 3.24 Hysteretic energy dissipated by 10-story structure subjected to near-fault ground motions without pulse in (a) longitudinal, and (b) transverse directions

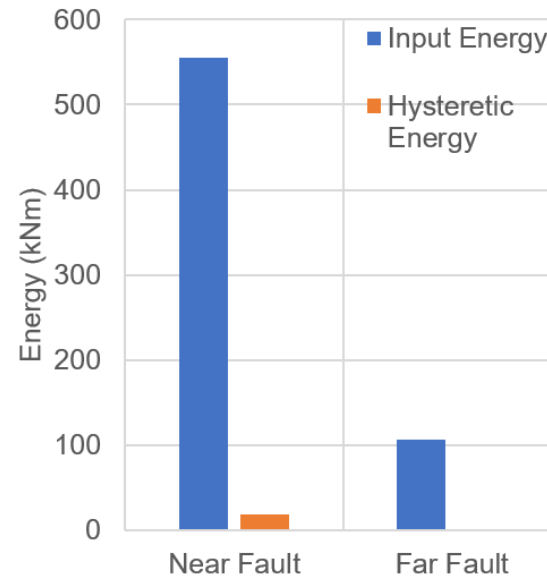
Figure 3.23 shows the energy dissipation at each floor when subjected to near-fault ground motions with pulse. It is observed that energy dissipation is maximum at the higher storeys (i.e., 7<sup>th</sup> and 8<sup>th</sup> storeys) when subjected to Japan earthquake. But the dissipation is maximum at lower floors when subjected to Northridge earthquake. Similar figure for the maximum drift obtained when subjected to near-fault ground motions without pulse is shown in figure 3.24. It is observed that the energy dissipation is maximum at higher storeys (i.e., 7<sup>th</sup> and 8<sup>th</sup> storey) for both Northridge and Japan earthquakes.

### 3.4.2 *Vertical Shaking*

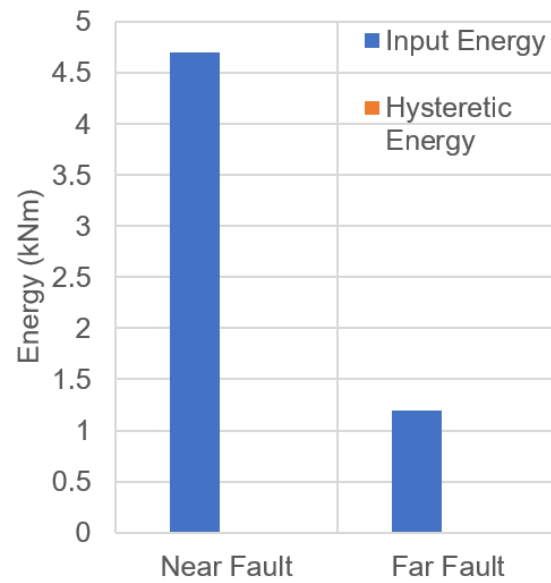
The nonlinear analysis of 5-storey structure subjected to vertical ground motion indicates that vertical component results in considerable higher peak values. The comparisons are made in terms of energy imparted and energy dissipated in the structure. Figure 3.25 shows the comparison of input energy imparted and hysteretic energy dissipated when subjected to the ground motion cases as defined above in longitudinal direction. Similarly, Figure 3.26 shows the comparison of input energy imparted and hysteretic energy dissipated when subjected to the ground motion cases as defined above in transverse direction. In all the cases, the near fault ground motions indicate comparatively higher input energy imparted than the far fault ground motions. However, the values are considerably lower in the third case in which vertical ground motion along with 30% fault parallel ground motions are applied. Also, the first case in which only vertical ground motion is applied indicates lower values than the other two cases. In the other two cases, where fault normal component is applied in addition to the vertical ground motion, the structure reached nonlinearity dissipating a percentage of energy imparted to it. This indicates that vertical ground motion alone may not cause great threat to normal structures. The distribution of hysteretic energy dissipated at each floor is shown in Figure 3.27 and 3.28, in longitudinal and transverse directions, respectively. In both the directions, the energy dissipated is maximum at the first floor and gradually reduces at the top floor.



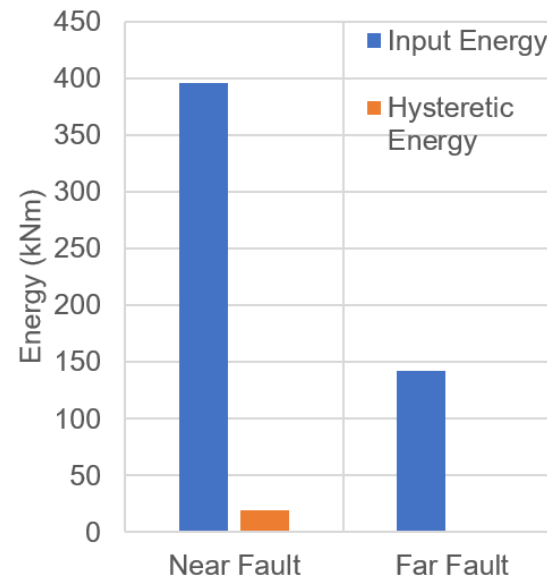
(a)



(b)

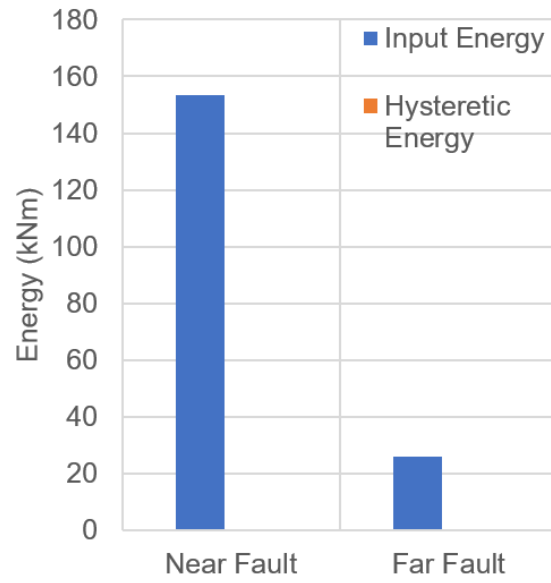


(c)

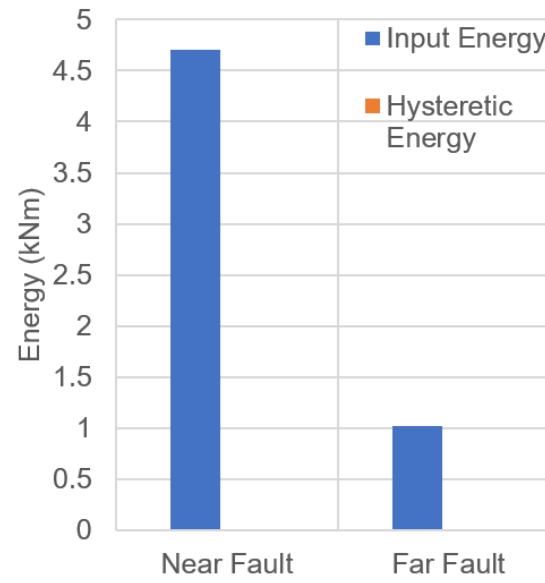


(d)

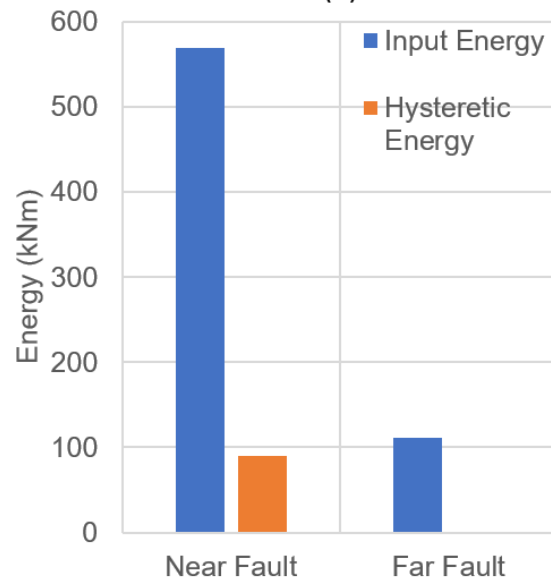
*Figure 3.25 Comparison on input energy and hysteretic energy of 5-storey structure in longitudinal direction subjected to (a) 100% Vertical, (b) 100% Vertical and 30% fault normal in longitudinal direction, (c) 100% Vertical and 30% fault parallel in transverse direction, and (d) 100% Vertical, 30% fault normal in longitudinal direction and 30% fault parallel in transverse direction*



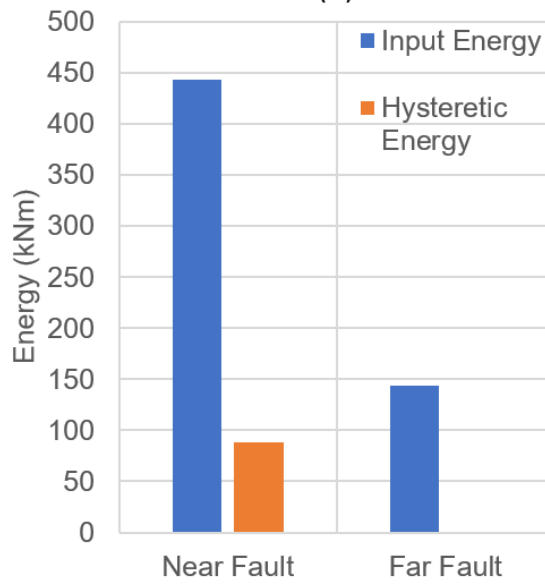
(a)



(b)



(c)



(d)

Figure 3.26 Comparison on input energy and hysteretic energy of 5-storey structure in transverse direction subjected to (a) 100% Vertical, (b) 100% Vertical and 30% fault normal in longitudinal direction, (c) 100% Vertical and 30% fault parallel in transverse direction, and (d) 100% Vertical, 30% fault normal in longitudinal direction and 30% fault parallel in transverse direction

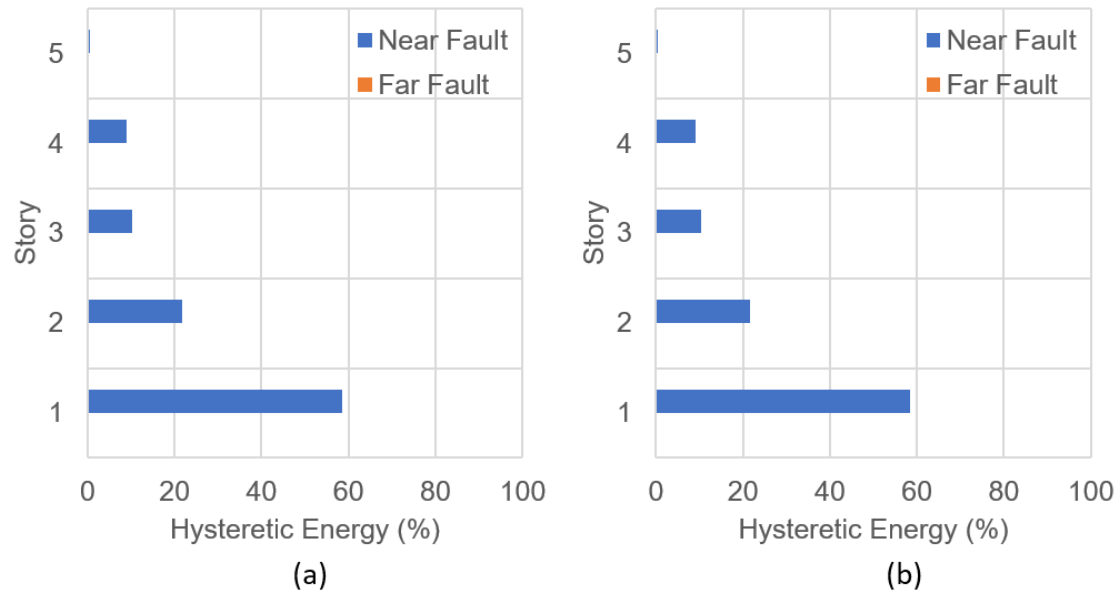


Figure 3.27 Distribution of hysteretic energy across floors of 5 storey structure in longitudinal direction obtained from nonlinear time history analysis when subjected to (a) 100% Vertical ground motion and 30% fault normal in longitudinal direction, and (b) 100% Vertical ground motion, 30% fault normal in longitudinal direction and 30% fault parallel in transverse direction

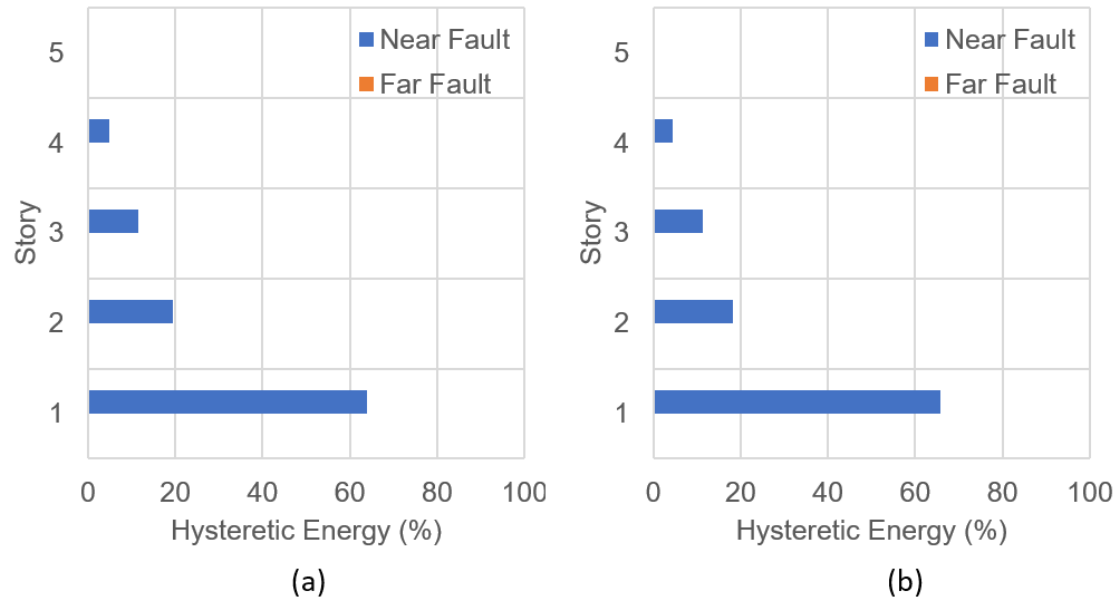
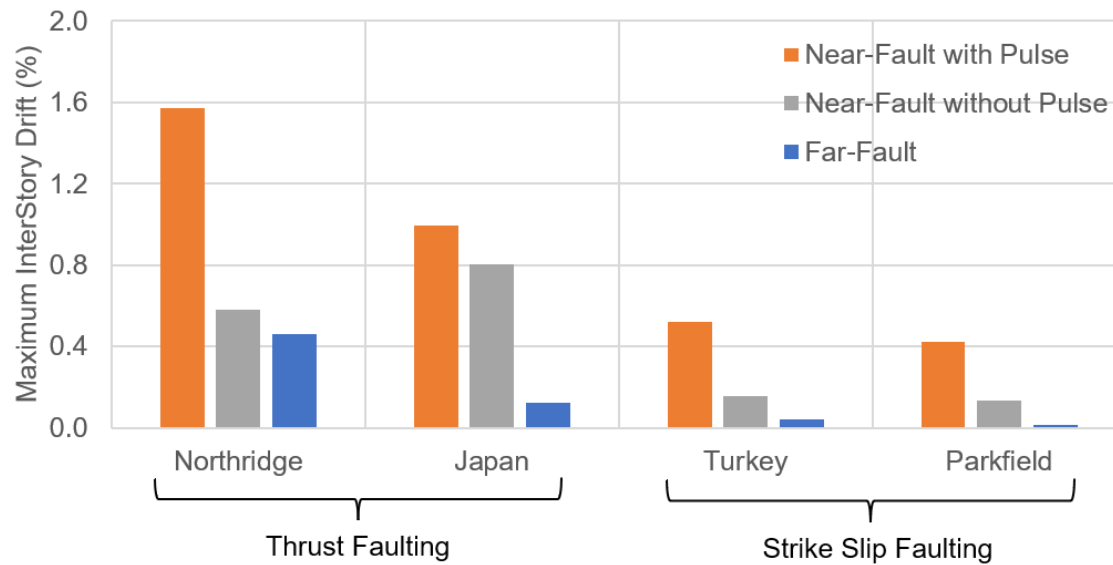


Figure 3.28 Distribution of hysteretic energy across floors of 5 storey structure in transverse direction obtained from nonlinear time history analysis when subjected to (a) 100% Vertical ground motion and 30% fault normal in longitudinal direction, and (b) 100% Vertical ground motion, 30% fault normal in longitudinal direction and 30% fault parallel in transverse direction

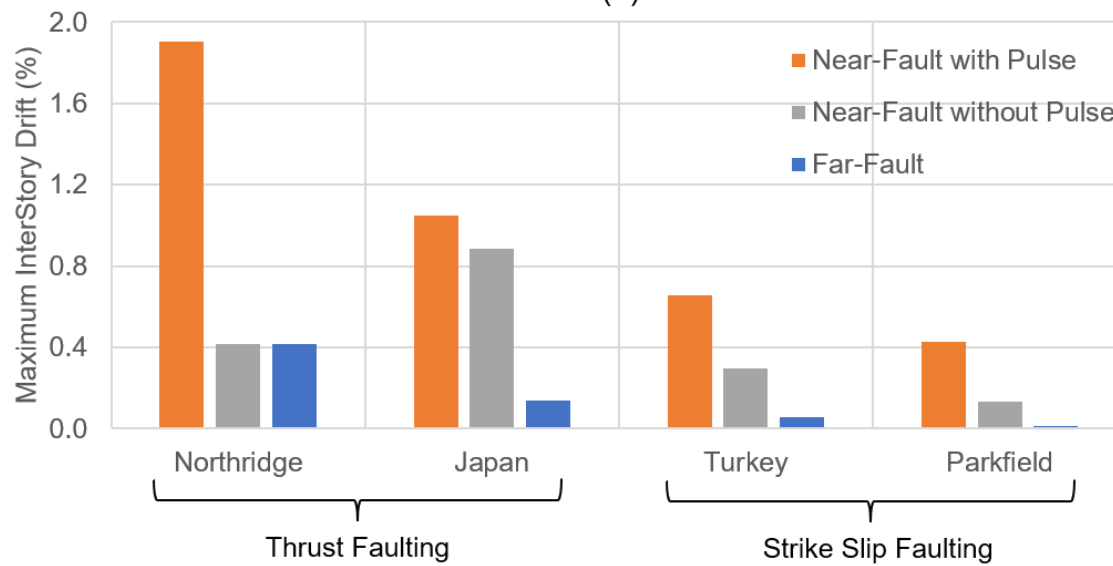
### 3.5 OBSERVATIONS

Figures 3.29 and 3.30 show the maximum inter storey drift of 5- and 10-storey structure when subjected to near and far-fault ground motions, respectively. The following observations about the behaviour of 5 and 10-storey buildings are made from the nonlinear time history analysis performed.



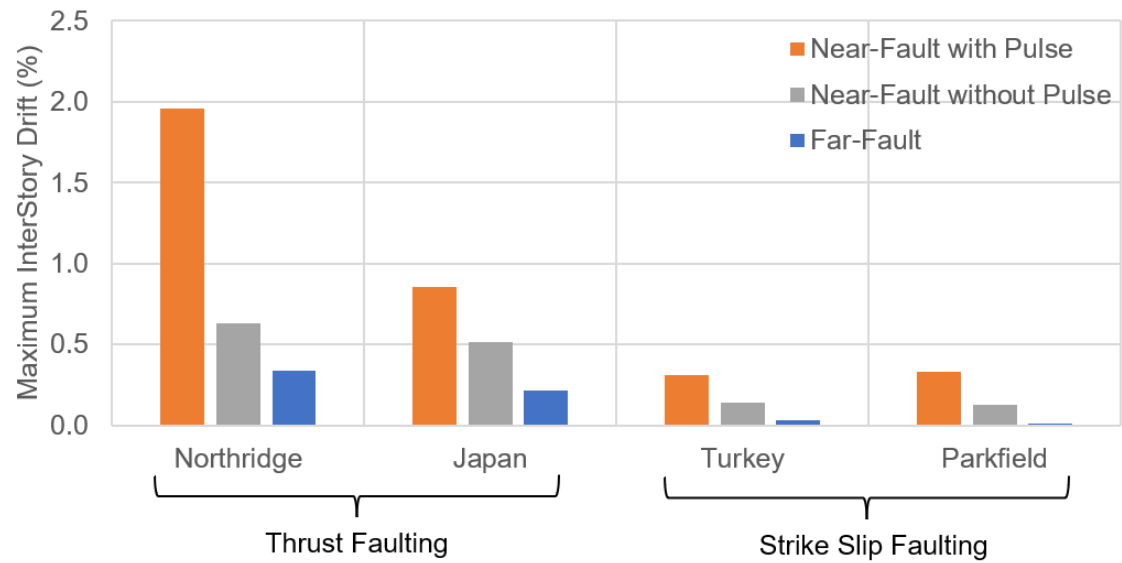


(a)

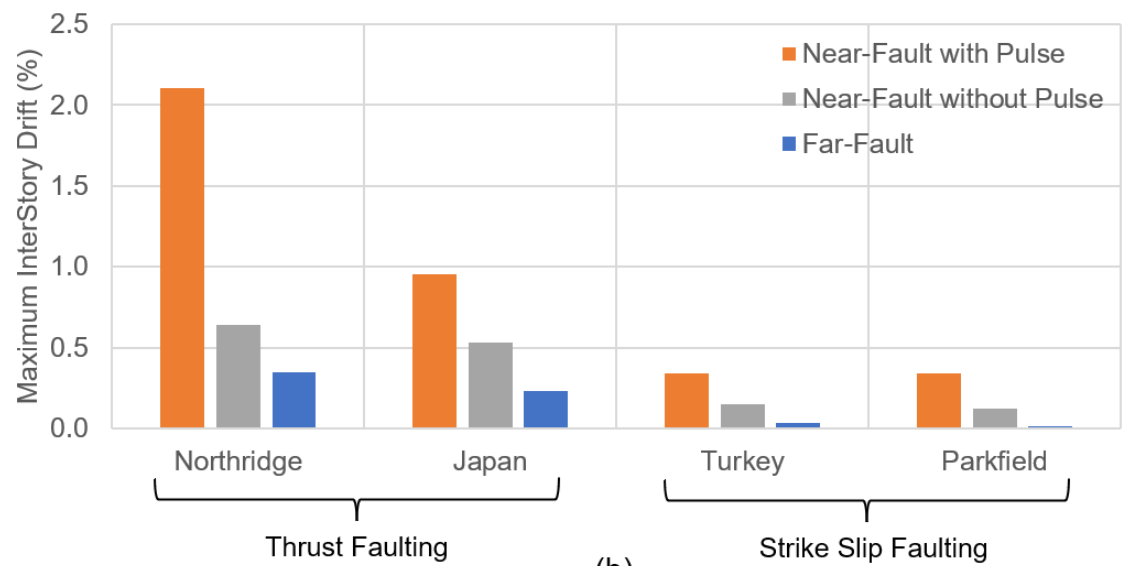


(b)

*Figure 3.29 Maximum inter storey drift (%) of 5-story structure when subjected to different ground motions in (a) longitudinal, and (b) transverse directions*



(a)



(b)

*Figure 3.30 Maximum inter storey drift (%) of 10-story structure when subjected to different ground motions in (a) longitudinal, and (b) transverse directions*

In view of the observations made in the structures when subjected to near and far-fault ground motions recorded during Northridge and Japan earthquakes, the results are consistent across the earthquakes in both the structures. Although, higher drifts are observed when subjected to near-fault ground motions in all the cases, the maximum drift is present in the lower floors when Northridge ground motions are applied. But higher storeys observe higher drift in the case of Japan earthquake. The low inter storey drift can be attributed to the peak ground acceleration of 0.53g for near-fault ground motion recorded during Japan earthquake. But it is usually anticipated to observe higher drifts for Japan earthquake since the buildings period (1.77 sec) matches with the pulse period of the Japan ground motions (1.78 sec) in contrast with Northridge ground motion (2.14 sec). Also, upper floors observed to dissipate more energy than the lower floors unlike Northridge earthquake.

It is observed that the structure attained inelastic drifts at the initial time instant after the start of the near fault double sided pulse. Another important aspect is that the response after the pulse is mostly elastic which indicates that the ground motion might not contain high amplitude pulse. This observation shows that the structure can withstand the near-fault ground motions if it can retain the high amplitude pulse in short duration.

### 3.6 CONCLUSIONS

The chapter deals with the nonlinear analysis of 5 and 10-storey buildings subjected to ground motions recorded in two thrust earthquakes and two strike slip earthquakes. The behaviour of the structures when near fault ground motions are observed to be comparatively vulnerable than that observed during far fault ground motions. The behaviour of the structures is studied by observing the maximum inter-storey drift (%) and the hysteretic energy dissipated with respect to the input energy imparted to the structure.

In the case of 5-storey structure, the maximum inter storey drift across all the analysis cases is obtained as 1.6% and 2% for near-fault ground motion with pulse in the longitudinal and transverse directions, respectively. Similarly, in the case of 10-storey structure, the maximum inter storey drift across all the analysis cases is obtained as 2.1% and 2.2% for near-fault ground motions with pulse in the longitudinal and transverse directions, respectively. This drift corresponds to moderate performance limit state according to the FEMA guidelines. In addition to the drifts, in the case of near fault ground motions with pulse, it is observed that the response time history of the structure attains elasticity in a short duration of time and later the structure may remain in elastic state. Thus, a moment resisting frame is insufficient to resist the near fault ground motions without modifications to the presence of structural wall even when classical earthquake resistant design principles are followed.

*Blank Page*

## 4 Effect of Near-Fault Ground Motions on Frame Buildings with Structural Walls

### 4.1 BACKGROUND

The most important difference between near fault and far fault ground motions is the presence of short duration impulse that occurs in the initial time instant of the near fault ground motion. Observations from the response of reinforced concrete moment resisting framed buildings reveal that although near fault ground motions contain short duration pulses, the number of plastic excursions are more for far fault ground motions. Also, far fault ground motions contain long period components that attenuate at very high distances. Therefore, the strategy of design of structures to resist near fault ground motions and far fault ground motions are different. In the case of far fault ground motions, the structure is required to dissipate the energy imparted in each cycle of ground motion through inelastic excursions yet retain the sufficient strength to carry the gravity loads. However, in the case of near fault ground motions, the structure is required to resist the short duration high amplitude pulse that occurs in the initial time instant only. Since, in most of the cases, the ground motion after the high amplitude pulse is less likely to cause large inelastic excursions.

The most intuitive mitigation technique to resist both near fault and far fault ground motions is to adopt structural walls in the moment resisting frames to impart sufficient strength to withstand high amplitudes, and required ductility to dissipate the huge inelastic energy demand imposed by the ground motion. Therefore, structural walls are adopted in the frames with varying structural plan density defined as the ratio of plan area of structural walls to that of the total plan area of the building. The improvements in the behaviour of structures with structural walls is observed and interpretations are derived.

## **4.2 GROUND MOTIONS CONSIDERED**

For the purpose of the study, two earthquakes in each of the source mechanisms are considered. 1995 Northridge earthquake and 2004 Japan earthquake are predominantly reverse/thrust faulting mechanism; 1999 Turkey earthquake and 2004 Parkfield earthquake are predominantly strike slip earthquakes. Table 3.1 shows the list of horizontal and vertical ground motion data set considered for carrying out the study similar to the moment frame buildings.

## **4.3 ANALYTICAL MODEL OF BUILDING**

Two buildings with 5-storey and 10-storey with same plan dimensions as that of moment resisting frames with floor-to-floor height of 4.5 m and with bay width of 4 m in 6 x 4 no. of bays in x and y directions, respectively are considered for the study. The same gravity loads are applied on the structure as that of moment resisting frame. Figure 4.1 shows the arrangement of structural walls in the building in three arrangements of walls with structural plan density 2.75, 3.75 and 9%. The prescribed 73 load combinations are defined to arrive at the design cross section sizes of beams, columns and structural walls. The first two models with partial structural walls are designed as dual systems in which the lateral load is resisted by a combining action of both moment resisting frames and structural walls. Hence, as prescribed by the codes, atleast 25% of the lateral loads are shared to the frames in arriving at the design forces. To ensure this clause, the reaction at the base of structural walls is subtracted from the total base reactions. This sum of reactions should be equal to or greater than 25% of the total base reactions. If it is less than the total base reactions, the design load combination are multiplied with a factor equal to the ratio of 0.25 times the total reactions and reactions at the columns bases obtained as above. The design is carried out in ETABS 2000 v19.

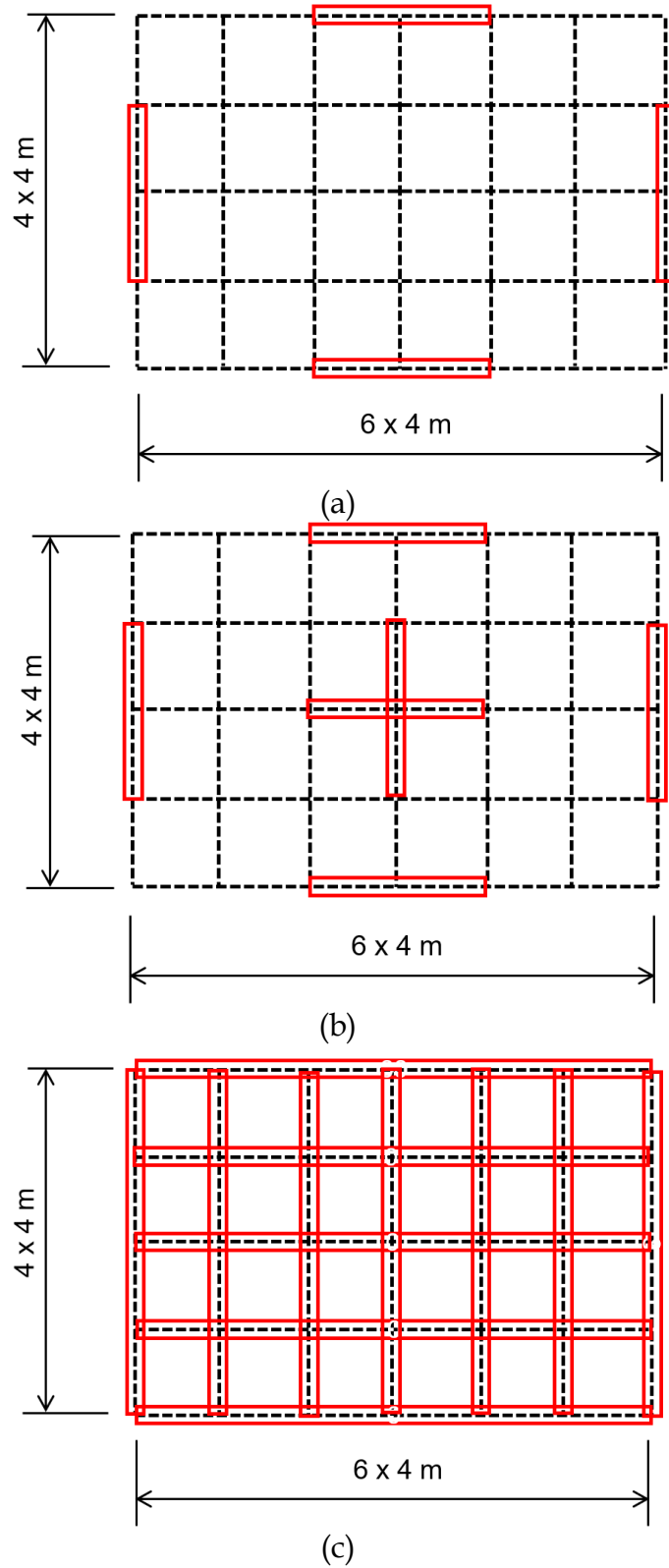


Figure 4.1 Structural plan showing (a) moment resisting frames and structural walls with SPD 2.75%, (b) moment resisting frames and structural walls with SPD 3.75%, and (c) complete structural walls with SPD 9%

## 4.4 NONLINEAR TIME HISTORY ANALYSIS

As discussed in the previous chapter, the nonlinearity in beams is modelled as a lumped plasticity model at the ends of the member and in columns as fibre hinges lumped at the ends of the members. Structural walls are modelled as wide columns with dummy beams supported by them to carry gravity loads. The density of the dummy beams is ensured to be zero not to transfer the self-weight of the beams. Also, the bending moments at the ends of the member are released not to transfer them to the columns [Kwan, 1993]. The reinforcement in the design section obtained are given to members through section designer module of the software SAP 2000 v23.

### 4.4.1 *Horizontal Shaking*

The primary focus of the study is to observe the earthquake response of the moment resisting frame building that is designed by conventional earthquake resistant design principles, drift gives a simple representation of the earthquake resistance. Hence, Inter-storey Drift Ratio (IDR) calculated as the relative displacement between two consecutive stories is the primary comparison parameter. Similarly, the damage observed is indicated by calculating the dissipated hysteretic energy from the hysteretic moment rotation relationship obtained from the analysis.

#### 4.4.1.1 5-Storey

Figure 4.2 shows the improvement in the response of structure with addition of structural walls. Figures 4.3 and 4.4 shows the plots of maximum IDR obtained for 5-storey structure with different structural systems subjected to the considered near-fault ground motions with pulse in the longitudinal and transverse directions, respectively. The same information is shown in table 4.1. It is observed that maximum inter-storey drift reduced with increase in structural plan density of walls provided. Out of all the ground motions, Northridge earthquake imposed higher drift demands

on the structures that can be justified by the large amplitude of the pulse present in the ground motion.

Table 4.1 Improvement in the Maximum Inter-Storey Drift (%) at each storey of 5-story structure subjected to near-fault ground motions with pulse in 4 earthquakes.

Storey	Earthquake	MRF	MRF+SW1	MRF+SW2	MR+SW3
5	Sylmar, 1994 Northridge Eq.	0.84	0.59	0.24	0.08
	NIGH11, 2004 Japan Eq.	0.71	0.50	0.13	0.06
	IGIRM, 1999 Turkey Eq.	0.38	0.21	0.11	0.06
	Eades, 2004 Parkfield Eq.	0.19	0.18	0.06	0.03
4	Sylmar, 1994 Northridge Eq.	1.25	1.28	0.31	0.11
	NIGH11, 2004 Japan Eq.	0.99	0.56	0.17	0.08
	IGIRM, 1999 Turkey Eq.	0.52	0.23	0.13	0.08
	Eades, 2004 Parkfield Eq.	0.37	0.20	0.07	0.04
3	Sylmar, 1994 Northridge Eq.	1.49	1.28	0.41	0.14
	NIGH11, 2004 Japan Eq.	0.89	0.59	0.22	0.09
	IGIRM, 1999 Turkey Eq.	0.47	0.24	0.14	0.11
	Eades, 2004 Parkfield Eq.	0.42	0.19	0.08	0.04
2	Sylmar, 1994 Northridge Eq.	1.57	1.52	0.45	0.15
	NIGH11, 2004 Japan Eq.	0.63	0.53	0.24	0.09
	IGIRM, 1999 Turkey Eq.	0.35	0.21	0.14	0.09
	Eades, 2004 Parkfield Eq.	0.39	0.16	0.08	0.04
1	Sylmar, 1994 Northridge Eq.	1.45	1.02	0.46	0.13
	NIGH11, 2004 Japan Eq.	0.46	0.37	0.23	0.06
	IGIRM, 1999 Turkey Eq.	0.36	0.15	0.11	0.06
	Eades, 2004 Parkfield Eq.	0.31	0.10	0.05	0.02

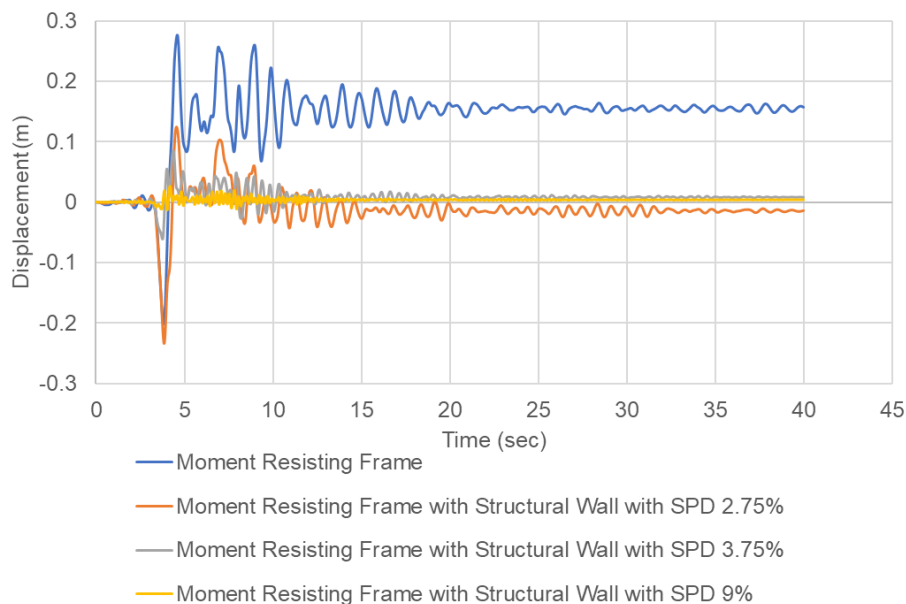


Figure 4.2 Displacement time history of 5-storey structure subjected to near-fault ground motion with pulse recorded during 1994 Northridge earthquake with (a) Moment resisting frame (b) Moment resisting Frame with structural wall of SPD 2.75%, (c) Moment resisting frame with structural walls of SPD 3.75%, and (d) Structural wall with SPD 9%

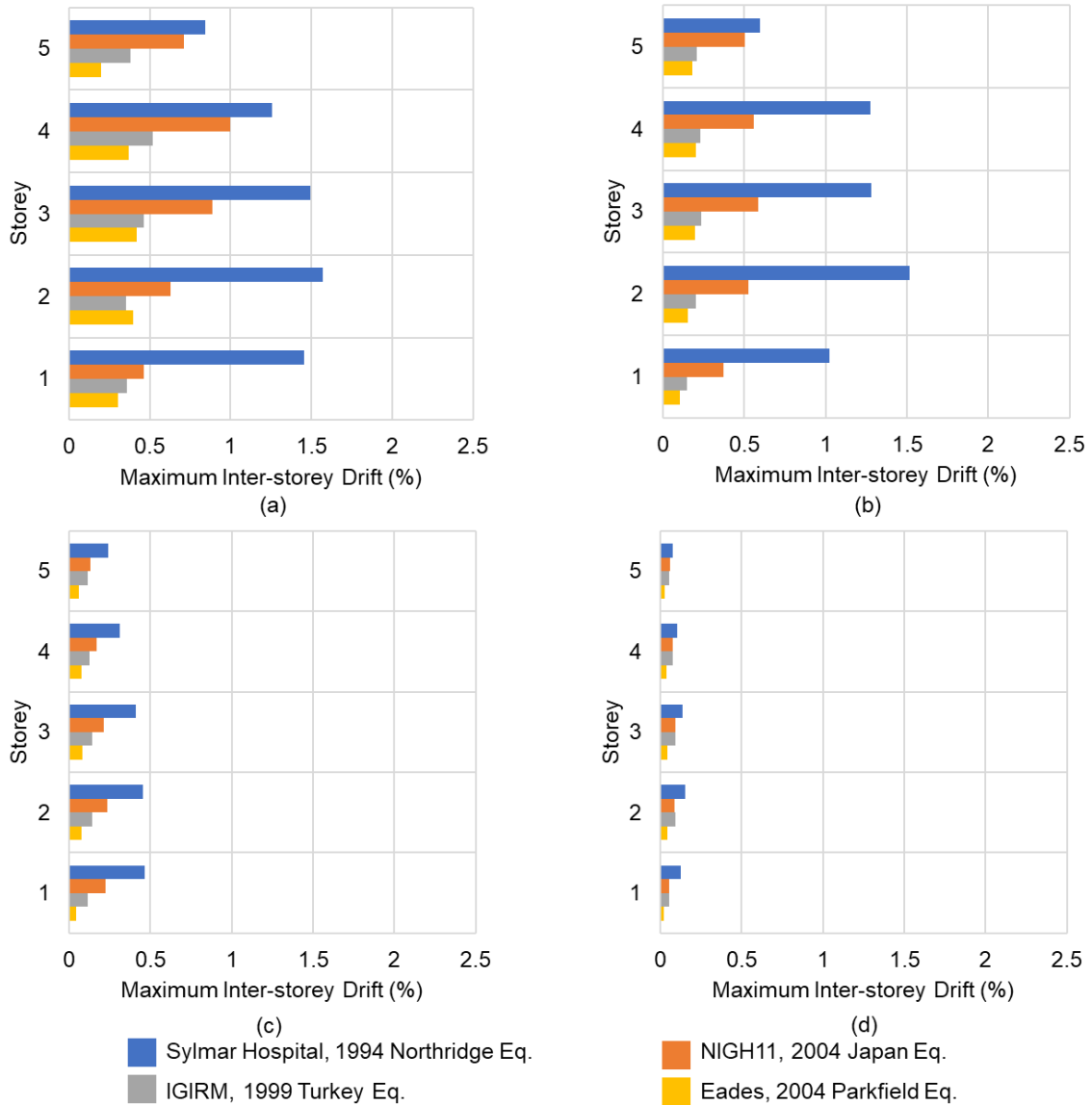


Figure 4.3 Maximum IDR in longitudinal direction at each floor of 5-storey building subjected to near-fault ground motions with pulse with different lateral force resisting systems (a) moment resisting frame, (b) moment frame with wall of SPD 2.75%, (c) moment frame with wall of SPD 3.75%, and (d) wall with SPD 9%

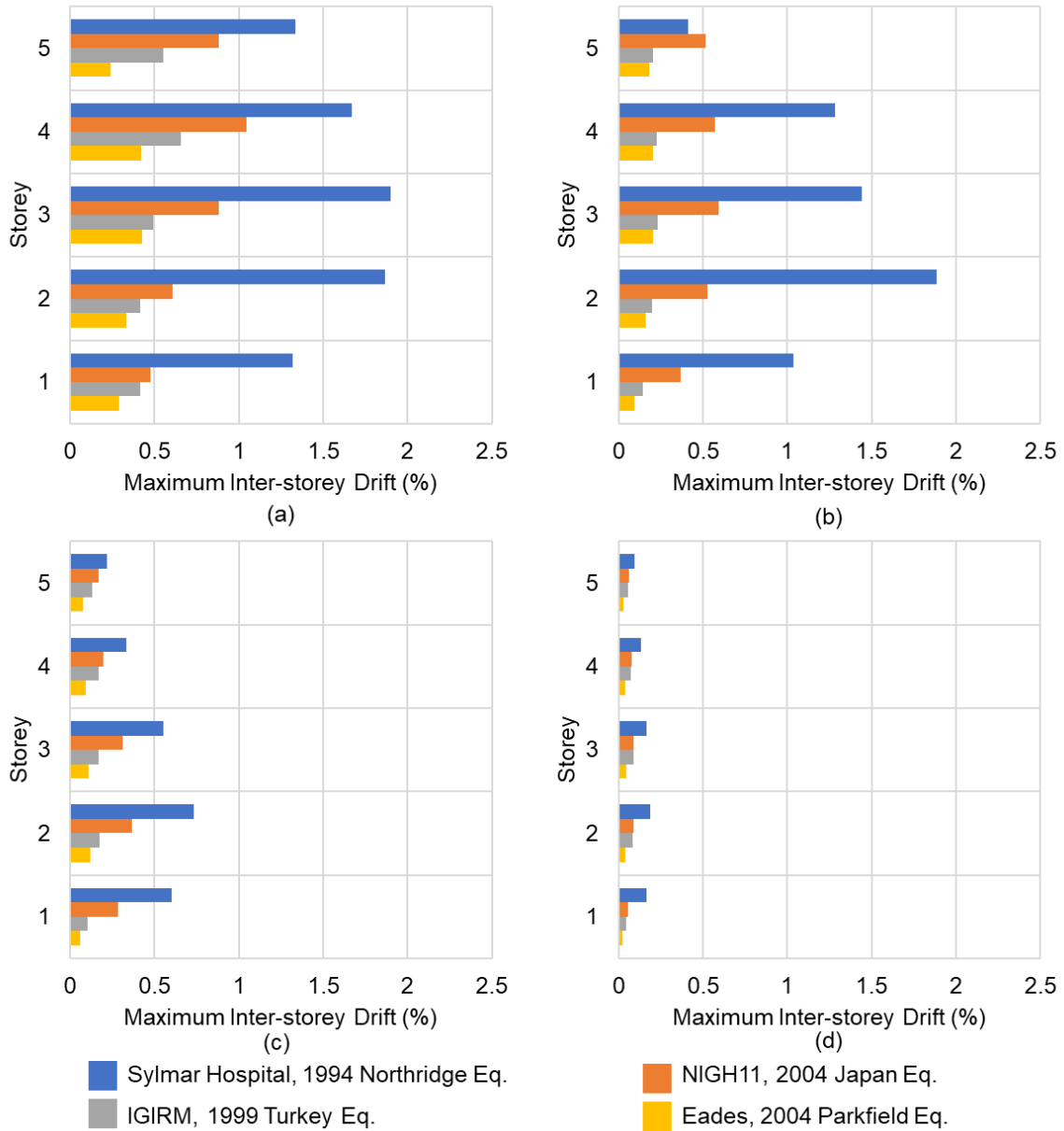


Figure 4.4 Maximum IDR in transverse direction at each floor of 5-storey building subjected to near-fault ground motions with pulse with different lateral force resisting systems (a) moment resisting frame, (b) moment frame with wall of SPD 2.75%, (c) moment frame with wall of SPD 3.75%, and (d) wall with SPD 9%

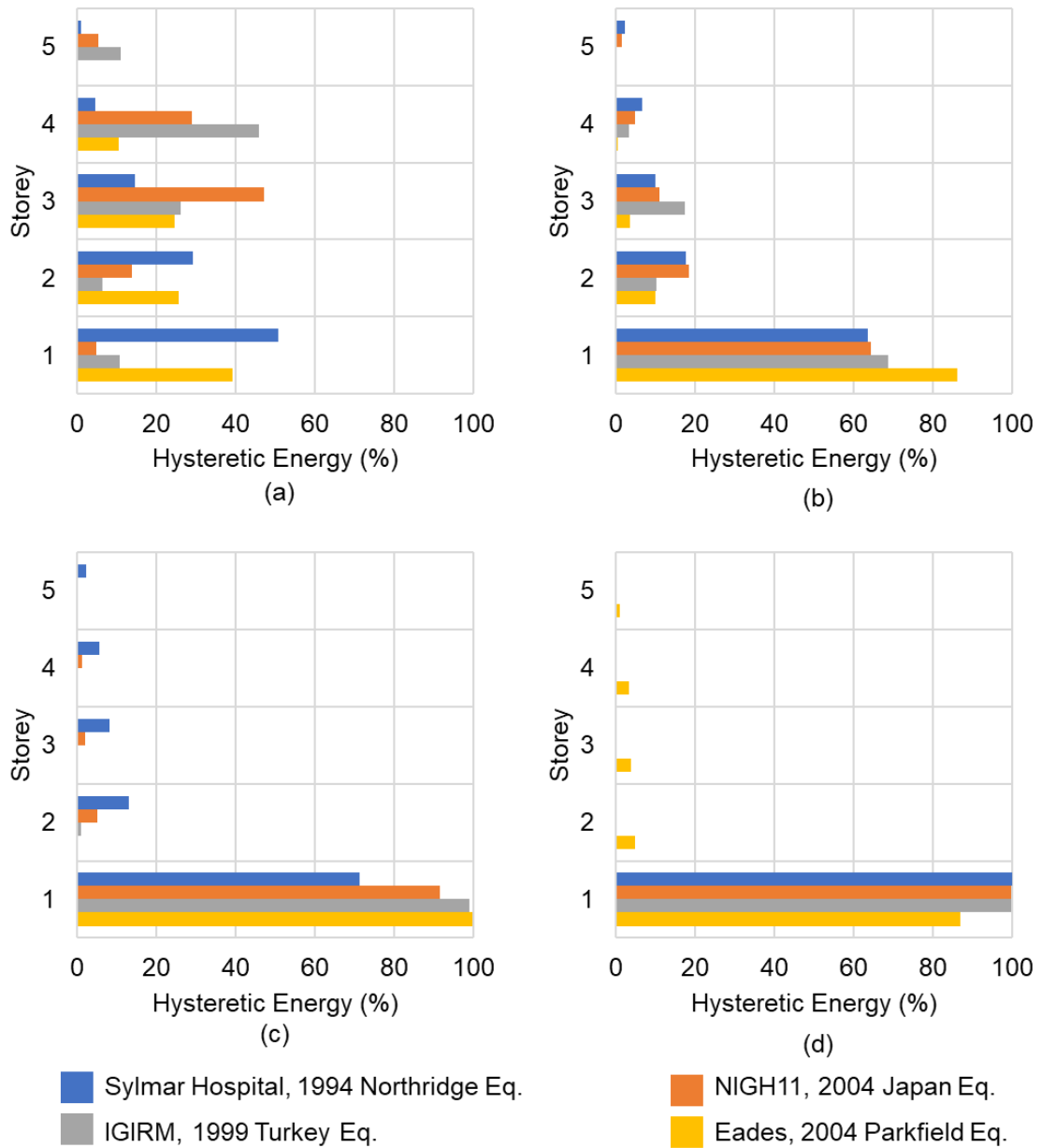


Figure 4.5 Distribution of hysteretic energy in longitudinal direction at each floor of 5-storey building subjected to near-fault ground motions with pulse with different lateral force resisting systems (a) moment frame, (b) moment frame with wall of SPD 2.75%, (c) moment frame with wall of SPD 3.75%, and (d) wall of SPD 9%

Figures 4.5 and 4.6 represent the distribution of hysteretic energy across all the storeys subjected to near-fault ground motions with pulse. It is observed that the energy dissipated increases as the SPD of walls increases. This increase is due to the enhanced ductility of the structure because of the presence of structural walls.

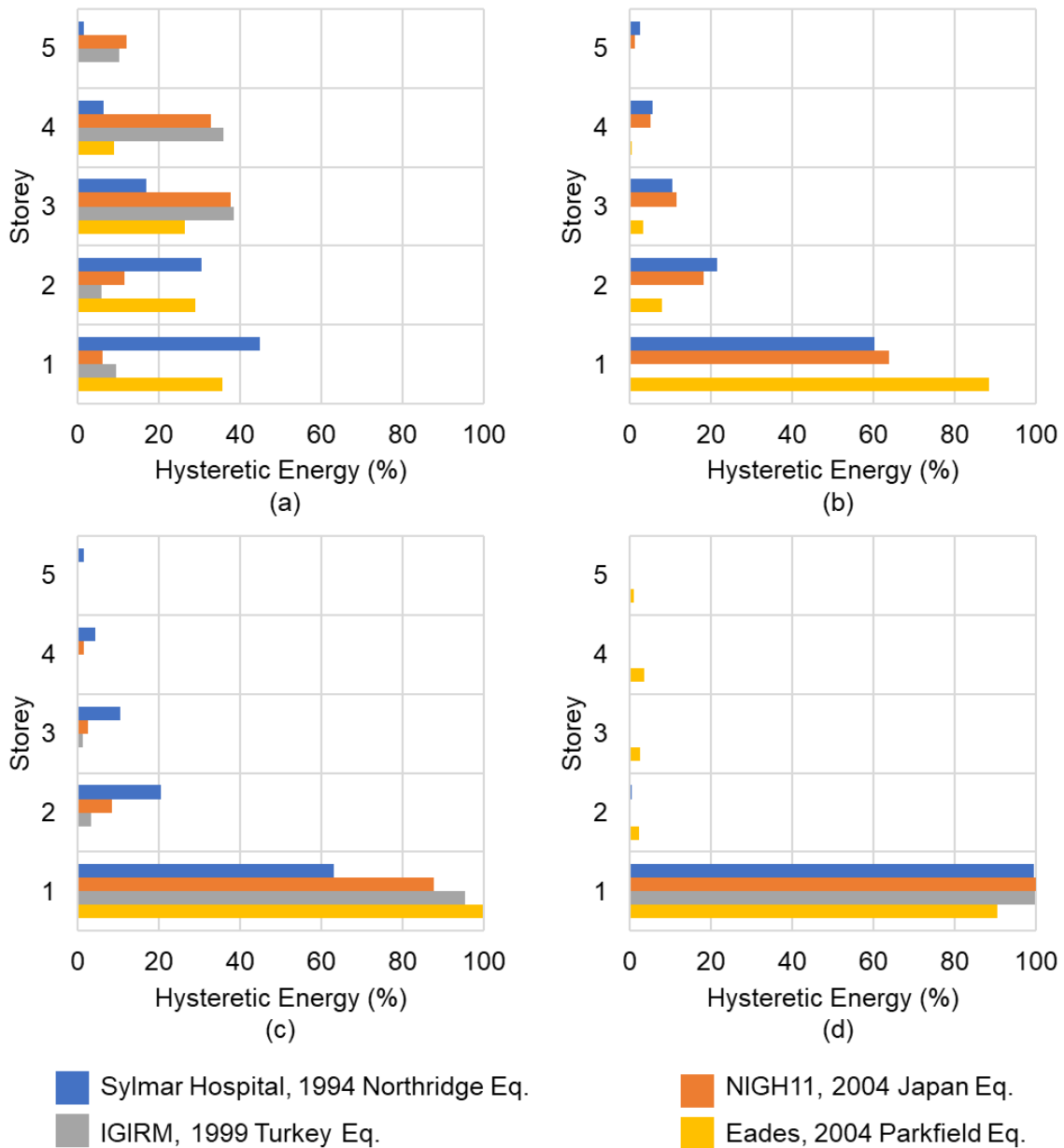


Figure 4.6 Distribution of hysteretic energy in transverse direction at each floor of 5-storey building subjected to near-fault ground motions with pulse with different lateral force resisting systems (a) moment resisting frame, (b) moment frame with wall of SPD 2.75%, (c) moment frame with wall of SPD 3.75%, and (d) wall with SPD 9%

The large energy dissipation allows the structure to withstand large amplitudes of ground motion. Also, most of the damage is concentrated at the base of the structure unlike moment frame building.

#### 4.4.1.2 10-Storey

Similar results are observed in the case of 10-storey structure represented by IDR and energy dissipation. Figure 4.7 shows the plot of IDR at each storey for both moment frame and the wall-frame system with SPD 9%. It is observed that the drift decreased considerably with the addition of structural walls.

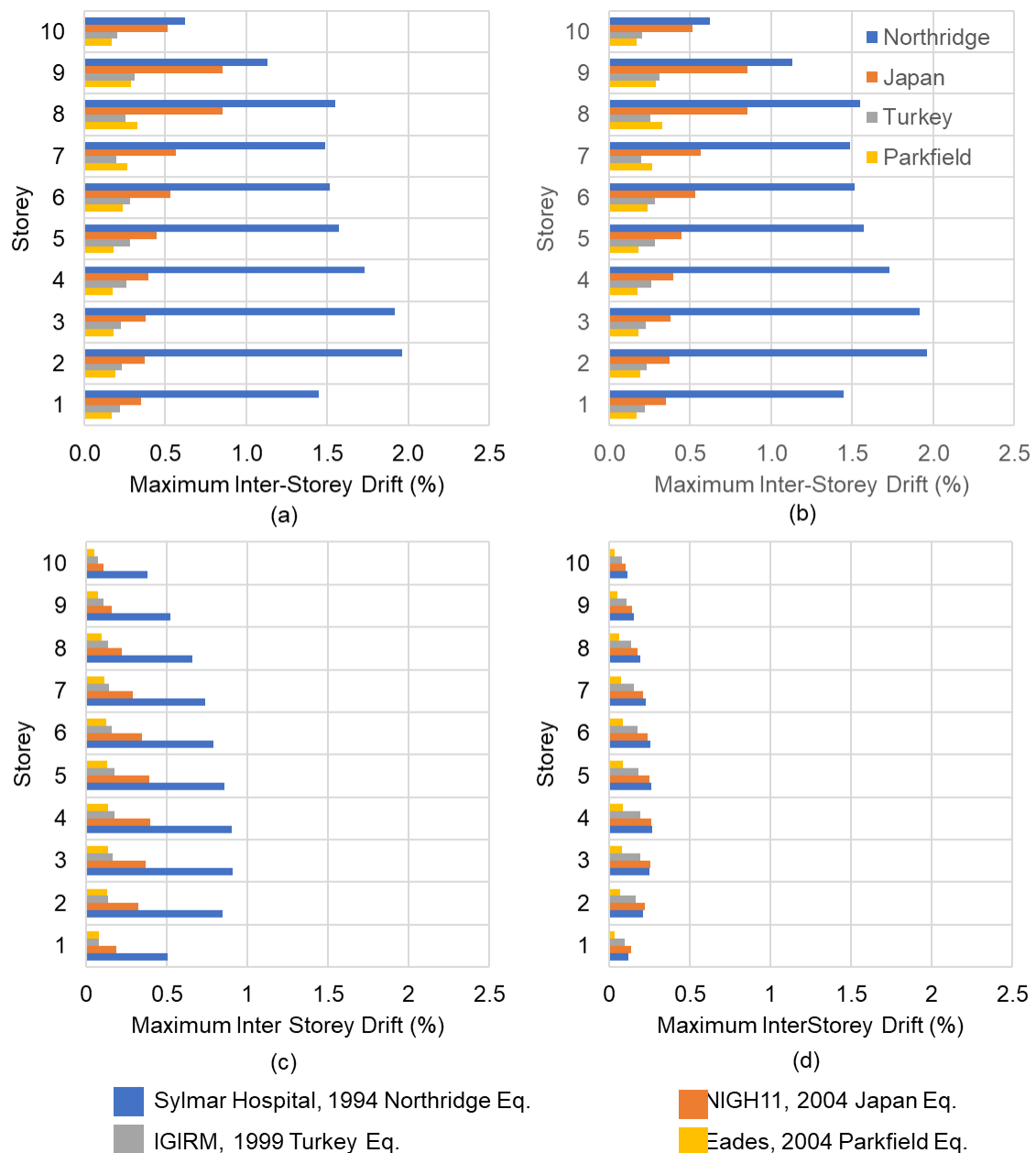


Figure 4.7 Maximum IDR in longitudinal direction at each floor of 10-storey structure subjected to near-fault ground motion without pulse with different lateral load resisting systems (a) moment resisting frame, and (b) wall-frame system with SPD 2.5%, (c) wall-frame system with SPD 3.75%, and (d) wall-frame system with SPD 9%

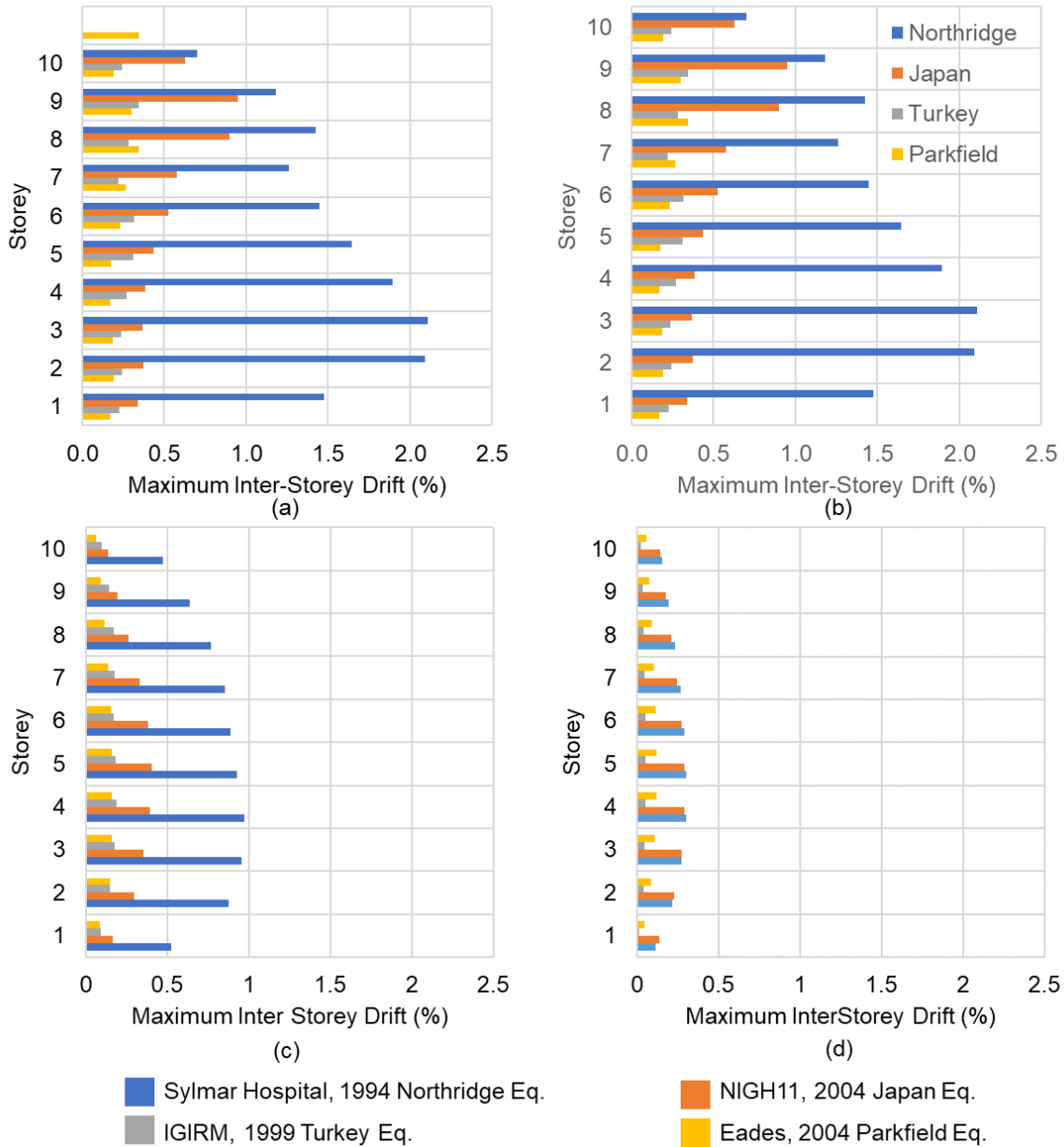


Figure 4.8 Maximum IDR in transverse direction at each floor of 10-storey structure subjected to near-fault ground motion without pulse with different lateral load resisting systems (a) moment resisting frame, and (b) wall-frame system with SPD 2.5%, (c) wall-frame system with SPD 3.75%, and (d) wall-frame system with SPD 9%

Also, the response amplitude of the Northridge earthquake decreased to an extent such that the effect of pulse in the ground motion is negligible. On the other hand, the energy dissipation of the structural with walls indicate large dissipation at the base of the structure. This indicates the ductility of the structural wall to allow large inelastic displacements.

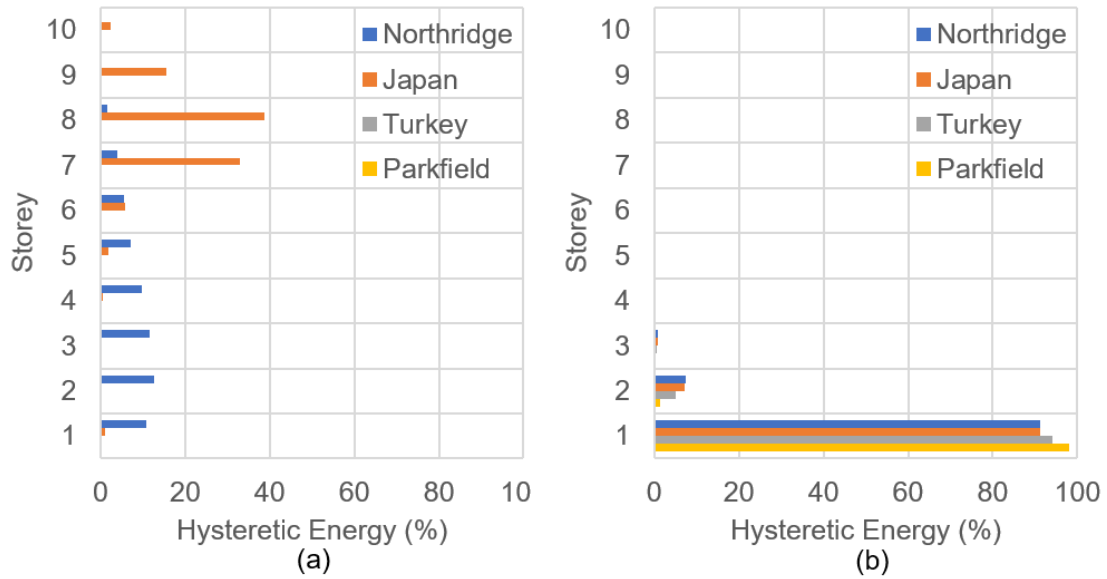


Figure 4.9 Dissipated energy at each storey of 10-storey structure subjected to near-fault ground motion with pulse for (a) moment resisting frame, and (b) wall-frame system with SPD 9% in the longitudinal direction

#### 4.4.2 Vertical Shaking

The same vertical ground motions considered in the previous chapter are applied on the structure with complete structural walls with 9% structural plan density. As expected, the structures respond elastically in all the analysis cases. Figure 4.10 shows the hysteretic energy with respect to the input energy imparted to the structure. It is observed that no energy dissipation takes place at all the structures with walls subjected to near-fault ground motions with pulse. This indicates the elastic behaviour of the structure.

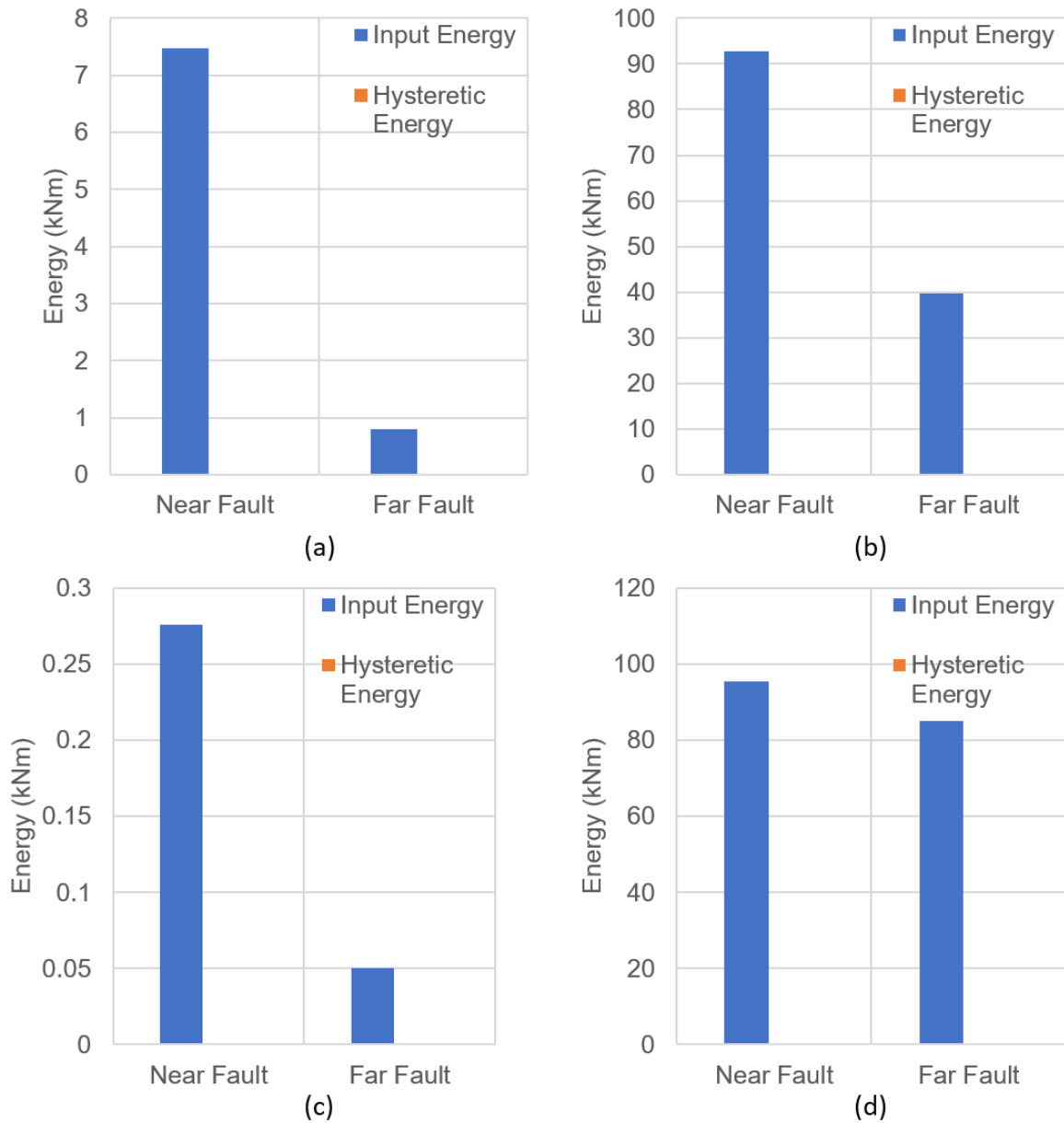


Figure 4.10 Comparison on input energy and hysteretic energy of 5 storey structure with structural walls SPD 9% in longitudinal direction when subjected to (a) 100% Vertical, (b) 100% Vertical and 30% fault normal in longitudinal direction, (c) 100% Vertical and 30% fault parallel in transverse direction, and (d) Vertical, 30% fault normal in longitudinal direction and 30% fault parallel in transverse direction

## 4.5 OBSERVATIONS

Figure 4.11 shows the consolidated maximum value of IDR obtained from nonlinear time history analysis of 5-storey structure subjected to near fault with and without pulse and far-fault ground motion recorded in different earthquake.

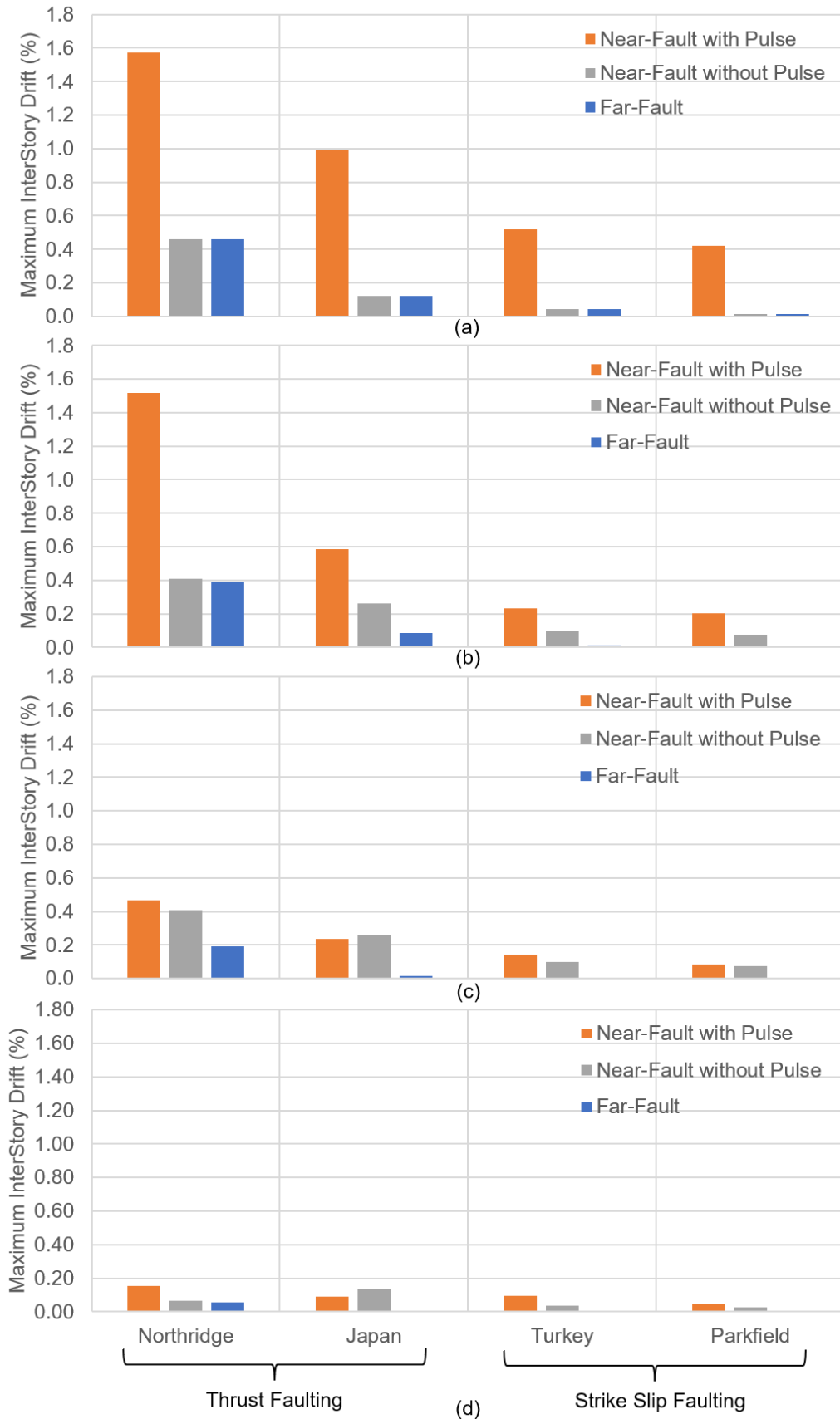


Figure 4.11 IDR of 5-storey building with (a) moment frames (b) frame with wall of SPD 2.75%, (c) frame with wall of SPD 3.75%, and (d) structural wall of SPD 9%

It is clearly observed that the structure with walls controlled the response of the structure in all the cases. Also, as the SPD of the structural walls increase the difference between the response of all the three types of ground motions decreases. This indicates that the structural wall reduces the impulsive behaviour of the near-fault ground motions with pulse. Similar results are obtained for the 10-storey structure.

## 4.6 CONCLUSIONS

The structure with structural walls with increase in SPD result in decrease of overall inter-storey drift and the difference in drifts between near fault ground motions with and without pulse. The distribution of drifts among the floors of 10 storey structure reveal that the flexural behaviour of the structure is largely improved with the presence of structural walls. This indicates that the structural walls are effective enough to resist the large amplitude pulse present in the ground motions. This is verified to be true in the case of vertical ground motion recorded during the Northridge earthquake.

The reinforced concrete structures of height less than 10 stories are required to be designed using dynamic analysis i.e., time history analysis by considering a ground motion suite containing atleast 25% of near fault ground motions in all the three directions. For such structures in the vicinity of probable fault, it is mandatory to consider structural wall system designed with suggested guidelines. If in any case, the structural wall cannot be adopted, a dual system with structural walls with structural plan density greater than or equal to 3.75% cannot be avoided.

*Blank Page*

## 5 Summary and Conclusions

### 5.1 SUMMARY

The only way to avoid life loss in the event of an earthquake is to mitigate the severe structural failures and ensure structures to withstand even the severe earthquakes. One such challenge to the structure lies in resisting the near fault ground motions that contain double sided velocity pulse in addition to the proximity effect observed in the near fault regions.

A detailed study is carried out on the ground motions recorded during 1999 Chi-Chi earthquake that are spatially distributed throughout the country. The characteristic differences in the near fault and far fault ground motions are observed with special attention on the near fault regions. Since the earthquake is predominantly thrust faulting mechanism, the ground motions exhibit strong hanging wall effect in the regions on the hanging wall that indicate high peak ground acceleration. From the observations, it can be concluded that the ground motions in the near fault region show that the PGA ratio of Fault normal to that of fault parallel equal to or more than 1. This helps in demarcating the near fault region for a particular earthquake, which in general do not have sufficient authenticity. In addition to the hanging wall effect, the most prominent and serious aspect of near fault ground motions is the presence of pulses that are more damaging for the structure and its failure.

To delineate the seismic behaviour of structures subjected to near fault ground motions with velocity pulses, a study is carried out on 5 storey and 10 storey reinforced concrete moment resisting frames subjected to near fault ground motions with and without pulses in comparison with far fault ground motions. Nonlinear time history analysis is carried out on both the structures when subjected to two thrust earthquake and two strike slip earthquakes. A plot of maximum inter storey drift obtained at each floor for ground motions recorded during each of the earthquake reveals that the near fault ground motions observe comparatively higher drifts than

the far fault ground motions. Also, the near fault ground motions with pulse observe higher drifts than those without pulse. This observation is reinforced with the input energy imparted and the hysteretic energy dissipated. The consideration of different earthquakes reveals that the immediate parameter that influence the structure response is the pulse period. However, after completion of the impulse present in the ground motions the structural response depends on the conventional characteristics such as peak ground acceleration, predominant frequency and effective duration. Therefore, it is identified that in order to improve the structural behaviour, the structural system needs to be improved such that the structure can withstand predominantly the high amplitude pulse that occurs in the initial time instant.

Structural wall system in addition to the moment resisting frame system is adopted with increase in structural plan density is found to be an intuitive solution to resisting the near fault ground motions. Therefore, three structures with two dual systems and one complete structural wall are verified by performing nonlinear time history analysis in all the previous cases that are studied in the moment resisting frame building. The results reveal that the increase in SPD of the walls reduces the overall maximum inter storey drift of the structure, in addition, decrease the difference in drifts observed due to near fault ground motions with and without pulse. The results of the 10-storey structure help in concluding another issue that the structure with structural walls improve the flexural behaviour of the structure by ensuring the uniform drifts at all floors.

## 5.2 CONCLUSIONS

The overall observations and conclusions reveal that the structural walls greatly enhance the overall seismic behaviour of the moment resisting frame in resisting the fault normal component of near fault ground motions without residual displacements. It may also be suggested that to achieve a sufficient elastic behaviour of the structure, structural walls with minimum 3.5% structural plan density is required to resist the near fault ground motions with pulses.

### 5.3 POSSIBLE FUTURE WORK

The present study can further be progressed in the following directions to properly mitigate the reinforced concrete structures:

1. The influence of shear hinges in the nonlinear response of the structure is required to be studied when subjected to near-fault ground motions
2. The behaviour of high-rise buildings with different structural systems when subjected to near and far-fault ground motions must be studied.

...

*Blank Page*

## 6 References

1. Aagaard, B. T., Hall, J. F., and Heaton, T. H., (2004) Effect of Fault Dip and Slip Rake Angles on Near-Source Ground Motions: Why Rupture Directivity was Minimal in the 1999 Chi-Chi, Taiwan, Earthquake. *Bulletin of the Seismological Society of America*, 94(1), 155–170.
2. Alavi, B., and Krawinkler, H., (2004) Behavior of Moment-Resisting Frame Structures Subjected to Near-Fault Ground Motions. *Earthquake Engineering and Structural Dynamics*, 33(6), 687–706. John Wiley and Sons Ltd. DOI: 10.1002/eqe.369.
3. Alavi, B., and Krawinkler, H., (2004) Strengthening of Moment-Resisting Frame Structures against Near-Fault Ground Motion Effects. *Earthquake Engineering and Structural Dynamics*, 33, 707-722. John Wiley and Sons Ltd. DOI:10.1002/eqe.370.
4. Anderson, J. C., and Bertero, V. v., (1997) Implications of the Landers and Big Bear Earthquakes on Earthquake Resistant Design of Structures. Berkeley.
5. Andrews, D. J., (1976a) Rupture Velocity of Plane Strain Shear Cracks. *Journal of Geophysical Research*, 81(32), 5679–5687. DOI: 10.1029/JB081i032p05679.
6. Andrews, D. J., (1976b) Rupture Propagation with Finite Stress in Antiplane Strain. *Journal of Geophysical Research*, 81(20), 1896–1977. DOI: 10.1029/JB081i020p03575.
7. Archila, M., (2014) December. Directionality Effects of Pulse-Like Near Field Ground Motions on Seismic Response of Tall Buildings. Vancouver.
8. Archuleta, R. J., (1984) A Faulting Model for the 1979 Imperial Valley Earthquake. *Journal of Geophysical Research*, 89(B6), 4559–4585. DOI: 10.1029/JB089iB06p04559.
9. Baker, J. W., (2007) Quantitative Classification of Near-Fault Ground Motions using Wavelet Analysis. *Bulletin of the Seismological Society of America*, 97(5), 1486–1501. DOI: 10.1785/0120060255.

10. Boore, D. M., (2001) Effect of Baseline Corrections on Displacements and Response Spectra for Several Recordings of the 1999 Chi-Chi, Taiwan, Earthquake. *Bulletin of the Seismological Society of America*, 91(5), 1199–1211.
11. Boore, D. M., and Atkinson, G. M., (1987) Stochastic Prediction of Ground Motion and Spectral Response Parameters at Hard-Rock Sites in Eastern North America. *Bulletin of the Seismological Society of America*, 77(2), 440–467.
12. Boore, D. M., and Bommer, J. J., (2005) Processing of Strong-Motion Accelerograms: Needs, Options and Consequences. *Soil Dynamics and Earthquake Engineering*, 25(2), 93–115. DOI: 10.1016/j.soildyn.2004.10.007.
13. Brune, J. N., (1970) Tectonic Stress and the Spectra of Seismic Shear Waves from Earthquakes. *Journal of Geophysical Research*, 75(26), 4997–5009. DOI: 10.1029/JB075i026p04997.
14. Burks, L. S., and Baker, J. W., (2014) Fling in the Near-Fault Ground Motions and its Effect on Structural Collapse Capacity. *Proceedings of Tenth U.S. National Conference on Earthquake Engineering*. Anchorage, Alaska: Earthquake Engineering Research Institute.
15. Cormier, V. F., and Spudich, P., (1984) Amplification of Ground Motion and Waveform Complexity in Fault Zones: Examples from the San Andreas and Calaveras Faults. *Geophysical Journal International*, 79(1), 135–152. DOI: 10.1111/j.1365-246X.1984.tb02846.
16. Murty C V R, Ragukanth S T G, Menon, A., Goswami, R., A R, Vijaynarayan, Gandhi, S. R., Kalidindi, S. N., et al., (2012) The Mw 6.9 Sikkim-Nepal Border Earthquake of September 18, 2011.
17. Hall, J. F., Heaton, T. H., Halling, M. W., and Wald, D. J., (1995) Near Source Ground Motions and its Effects on Flexible Buildings. *Earthquake Spectra*, 11(4), 569–605.
18. Hanks, T. C., (1975) Strong ground motion of the San Fernando, California, earthquake: Ground displacements. *Bulletin of the Seismological Society of America* 193–225., 65(1), 193–225.
19. Hartzell, S. H., and Heaton, T. H., (1983) Inversion of Strong Ground Motion and Teleseismic Waveform Data for the Fault Rupture History of the 1979 Imperial

- Valley, California, Earthquake. *Bulletin of Seismological Society of America*, 73(6), 1563–1583.
20. Hartzell, S., and Helmberger, D. v., (1982) Strong Motion Modeling of the Imperial Valley Earthquake of 1979. *Bulletin of Seismological Society of America*, 72(2), 571–596.
  21. Heaton, T. H., and Hartzell, S. H., (1988) Earthquake Ground Motions. *Annual Review of Earth and Planetary Sciences*, 16, 121–145.
  22. Heaton, T. H., and Helmberger, D. v., (1979) Generalized Ray Models of the San Fernando Earthquake. *Bulletin of the Seismological Society of America*, 69(5), 1311–1341.
  23. Ida, Y., (1972) Cohesive Force Across the Tip of a Longitudinal-Shear Crack and Griffith's Specific Surface Energy. *Journal of Geophysical Research*, 77(20), 3796–3805. DOI: 10.1029/JB077i020p03796.
  24. Ishihara, K., Shimizu, K., and Yamada, Y., (1981) Pore Water Pressures Measured in Sand Deposits During an Earthquake. *Soils and Foundations*, 21(4), 85–100. DOI: 10.3208/sandf1972.21.4\_85.
  25. Jain, S. K., Murty, C. V. R., Chandak, N., Seeber, L., and Jain, N. K., (1993) The September 29, 1993, M6.4 Killari, Maharashtra Earthquake in Central India. EERI Special Earthquake Report (Vol. 28).
  26. Joyner, W. B., and Boore, D. M., (1982) Prediction of Earthquake Response Spectra. Menlo Park, California.
  27. Kalkan, E., and Kunnath, S. K., (2006) Effects of Fling Step and Forward Directivity on Seismic Response of Buildings. *Earthquake Spectra*, 22(2), 367–390. Earthquake Engineering Research Institute. DOI: 10.1193/1.2192560.
  28. Kwan A. K. H. (1993), Improved Wide-Column Frame Analogy for Shear/Core Wall Analysis, *Journal of Structural Engineering*, 119(2), 420.
  29. Liu, H.-L., and Heaton, T. H., (1984) Array Analysis of the Ground Velocities and Accelerations from the 1971 San Fernando, California Earthquake. *Bulletin of Seismological Society of America*, 74(5), 1951–1968.

30. Liu, H.-L., and Helmberger, D. v., (1985) The 23:19 Aftershock of the 15 October 1979 Imperial Valley Earthquake: More Evidence for an Asperity. *Bulletin of Seismological Society of America*, 75(3), 689–706.
31. Mander, J. B., Priestley, M. J. N., and Park, R., (1988) Theoretical Stress-Strain Model for Confined Concrete. *Journal of Structural Engineering, ASCE*, 114(8), 1804–1826.
32. Muin, S., Astaneh-Asl, A., and Topkaya, C., (2020) The Response of Tall Buildings to Far-Field Earthquakes and the Case of a 49-Storey Steel Building. *International Journal of Earthquake and Impact Engineering*, 3(1), 15–39.
33. Oglesby, D. D., Archuleta, R. J., and Nielsen, S. B., (2000) Dynamics of Dip-Slip Faulting: Explorations in Two Dimensions. *Journal of Geophysical Research*, 105(B6), 13643–13653.
34. Olson, A. H., and Apsel, R. J., (1982) Finite Faults and Inverse Theory with Applications to the 1979 Imperial Valley Earthquake. *Bulletin of the Seismological Society of America*, 72(6A), 1969–2001. DOI: 10.1785/BSSA07206A1969.
35. Papageorgiou, A. S., and Aki, K., (1983a) A Specific Barrier Model for the Quantitative Description of Inhomogeneous Faulting and the Prediction of Strong Ground Motion. Part I. Description of the Model. *Bulletin of Seismological Society of America*, 73(3), 693–722.
36. Papageorgiou, A. S., and Aki, K., (1983b) A Specific Barrier Model for the Quantitative Description of Inhomogeneous Faulting and the Prediction of Strong Ground Motion. Part II. Applications of the Model. *Bulletin of the Seismological Society of America*, 73(4). DOI: 10.1785/BSSA0730040953.
37. Plafker, G., (1965) Tectonic Deformation Associated with the 1964 Alaska Earthquake: The Earthquake of 27 March 1964 Resulted in Observable Crustal Deformation of Unprecedented Areal Extent. *Science*, 148(3678), 1675–1687. DOI: 10.1126/science.148.3678.1675.
38. Ramancharla, P. K., and Murty C. V. R., (2014) Earthquake Safety of Houses in India: Understanding the Bottlenecks in Implementation. *Indian Concrete Journal*, 88(9), 51–63.

39. Shabestari, K. T., and Yamazaki, F., (2003) Near-Fault Spatial Variation in Strong Ground Motion due to Rupture Directivity and Hanging Wall Effects from the Chi-Chi, Taiwan Earthquake. *Earthquake Engineering and Structural Dynamics*, 32(14), 2197–2219. John Wiley and Sons Ltd. DOI: 10.1002/eqe.323.
40. Shin, T.-C., and Teng, T.-L., (2001) An Overview of the 1999 Chi-Chi Taiwan Earthquake. *Bulletin of Seismological Society of America*, 91(5), 895–913.
41. Singh, S. K., Mena, E., and Castro, R., (1988) Some aspects of source characteristics of the 19 September 1985 Michoacan earthquake and ground motion amplification in and near Mexico City from strong motion data . *Bulletin of the Seismological Society of America*, 78(2), 451–477.
42. Somerville, P., and Graves, R., (1993) Conditions that Give Rise to Unusually Large Long Period Ground Motions. *The Structural Design of Tall Buildings*, 2(3), 211–232. DOI: 10.1002/tal.4320020304
43. United States Geological Survey, Strong Motion Virtual Data Centre (COSMOS), Accessed on 10 Dec 2018, California.
44. Thatcher, W., (1975) Strain Accumulation and Release Mechanism of the 1906 San Francisco Earthquake. *Journal of Geophysical Research*, 80(35), 4862–4872. DOI: 10.1029/JB080i035p04862.
45. Todd, D. R., Carino, N. J., Chung, R. M., Lew, H. S., Taylor, A. W., and Walton, W. D., (1994) 1994 Northridge earthquake: Performance of Structures, Lifelines and Fire Protection Systems. Gaithersburg, MD. DOI: 10.6028/NIST.IR.5396.
46. Tremblay, R., Timler, P., Bruneau, M., and Filiatrault, A., (1995) Performance of steel structures during the 1994 Northridge earthquake. *Canadian Journal of Civil Engineering*, 22, 338–360.
47. Trifunac, M. D., (1976) Preliminary Analysis of the Peaks of Strong Earthquake Ground Motion - Dependence of Peaks on Earthquake Magnitude, Epicentral Distance, and Recording Site Conditions. *Bulletin of the Seismological Society of America*, 66(1), 189–219.
48. Trifunac, M. D., and Brady, A. G., (1975) A Study on the Duration of Strong Earthquake Ground Motion. *Bulletin of the Seismological Society of America*, 65(3), 581–626.

49. Tsai, N. C., (1969) May 28. Influence of Local Geology on Earthquake Ground Motions. Pasadena, California.
50. Udias, A., Madariaga, R., and Buforn, E., (2014) Source Mechanisms of Earthquakes Theory and Practice (1st ed., Vol. 1). Cambridge: Cambridge University Press.
51. Vidale, J. E., (1987) Application of Two-Dimensional Finite-Difference Wave Simulation to Earthquakes. Pasadena.
52. Yadav, K. K., and Gupta, V. K., (2017) Near-Fault Fling-Step Ground Motions: Characteristics and Simulation. *Soil Dynamics and Earthquake Engineering*, 101, 90–104. Elsevier Ltd. DOI: 10.1016/j.soildyn.2017.06.022.
53. Zeevaert, L., (1964) Strong Ground Motions Recorded during Earthquakes of May the 11th and 19th, 1962 in Mexico City. *Bulletin of the Seismological Society of America*, 54(1), 209–231. DOI: 10.1785/BSSA0540010209

...